AD

AFFDL-TR-74-144

C-5A CARGO DECK LOW-FREQUENCY VIBRATION ENVIRONMENT

TECHNICAL REPORT AFFDL-TR-74-144

FEBRUARY 1975

AIR FORCE FLIGHT DYNAMICS LABORATORY
AIR FORCE SYSTEMS COMMAND
WRIGHT-PATTERSON AIR FORCE BASE, OHIO 45433

NOTICE

When Government drawings, specifications, or other data are used for any purpose other than in connection with a definitely related Government procurement operation, the United States Government thereby incurs no responsibility nor any obligation whatsoever; and the fact that the government may have formulated, furnished, or in any way supplied the said drawings, specifications, or other data, is not to be regarded by implication or otherwise as in any manner licensing the holder or any other person or corporation, or conveying any rights or permission to manufacture, use, or sell any patented invention that may in any way be related thereto.

This technical report has been reviewed and is approved for publication.

Walter J. Mykytow

WALTER J. MYKYTOW
Asst. for Research and Technology
Vehicle Dynamics Division
AF Flight Dynamics Laboratory

Copies of this report should not be returned unless return is required by security considerations, contractual obligations, or notice on a specific document.

SECURITY CLASSIFICATION OF THIS PAGE (When Data Entered)

REPORT DOCUMENTATION PAGE

READ INSTRUCTIONS BEFORE COMPLETING FORM

1. REPORT NUMBER: AFFDL-TR-74-144	2. GOVT ACCESSION NO.
3. RECIPIENT'S CATALOG NUMBER	
4. TITLE (and Subtitle): C-5A Cargo Deck Low-Frequency Vibration Environment	5. TYPE OF REPORT & PERIOD COVERED: Final report. Mar 73 - Aug 74
6. PERFORMING ORG. REPORT NUMBER	
7. AUTHOR(s): JEROME PEARSON, ROGER E. THALLER, ANTHONY R. BAYER, JR.	8. CONTRACT OR GRANT NUMBER(s)
9. PERFORMING ORGANIZATION NAME AND ADDRESS: Air Force Flight Dynamics Laboratory, Wright-Patterson Air Force Base, Ohio 45433	10. PROGRAM ELEMENT, PROJECT, TASK AREA & WORK UNIT NUMBERS: 410A0201
11. CONTROLLING OFFICE NAME AND ADDRESS: "	12. REPORT DATE: February 1975
	13. NUMBER OF PAGES: 108
14. MONITORING AGENCY NAME & ADDRESS (if different from Controlling Office)	15. SECURITY CLASS. (of this report): UNCLASSIFIED
	15a. DECLASSIFICATION DOWNGRADING SCHEDULE

16. DISTRIBUTION STATEMENT (of this Report)

Distribution limited to U.S. Government agencies only; test and evaluation; statement applied December 1974. Other requests for this document must be referred to AF Flight Dynamics Laboratory (FYS) Wright-Patterson AFB, Ohio 45433.

17. DISTRIBUTION STATEMENT (of the abstract entered in Block 20, if different from Report)

Approved for public release; distribution unlimited.

18. SUPPLEMENTARY NOTES

19. KEY WORDS (Continue on reverse side if necessary and identify by block number)

Jet Transport Planes, Vibration, C-5 Aircraft, C-5A Aircraft, Flight Testing, Dynamic Response, Landing Impact, Taxiing, Turbulence, Statistical Analysis.

20. ABSTRACT (Continue on reverse side if necessary and identify by block number)

The low-frequency vibration environment of the C-5A cargo deck is defined in terms of the accelerations experienced during takeoff, cruise, landing, and turbulence simulated by low-altitude terrain following. The accelerations presented are the peaks and the percentage occurrence levels versus one-third octave frequency band from 0.4 to 31.5 Hz. These percentage occurrence curves allow the prediction of the probability of exceeding a given level of acceleration for a given flight profile. They can be used to develop

DD FORM 1 JAN 73 1473 EDITION OF 1 NOV 65 IS OBSOLETE

UNCLASSIFIED

SECURITY CLASSIFICATION OF THIS PAGE (When Data Entered)

20. Continued

vibration test curves for C-5A cargoes which are sensitive to low-frequency acceleration, such as large, flexible spacecraft and launch vehicles mounted horizontally. Sample calculations are presented which show two methods of predicting the probability of occurrence of given levels of acceleration for typical flight profiles, based on the Gaussian and the binomial distributions.

FOREWORD

The research described in this report was performed by personnel of the Vehicle Dynamics Division, Air Force Flight Dynamics Laboratory, Air Force Systems Command, Wright-Patterson Air Force Base, Ohio.

The Project Engineer was Mr. Jerome Pearson, the Mathematical Analyst was Mr. Roger E. Thaller, and the Instrumentation Engineer was Mr. Anthony R. Bayer, Jr. The work was performed between March 1973 and August 1974.

This report was submitted by the authors on 25 September 1974.

TABLE OF CONTENTS

LIST OF ILLUSTRATIONS

LIST OF TABLES

I. INTRODUCTION

The availability of large transport aircraft has allowed the transporting by air of many large, fragile aerospace payloads. Some of these payloads, such as horizontally mounted launch vehicles and spacecraft with flexible appendages, are very sensitive to low levels of vibration at frequencies below five hertz. In order to protect these payloads during air transportation, it is necessary to know the low-frequency vibration environment of these aircraft cargo decks.

The measurement of cargo deck vibration environments has a long history (references 1, 2), but most of these studies have dealt with the frequency range above five or ten hertz. This lack of data below five hertz confronted the Air Force Space and Missile Systems Organization (SAMSO) when it required payloads with known high responses to 0.5 to 2 Hz excitation to be transported aboard C-5A aircraft. The Air Force Flight Dynamics Laboratory was requested by SAMSO to perform the flight tests necessary to define the low-frequency vibration environment of the C-5A cargo deck. These measurements were needed to determine the risks of occurrence of given levels of acceleration during all phases of C-5A operations. The tests were performed and the environmental vibrations were presented in a limited-distribution report (3).

1. Magrath, H.A., Rogers, O.R., and Grimes, C.K.: Shock and Vibration Handbook (C.M. Harris and C.E. Crede, Eds.), Vol. 3, Chap 47, McGraw-Hill, New York, 1961.
2. Ostrem, F.E., "A Survey of the Transportation Shock and Vibration Input to Cargo," Shock and Vibration Bulletin No. 42, Part 1, pp. 137-151, January 1972.
3. Pearson, Jerome, Thaller, Roger E., and Bayer, Anthony R. Jr., C-5A Cargo Deck Flight Vibration Measurements, AFFDL/FYS/73-12, Wright-Patterson AFB, Ohio, November 1973.

The objective of this report is to present these new low-frequency measurements and additional data in conjunction with statistical criteria. The environmental vibrations are presented for the test conditions of taxi, takeoff, climb, cruise, turbulence simulated by terrain-following, descent, and landing. These data and the statistical criteria can be used to approximate the probability of occurrence of given levels of acceleration for flight profiles constructed from these flight conditions.

The calculations in this report used only the vibration data measured by the Flight Dynamics Laboratory. Other vibration data on the C-5A have been compiled, including fatigue studies of VGH data from many landings. The results of these studies may be found in reports such as reference 4.

4. Anon., C-5A Acceleration Data Reduction and Analysis Program Semi-Annual Report. Lockheed-Georgia Company Report LG1US613/M-2-3, 31 May 1974.

II. FLIGHT TESTS AND RESULTS

The test results presented in this report were measured on C-5A aircraft number 68 during a series of test flights. This aircraft has been used as a testbed for many new C-5A systems. It was equipped with an automatic landing system called Autoland.

The C-5A cargo deck, shown in Figure 1, extends from fuselage station 507 to station 1970 and is 19 feet wide. The station numbers are the distance in inches from a reference point forward of the aircraft nose.

1. Instrumentation

In order to measure the vibration environment of equipment carried on the cargo deck, accelerometers were mounted in pairs at the six locations marked in Figure 1. All the 3.5-ounce accelerometers were mounted on aluminum blocks attached to the permanent cargo tie-down rails at the sides of the cargo deck. The accelerometers at the forward end of the cargo deck at station 530 sensed vertical and lateral accelerations. The accelerometers near the middle of the cargo deck were located just forward of the wheel wells at station 1150, and sensed vertical and longitudinal accelerations. The accelerometers at the aft end of the cargo deck were located at station 1940, just forward of the rear loading ramp. They were positioned to sense vertical and lateral accelerations. The accelerometers had an upper frequency limit of 1550 Hz, a sensitivity of 100 millivolts (RMS) per g (peak), and an output noise of less than 5 mv RMS.

These twelve sensors were used to define the vertical, lateral, and longitudinal accelerations of the cargo deck. Roll, pitch, and yaw angular accelerations were derived by taking the difference between the real-time signals from pairs of sensors. These angular measurements give only a

rough estimate of the angular vibration environment because of the large distance between the sensors. For the low-frequency data, the accelerometer outputs were filtered to pass frequencies between 0.15 and 30 Hertz. The low frequencies were attenuated 6 dB per octave, down 3 dB at 0.15 Hz; the high frequencies were attenuated at 48 dB per octave, down 3 dB at 30 Hz. For the full frequency range data, the 30 Hz low-pass filter was removed and the accelerations were recorded at frequencies up to the accelerometer frequency limit of about 1600 Hz.

The 12 channels of data were amplified and recorded in flight by a compact instrument package which contained the amplifiers, power supply, time code generator, filters, and an FM tape recorder; the system block diagram is shown in Figure 2. The amplifiers were equipped with automatic gain controls which adjusted the amplifier gains in 10 dB steps over a 70 dB range to ensure that the signals were recorded with the proper amplitude. The automatic gain change was triggered when the signal was out of the amplifier range for more than 0.3 seconds. Most flight conditions could thus be recorded properly without advance knowledge of the vibration levels. However, for the landing data the amplifiers were locked into a pre-calculated gain step in order to avoid clipping the response at the instant of runway impact.

The fourteen-channel analog FM tape machine recorded at 3-3/4 ips with a center frequency of 6.75 KHz. This gave 96 minutes of recording time per flight with a signal-to-noise ratio of 38 dB and a bandwidth of 1.25 KHz. The landing data were recorded at 30 ips with a center frequency of 54 KHz. This gave 12 minutes of recording time per flight with a signal-to-noise ratio of 42 dB and a bandwidth of 10 KHz.

2. Test Procedure

The complete instrument package was mounted on a 24-inch square aluminum plate and tied down to the cargo deck by straps during the flight tests, as shown in Figure 3. The tape recorder was operated in flight by a crewman on the upper deck using a remote control unit. The crewman recorded the test conditions by voice on an extra tape recorder channel.

Before each test flight, a known calibration signal was recorded. Vibration was then measured with all aircraft engines and power off to measure the instrumentation system noise levels.

Vibration was measured during takeoff, climb, cruise, turbulence simulated by low-altitude terrain following, descent, landing, and taxi. Measurements were made during 27 takeoffs and landings on three runways; the gross weights ranged from 455,000 pounds to 673,000 pounds; and four hours of cruising time were recorded in conditions ranging from smooth air to the severe vibration induced by terrain following at low altitude.

3. Data Analysis

The data were recorded on magnetic tapes during flight, played back on a laboratory recorder meeting IRIG Standard #106-72, and were analyzed by several methods. The first method was applied to 0-10KHz data obtained during climb, cruise in smooth air, and descent. To acquire a general overview of the high frequency vibration, the root-mean-square acceleration, g rms, was determined over one-third octave bands from 3.15 Hz to 10 KHz center frequencies. The filters conformed to USASI 51.11-1966, Class III standards. More detailed analysis of the low-frequency data was performed to determine the risk of encountering given levels of acceleration. This

determination required definition of the distribution of acceleration amplitudes.

It was desired to determine the acceleration levels within the one-third octave bands with center frequencies of 0.4 Hz to 31.5 Hz. Since the filters from standard one-third octave analysis systems have center frequencies only as low as 3.15 Hz, it was necessary to play back the data through the filters at eight times the recording speed. The 0.4 Hz band data were thus derived from the 3.15 Hz band filter on the standard one-third octave system, and so on up to the 31.5 Hz band data, which were derived from the 250 Hz band filters. Since the commercially available one-third octave systems are not precisely spaced at the mathematically correct frequencies, a negligible error in frequency was introduced by this procedure.

This procedure was applied to low-frequency data recorded during climb, cruise in smooth air, and descent. The resulting filtered time histories were averaged to obtain root-mean-square acceleration, g rms, over one-third octave bands with center frequencies from 0.4 Hz to 31.5 Hz. Because these g rms levels were less than the levels observed during other conditions, a comparatively small engineering risk was associated with underestimating the distribution of these data. The Gaussian distribution was applied to the low-level climb, cruise, and descent data, based upon previous data analyses (5).

For the flight conditions causing the highest accelerations, a more detailed analysis was used. The landing, taxiing, and terrain-following

5. Magnuson, C.F., "Dynamic Environment Study of Turbojet Cargo Aircraft," Proceedings of the Institute of Environmental Sciences 18th Annual Technical Meeting, pp. 420-425, May 1972.

records were filtered into one-third octave bands with center frequencies of 0.4 Hz to 31.5 Hz.

These twenty filtered time histories were each sampled 124 times per second and digitized by an analog-to-digital converter and recorded on a second magnetic tape. The converter had an aperture time of 50 nanoseconds, a full-scale input of $\pm$2.5 VDC, and a resolution of 1.22 millivolts. These digitized time histories were input to a computer with a 16-bit integer word length. This computer used decimal words with a 23-bit mantissa and an exponent biased by hexadecimal 80. Using a Fortran IV compiler, the time histories were analyzed in terms of maximum accelerations and probability densities over each frequency band. Figure 4 shows a flow chart of this procedure.

In order to completely describe the distribution of accelerations, a histogram of acceleration versus number of occurrences and its statistical parameters such as mean and variance would be needed for each frequency band and for all sensors. Since this would require a prohibitive number of graphs, a simplified method to describe the distributions was used which required only one graph per sensor. In this method, the absolute values of the time histories were used to produce the acceleration histograms. The maximum value of acceleration for each frequency band was recorded, as were the levels of acceleration which encompassed 68.27% and 95.45% of all the data samples. These three values were then plotted by a digital plotter for all frequency bands for each sensor. These particular percentage levels were selected because they correspond to the values of σ and 2σ for a Gaussian distribution. Thus if the data were Gaussian, these two levels would be in the ratio of one to two. When these percentage levels are plotted together

with the maximum acceleration observed, it is possible to estimate with some confidence whether a distribution is Gaussian by this test. If the ratio is not one to two, the difference is a measure of how much the distribution differs from the Gaussian case.

The plotted data represent the distribution of accelerations during a given flight condition, and the probability of occurrence of a given acceleration can be estimated from the statistically significant σ and 2σ levels.

Previous work has presented vibration data in percentage occurrence levels, usually 99% or 90% levels (5,6). The advantage of using the peak, 95.45% and 68.27% levels is that they are more statistically convenient than the 99% or 90% levels. The drawback to plotting the peak level is that a stray digit in the computer can cause a great error in the maximum value of acceleration. In the present program, the highest values of acceleration were checked against the original time histories to ensure their accuracy.

A sample of data plotted by this method is shown in Figure 5 for a Gaussian signal. The 68.27% and 95.45% curves are in the ratio of one to two. The peak value curve is a function of the testing time in terms of frequency -- that is, the number of cycles of data measured. Theoretically, an infinitely long testing time will give an infinite peak value and an exact one-to-two ratio in the 68.27% and 95.45% curves.

5. Magnuson, C.F., "Dynamic Environment Study of Turbojet Cargo Aircraft," Proceedings of the Institute of Environmental Sciences 18th Annual Technical Meeting, pp. 420-425, May 1972.
6. Foley, J.T., Gens, M.B., and Magnuson, C.F.: "Current Predictive Models of the Dynamic Environment of Transportation." Proceedings of the Institute of the Environmental Sciences 18th Annual Technical Meeting, May 1972, pp. 162-171.

For practical testing times this ratio is still very close to 1:2, but the peak acceleration curve usually falls above 3σ (7). In addition, no realizable physical system exhibits infinite values of acceleration; the distribution is truncated at high levels of acceleration by physical limitations.

Within certain frequency bands, the display of landing data showed the largest maximum values and the ratios of 68.27% and 95.45% levels most different from 2:1. The landing data were most important and application of the Gaussian distribution to these data was least accurate. Therefore, analysis of the landing data was repeated using an alternate method.

For each landing, a tabulation was made of the maximum acceleration recorded in each of the selected frequency bands from impact to the end of taxi. These peaks could then be used directly to compile the probability of occurrence of specific values of acceleration using the binomial distribution. This analysis is described in detail later.

4. Results

The test data showed that the highest accelerations at low frequencies were experienced during landing. The other conditions producing high accelerations were high-speed taxiing and terrain following. Accelerations measured during these three conditions were analyzed in percentage occurrence levels. The results are summarized in Figure 6, which shows the peak, 95.45%, and 68.27% levels recorded over 27 landings and a sample of

7. Gray, C.L., "First Occurrence Probabilities for Extreme Random Vibration Amplitudes," Shock and Vibration Bulletin No. 35, Part IV, pp. 99-104, 1966.

low-altitude terrain following. The peak values from this figure were converted to equivalent double-amplitude based on sinusoidal vibration at each band center frequency and are plotted in Figure 7. The dashed line in the figure is an envelope derived from previous data on smaller aircraft.

The low-frequency vibration environment of the C-5A cargo deck is less severe than that of smaller aircraft. In general, the data appear to represent broad-band Gaussian excitation with enhanced responses at predominant frequencies which correspond to the fuselage resonances. Except for the landing data with the bands having center frequencies 8 Hz, 10 Hz, and 12.5 Hz, the 95.45% level is about twice the 68.27% level, indicating that the data do not differ greatly from Gaussian. Note that due to the filtering of the data at 30 Hz, the 31.5 Hz band has been attenuated slightly.

a. Taxiing

The responses for each sensor for taxiing are shown in Figures 8-19. The largest observed acceleration, 0.27g, was in the vertical direction at the left front of the cargo deck in the 31.5 Hz band. There were also significant accelerations in the 1-1.25 Hz and 8-10 Hz bands at different parts of the cargo deck. The longitudinal accelerations were the lowest observed, and were plotted on an expanded scale in Figures 13 and 15. The derived values of roll, pitch, and yaw angular accelerations are shown in Figures 20-22. The roll angular acceleration was obtained by subtracting the linear accelerations from the two vertical sensors at station 530 and dividing by the 228-inch distance between them; the pitch angular acceleration was obtained in the same manner from the two vertical sensors on the right side of the cargo deck at stations 530 and 1150; and

the yaw angular acceleration was obtained from the two longitudinal sensors at station 1150. The largest observed angular acceleration was 0.7 radians/second^2 of yaw in the 10 Hz band.

b. Climb, Cruise, Descent

The accelerations encountered in these flight conditions were the lowest measured. As discussed previously, these data were considered to be normally distributed and only the rms accelerations are plotted. Figures 23-34 show the responses of each sensor for these three conditions of climb, cruise, and descent. The first part of each figure, e.g., Figure 23a, shows the sensor response for the frequency range 0.4 to 31.5 Hz; the second part of each figure, e.g., Figure 23b, shows the same sensor response for the frequency range 3.15 Hz to 10 KHz. At the right side of each figure is the overall rms response for the sensor. The accelerations for each flight condition and sensor were relatively low; no single band acceleration exceeded 0.1g rms. Due to the recorder rolloff above 1.25 KHz, the higher frequencies are attenuated.

c. Turbulence

It was hoped that a good sample of flight in turbulence would be obtained, but only light turbulence was observed during this series of flight tests. However, during some test flights the aircraft was flown at a height of 1000 feet above ground level with the aid of terrain-following radar. This flight condition resulted in large accelerations as the aircraft flew very rapidly through the near-surface turbulence. This condition was intended to simulate flight through heavy turbulence at altitude and these data were used to estimate the aircraft responses in this condition. Figures 35-49 show all the sensor responses and the

derived roll, pitch and yaw accelerations during terrain following. These figures show generally lower responses than during taxiing, with the highest responses occurring at lower frequencies. Vertical responses in the 2 Hz band predominated at the forward station, and responses at 0.63 and 0.8 Hz were larger at the center and aft stations. The highest lateral responses were between 2.5 and 4 Hz and the highest longitudinal responses were at 1 and 1.25 Hz. Note that Figures 40-42, 47, and 48 are plotted on an expanded scale.

d. Landing

The responses for each sensor during landing are shown in Figures 50-61, and the derived roll, pitch, and yaw angular accelerations during landing are shown in Figures 62-64. These figures show that the vertical responses at the rear of the cargo deck represent the most severe environment. The largest responses were in the 10 Hz band, and less significant responses occurred in the 0.5, 3.15, and 20 Hz bands. The largest linear acceleration observed in any one frequency band was 0.5g in the 10 Hz band. The largest observed angular acceleration was roll in the 10 Hz band.

The landing data show the largest discrepancies from the normal distribution, which are particularly evident in the 8, 10, and 12.5 Hz frequency bands. In order to apply an alternate method of analysis to these data, the peak accelerations observed in each of these frequency bands for each sensor are tabulated in Tables 1-12. One maximum is listed for each sensor for each landing, but not all 27 landings were obtained for the vertical sensors at the rear of the cargo deck.

III. SAMPLE VIBRATION CALCULATIONS

In order to determine the risk of encountering an acceleration which would damage a sensitive payload, it is necessary to calculate the probability of exceeding the limiting acceleration for each flight condition and then to combine these into an overall probability for an entire flight profile. The profile is constructed from the time spent in each of the conditions of interest - taxi, cruise, cruise in turbulence, descent, landing impact, and rollout. These probabilities have been calculated by two different methods -- one based on the normal distribution and one based on the binomial distribution. Most of the C-5A flight vibration was distributed normally, as indicated by the 68.27% and 95.45% levels. However, for the landing and rollout data in the frequency bands centered on 8, 10, and 12.5 Hz, the binomial distribution was applied. These methods are described below and are accompanied by sample calculations.

1. Normal Distribution

In order to determine the probability of exceeding a given acceleration during a selected flight condition, first compare this acceleration to the measured 100% level or the 3σ level. If this acceleration is less than either of these values, it will be exceeded frequently during this flight condition. If the acceleration of interest is greater than these values, the following analysis applies.

For normally distributed data, the probability P of exceeding an acceleration a, where a is greater than three standard deviations ($a>3\sigma$), is given by

$$P \leq 2fTe^{\frac{-a^2}{2\sigma^2}} \qquad (1)$$

where f is the frequency of the vibration and T is the time in seconds spent in the flight condition (7). If P_1 through P_5 are the values of P for flight conditions 1 through 5, then the overall probability of exceeding acceleration a during the total flight profile is

$$P = 1 - [(1-P_1)(1-P_2)(1-P_3)(1-P_4)(1-P_5)] \qquad (2)$$

Table 13 has been compiled as an example of the application of the normal distribution to find the probability of exceeding a vertical acceleration of 0.1g in the 1.25 Hz frequency band at the right rear of the C-5A cargo deck. The flight profile assumed includes 500 seconds of taxiing, 1500 seconds in climb, and so on through all the values given in column 6 of Table 13, for a flight of about four hours. The 100% and 68.27% (or σ) values were obtained from Figure 16 for taxiing, from Figure 31 and for climb, cruise, and descent, from Figure 43 for turbulence (simulated by terrain following), and from Figure 58 for landing. The values required for the calculations are shown in columns 2-6. Column 7 shows the risk of exceeding the 0.1g acceleration for each flight condition, and the sum in column 9 then shows the overall probability of exceeding 0.1g acceleration in the 1.25 Hz frequency band for this flight profile, which is 0.418. The rms acceleration during climb, cruise, and descent is so low that the probability of exceeding 0.1g in these conditions is essentially zero. The proportion of time spent in turbulence may be estimated as a function of altitude, following Press and Steiner (8).

7. Gray, C.L., "First Occurrence Probabilities for Extreme Random Vibration Amplitudes," Shock and Vibration Bulletin No. 35, Part IV, pp. 99-104, 1966.
8. Press, Harry, and Steiner, Roy, An Approach to the Problem of Estimating Severe and Repeated Gust Loads for Missile Operations, NACA TN4332, 1958.

Additional information on the application of equation 1 may be found in Bendat (9) and Bendat et al. (10).

2. Binomial Distribution

The data measured in the 8, 10, and 12.5 Hz bands during landing do not show a ratio of 1:2 between the 68.27% and 95.45% levels and are apparently not normally distributed. In order to provide a better measure of the probability of occurrence of large accelerations during this condition, the binomial distribution may be applied. The probability P of exceeding acceleration "a" during at least one landing included in the flight is given by

$$P = 1 - (P_a)^n \qquad (3)$$

where P_a is the proportion of all landings in which the acceleration a was not exceeded and n is the number of landings planned for the flight. The values of P_a may be determined from a compilation of the peak accelerations recorded during the test landings. These are shown in Tables 1 through 12 for each of the twelve sensors. The peak acceleration for each landing is tabulated for the three frequency bands centered on 8, 10, and 12.5 Hz. The proportion P_a of the landings during which an acceleration a was not exceeded may thus be determined directly from the tables. When the probability P from equation 3 is determined, it may be combined with the probabilities determined for other flight conditions by equation 2. This overall probability can therefore be a combination of binomially and

9. Bendat, Julius S., Probability Functions for Random Responses: Prediction of Peaks, Fatigue Damage, and Catastrophic Failures, NASA CR-234, National Aeronautics and Space Administration, Washington, D.C., April 1964.

10. Bendat, J.S., Enochson, L.D., Klein, G.H., and Pierson, A.G., The Application of Statistics to the Flight Vehicle Vibration Problem, ASD TR 61-123, Wright-Patterson AFB, Ohio, December 1961.

normally derived probabilities.

Table 14 has been compiled as an example of the use of the binomial distribution for calculating the probability of exceeding 0.3g vertically at the right rear of the cargo deck in the 10 Hz frequency band. A flight profile of 920 seconds taxiing, 5000 seconds climb, and so forth, was used as shown in column 6, including one landing. The probabilities for taxi, climb, cruise, turbulence, and descent are calculated as before, but the binomial distribution is used for the landing. From Table 9, there were 3 landings during which 0.3g was exceeded in the 10 Hz band. The probability of exceeding 0.3g during a single landing is thus

$$P = 1 - (P_a)^n = 1 - (\frac{17}{20})^1 = 0.15$$

In this example, the overall probability of exceeding 0.3g is strongly dependent on the landing impact, and the overall probability is also 0.15.

IV. CONCLUSIONS

The low-frequency vibration environment of the C-5A cargo deck is not severe compared to smaller transport aircraft. The most severe vibration is the response of the aft end of the cargo deck due to the landing impact. A recommended sinusoidal vibration envelope has been developed as shown in Figure 7, to be compatible with the test methods of MIL STD 810B. For fragile payloads which cannot meet these requirements the results may be used in designing isolation mounts for the required attenuation over the frequency range of 0.4 to 30 Hz. The statistical methods described may also be used to determine the probability of exceeding a critical acceleration level at a particular frequency, in order to quantify the risk of damaging very expensive cargo. These data provide an estimate of the C-5A vibration environment, with a degree of confidence based on the sample size used. To increase the confidence that this accurately represents the actual environment, however, would require a much larger sample of data and a statistical correlation with the specific environmental parameters such as gust velocity, landing sink speeds, and cargo loading.

V. REFERENCES

1. Magrath, H.A., Rogers, O.R., and Grimes, C.K.: Shock and Vibration Handbook (C.M. Harris and C.E. Crede, Eds.), Vol. 3, Chap. 47, McGraw-Hill, New York, 1961.

2. Ostrem, F.E., "A Survey of the Transportation Shock and Vibration Input to Cargo," Shock and Vibration Bulletin No. 42, Part 1, pp. 137-151, January 1972.

3. Pearson, Jerome, Thaller, Roger E., and Bayer, Anthony R. Jr., C-5A Cargo Deck Flight Vibration Measurements, AFFDL/FYS/73-12, Wright-Patterson AFB, Ohio, November 1973.

4. Anon., C-5A Acceleration Data Reduction and Analysis Program Semi-Annual Report. Lockheed-Georgia Company Report LG1US613/M-2-3, 31 May 1974.

5. Magnuson, C.F., "Dynamic Environment Study of Turbojet Cargo Aircraft," Proceedings of the Institute of Environmental Sciences 18th Annual Technical Meeting, pp. 420-425, May 1972.

6. Foley, J.T., Gens, M.B., and Magnuson, C.F.: "Current Predictive Models of the Dynamic Environment of Transportation." Proceedings of the Institute of the Environmental Sciences 18th Annual Technical Meeting, May 1972, pp. 162-171.

7. Gray, C.L., "First Occurrence Probabilities for Extreme Random Vibration Amplitudes," Shock and Vibration Bulletin No. 35, Part 1V, pp. 99-104, 1966.

8. Press, Harry, and Steiner, Roy, An Approach to the Problem of Estimating Severe and Repeated Gust Loads for Missile Operations, NACA TN4332, 1958.

9. Bendat, Julius S., Probability Functions for Random Responses: Prediction of Peaks, Fatigue Damage, and Catastrophic Failures, NASA CR-234, National Aeronautics and Space Administration, Washington, D.C., April 1964.

10. Bendat, J.S., Enochson, L.D., Klein, G.H., and Pierson, A.G., The Application of Statistics to the Flight Vehicle Vibration Problem, ASD TR 61-123, Wright-Patterson AFB, Ohio, December 1961.

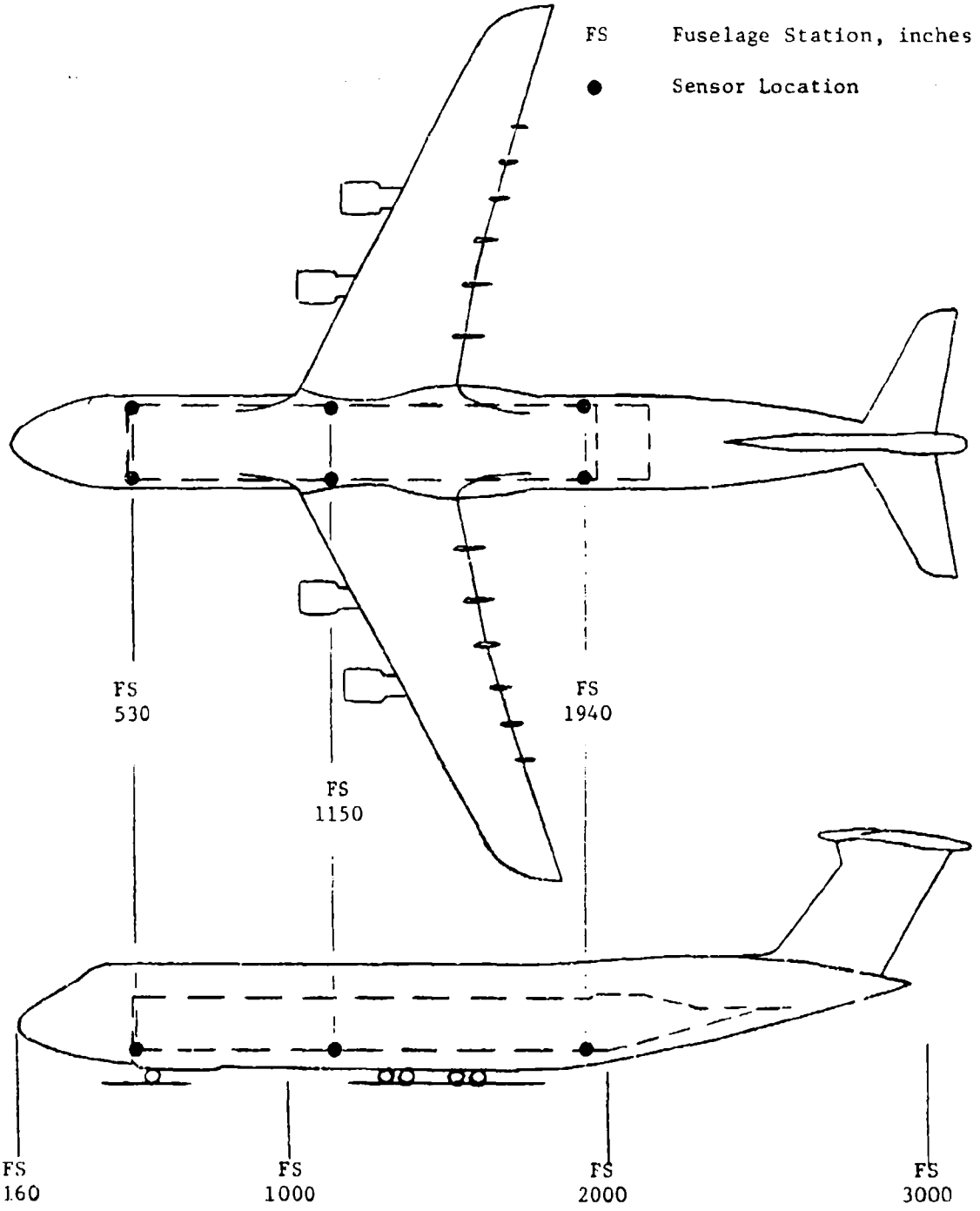

Figure 1. C-5A Aircraft and Transducer Locations.

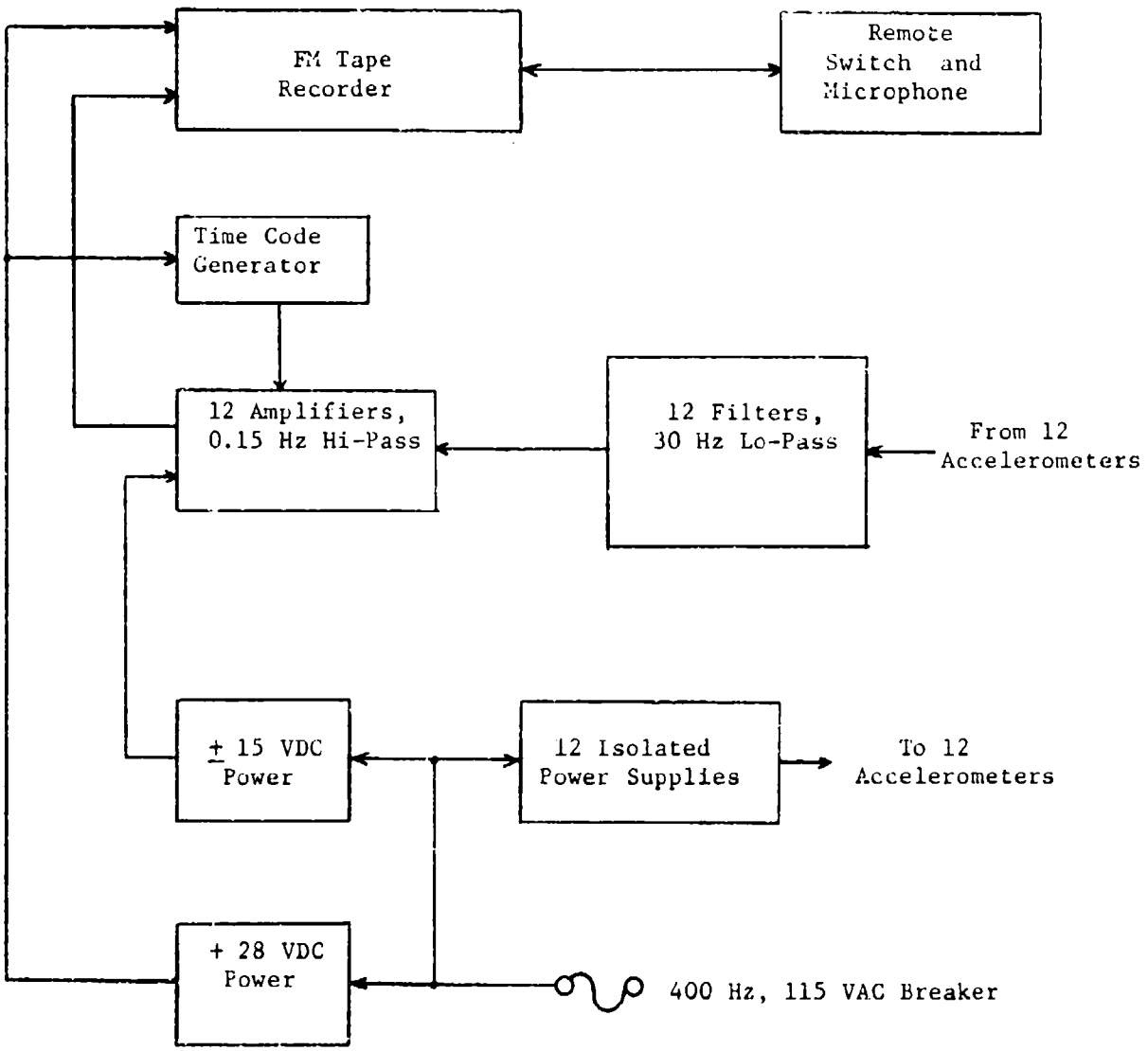

Figure 2. Block Diagram of Instrumentation System.

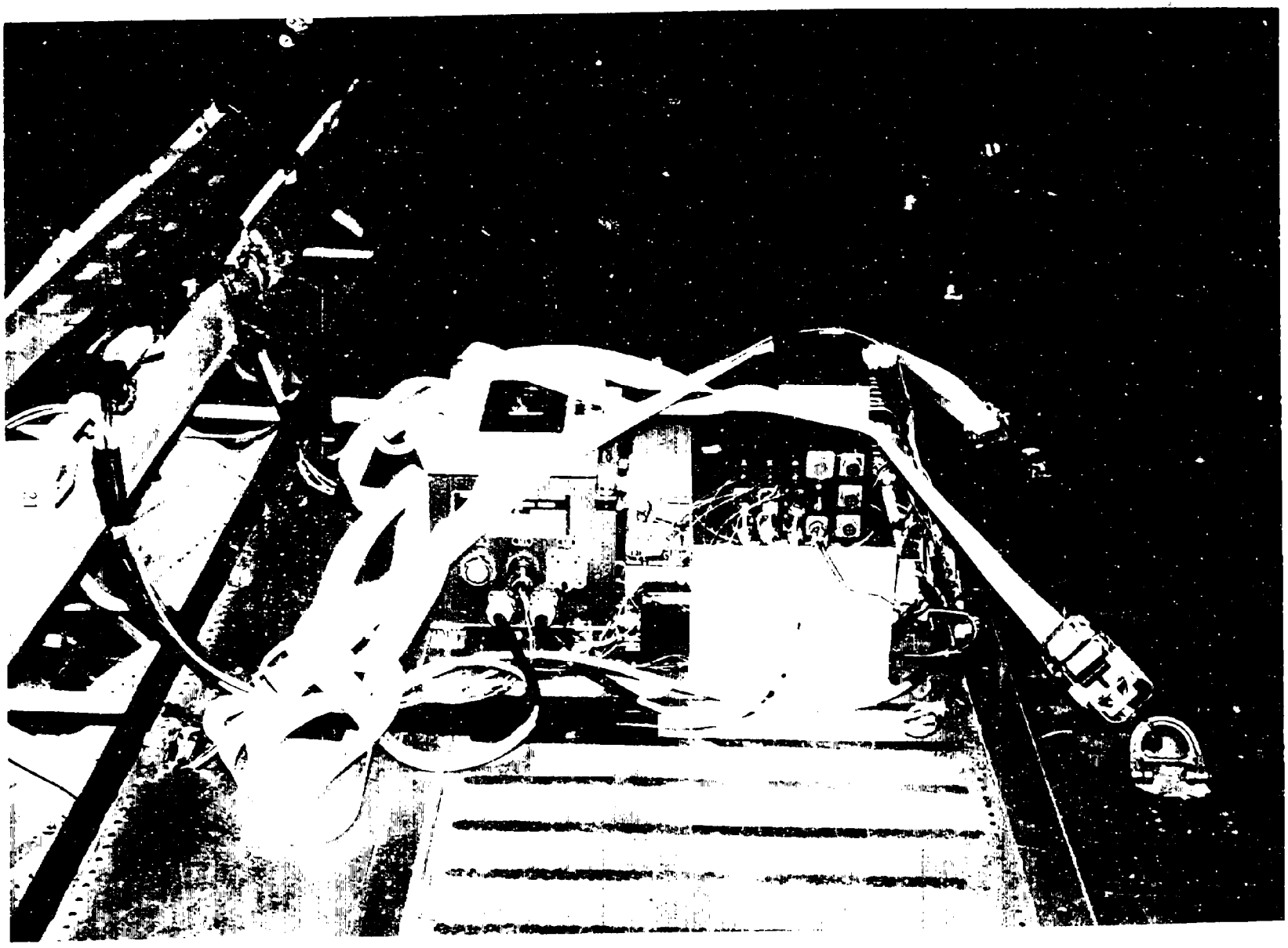

Figur 3. Instrumentation Package In Aircraft.

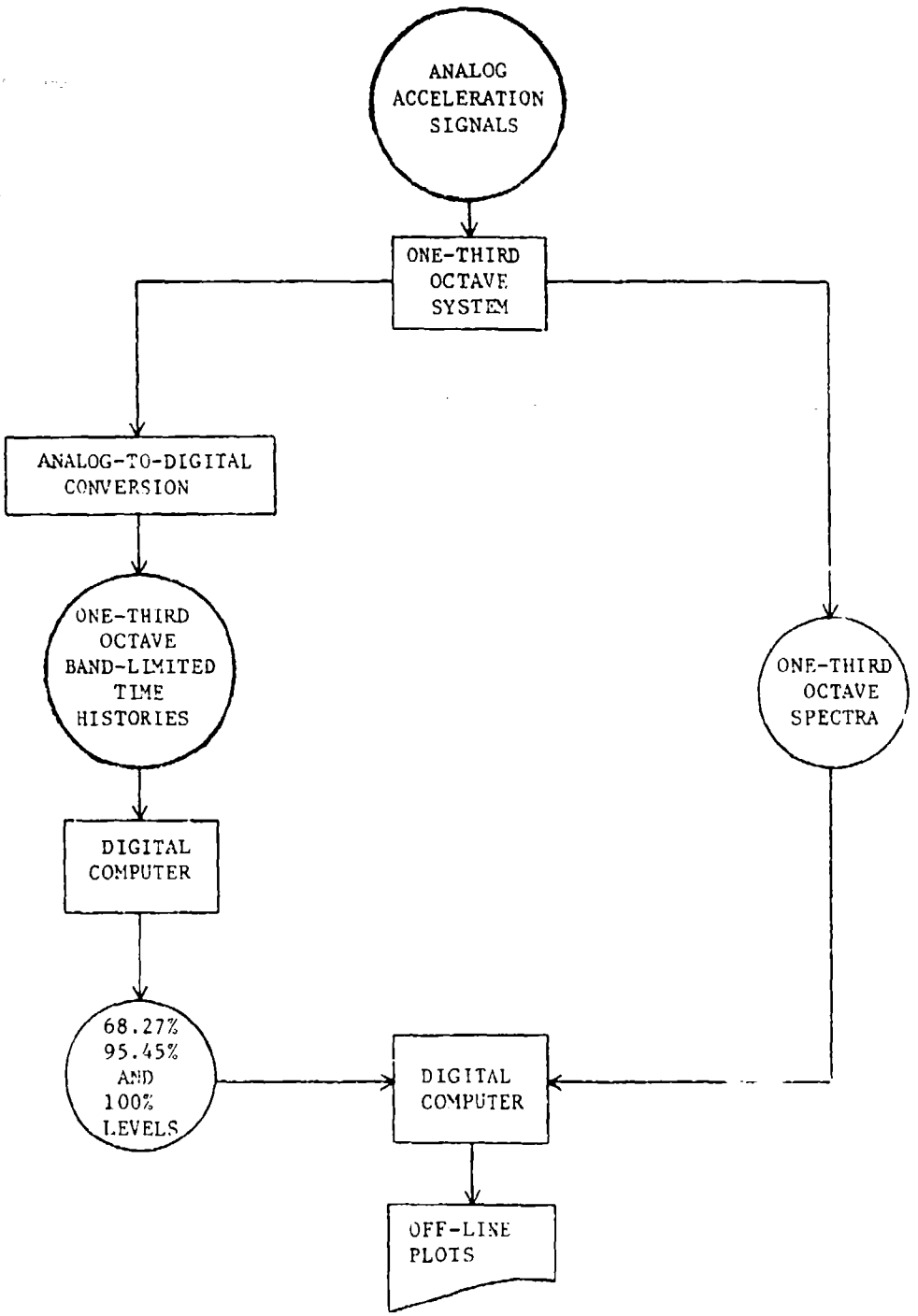

Figure 4. Flow Chart of Vibration Analyses.

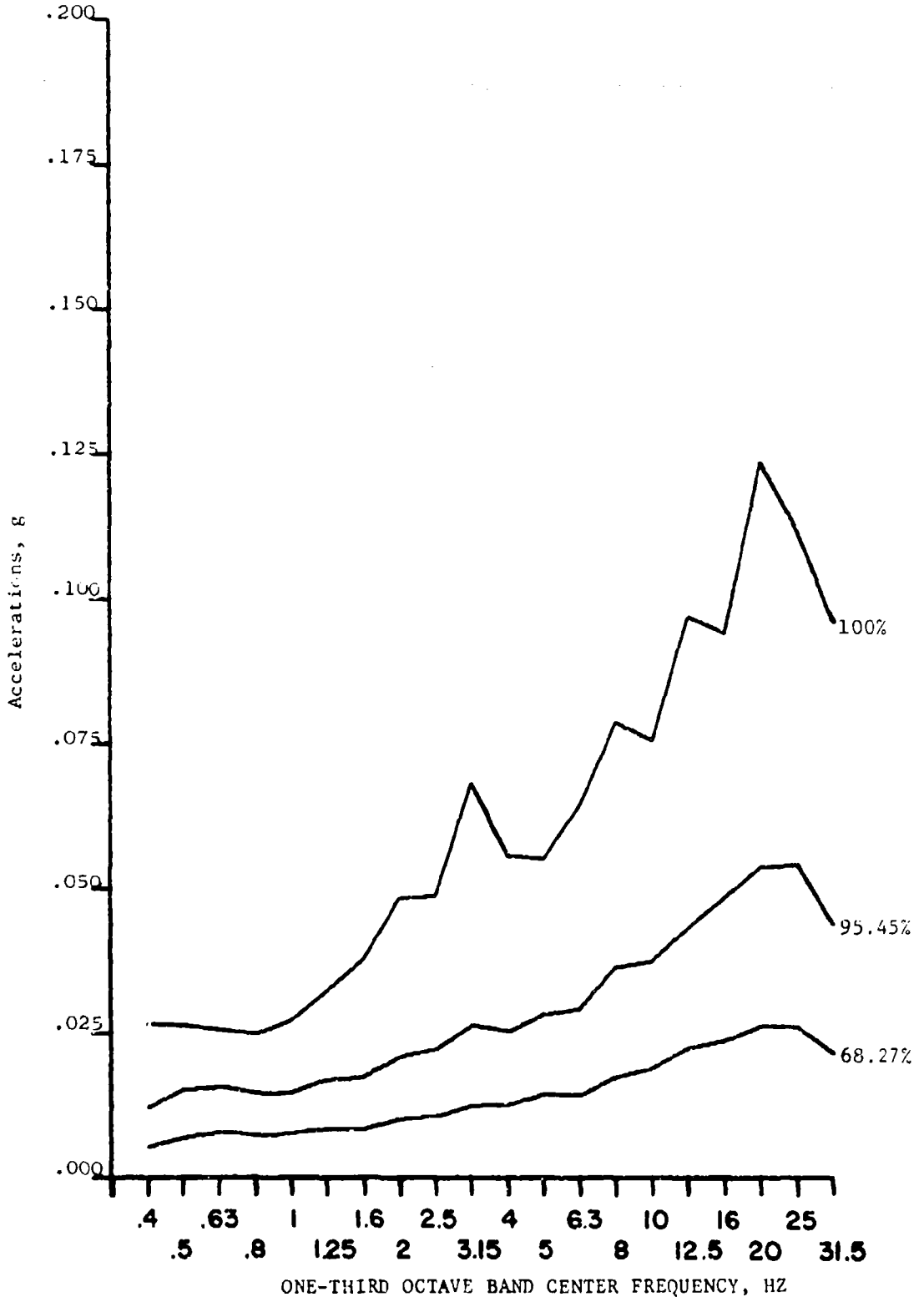

Figure 5. Results of Vibration Analysis on Gaussian Data.

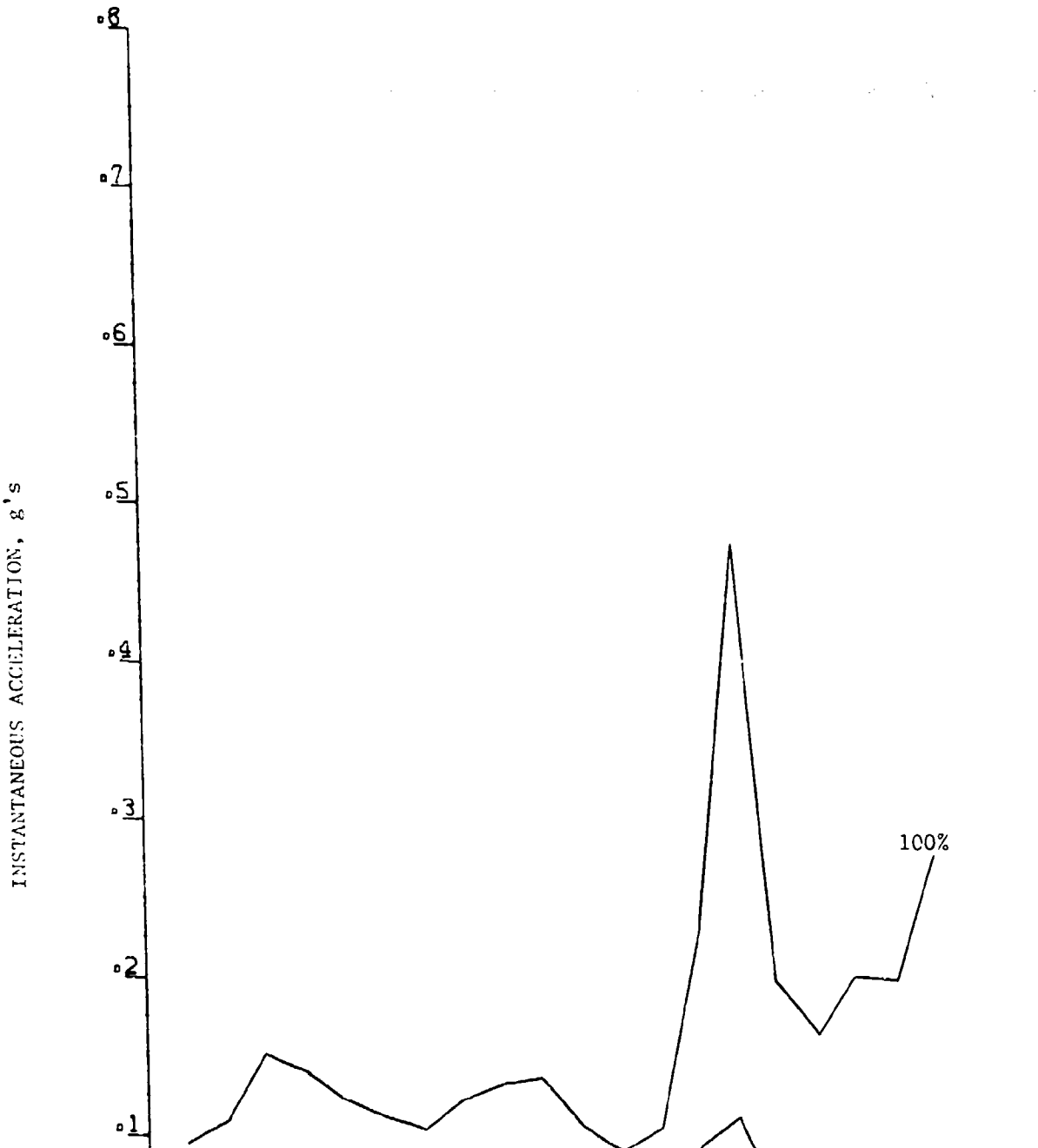

Figure 6. Maximum Accelerations for Landing, Taxiing, and Terrain-Following.

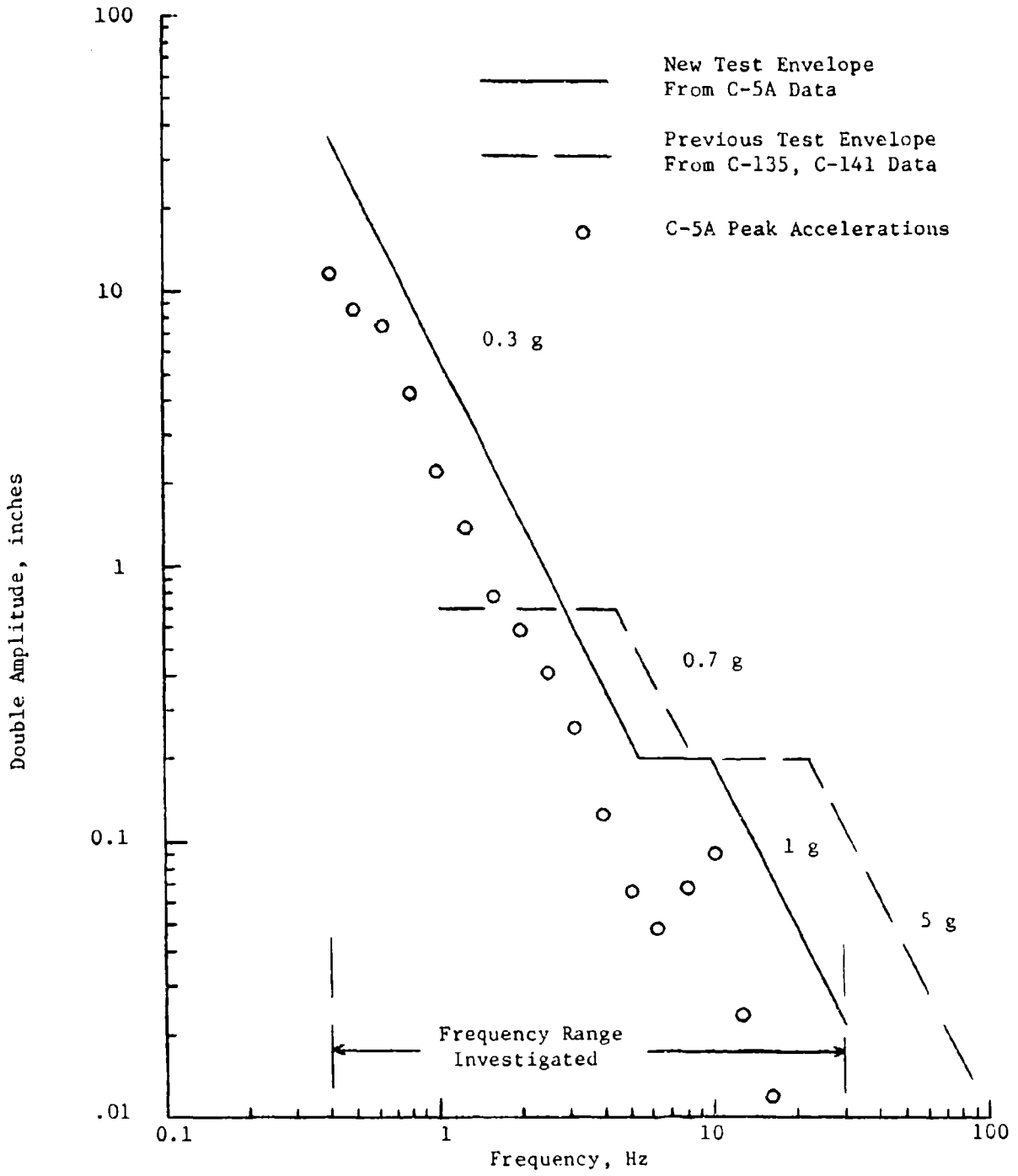

Figure 7. Recommended Sinusoidal Vibration Test Envelope.

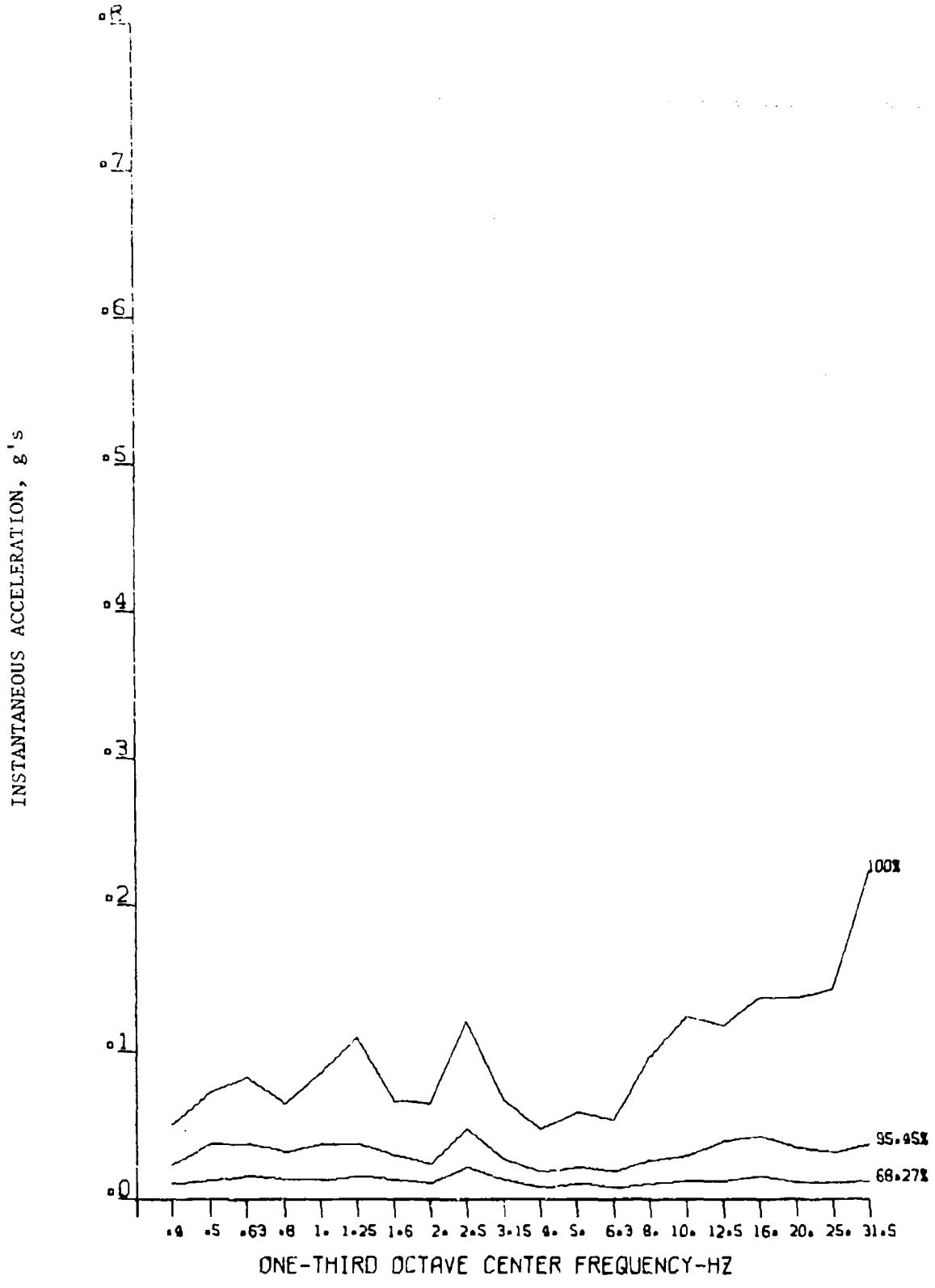

Figure 8. Vertical Taxiing Acceleration, Right Front Cargo Deck.

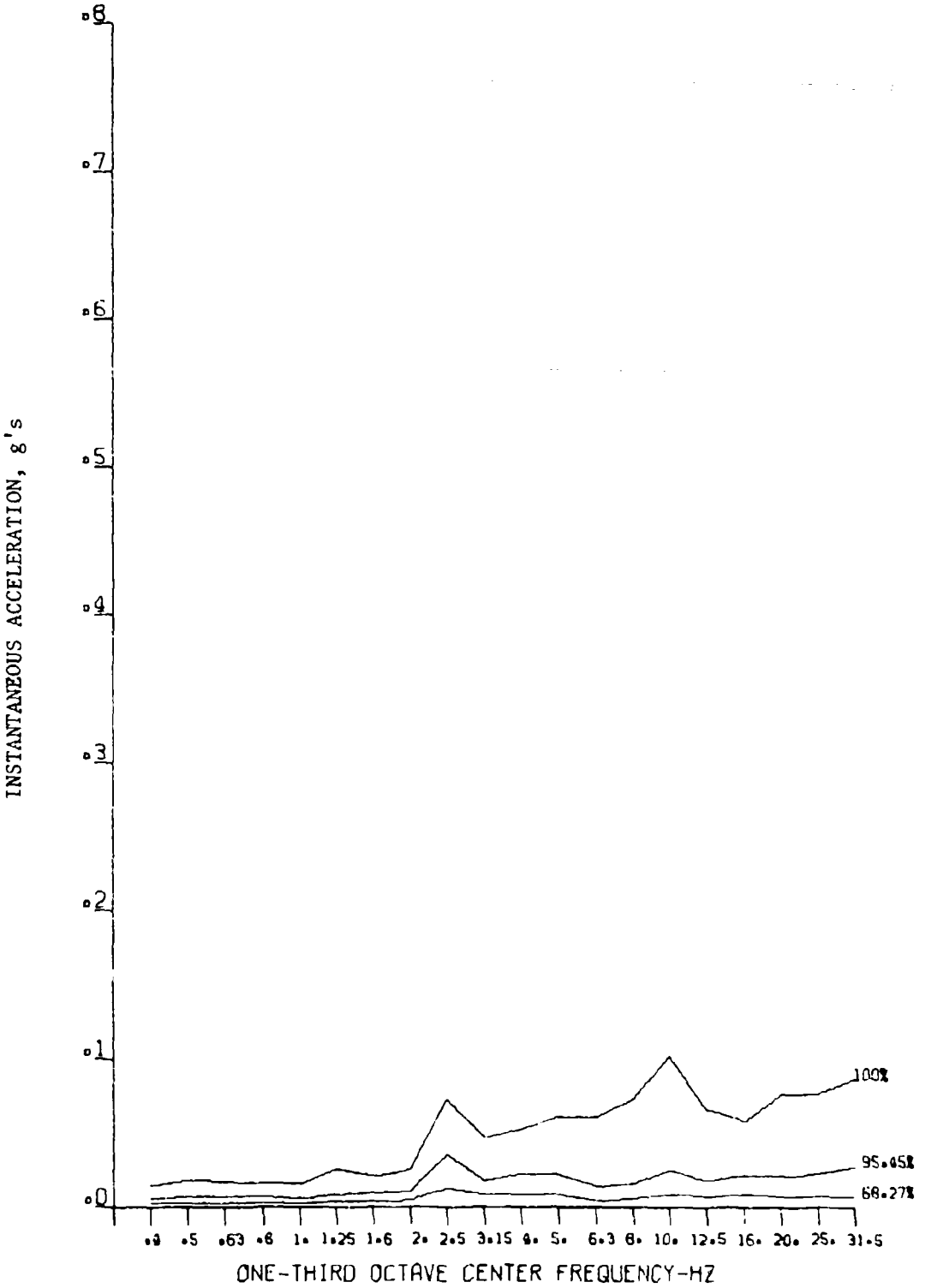

Figure 9. Lateral Taxiing Acceleration, Right Front Cargo Deck.

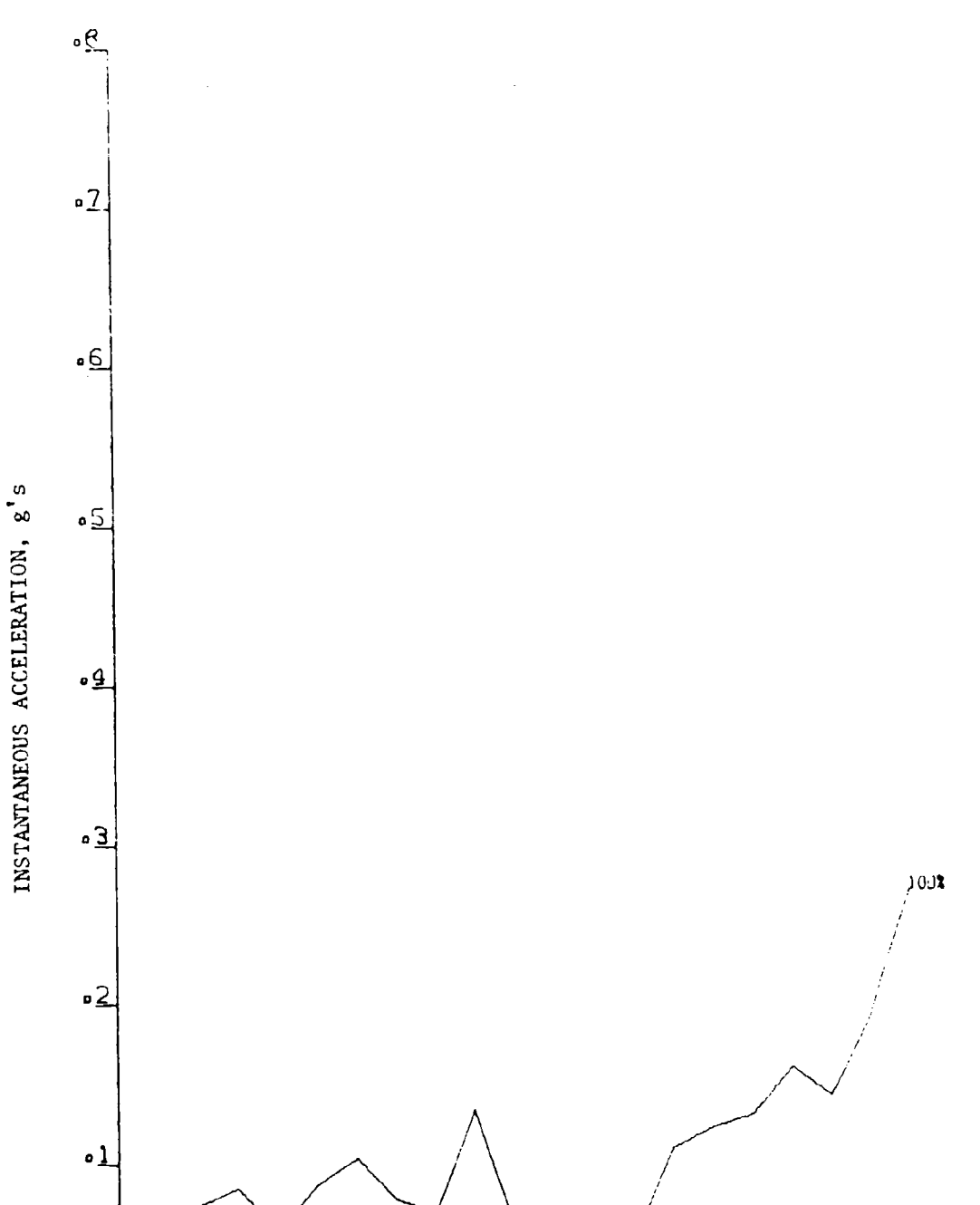

Figure 10. Vertical Taxiing Acceleration, Left Front Cargo Deck.

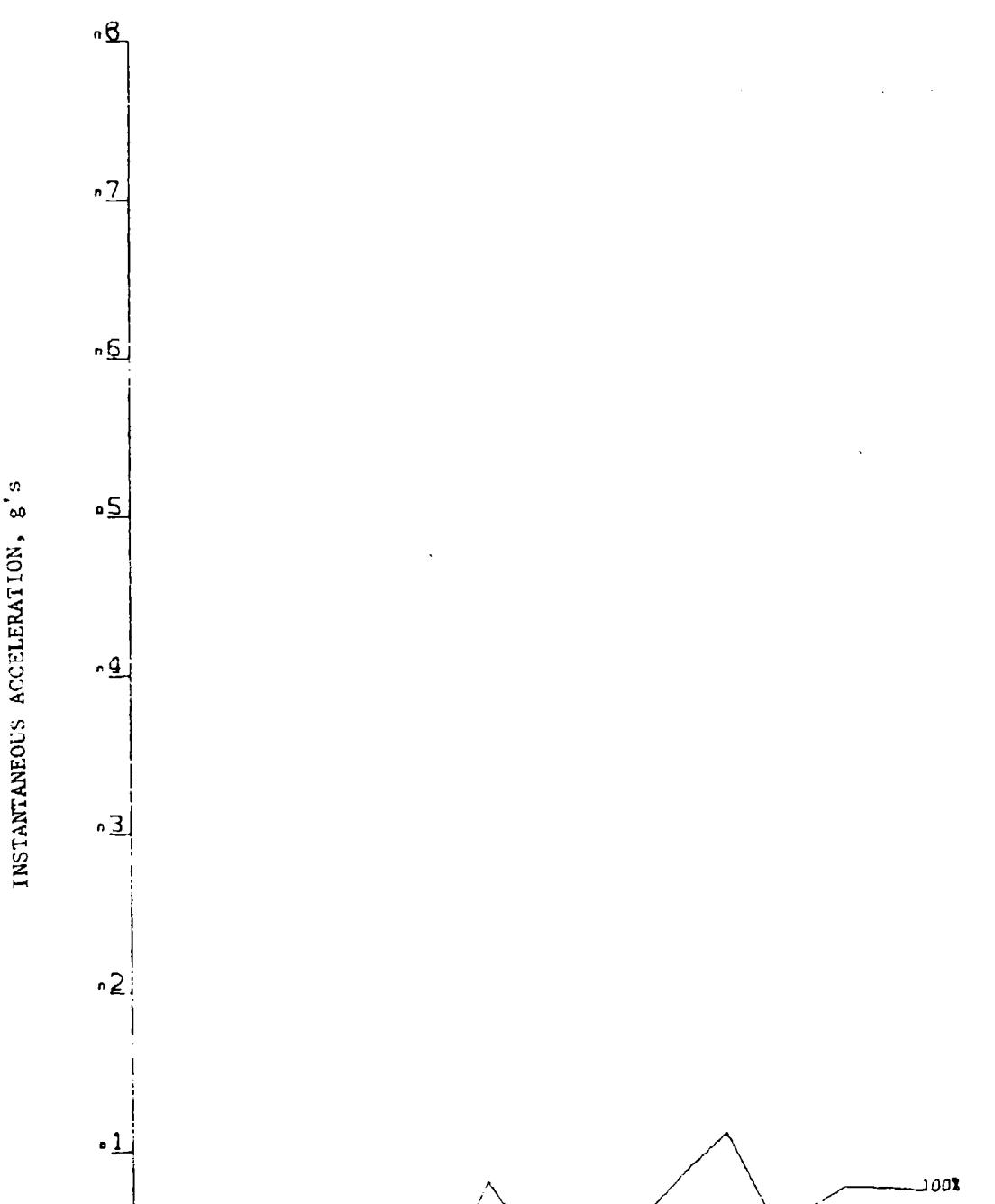

Figure 11. Lateral Taxiing Acceleration, Left Front Cargo Deck.

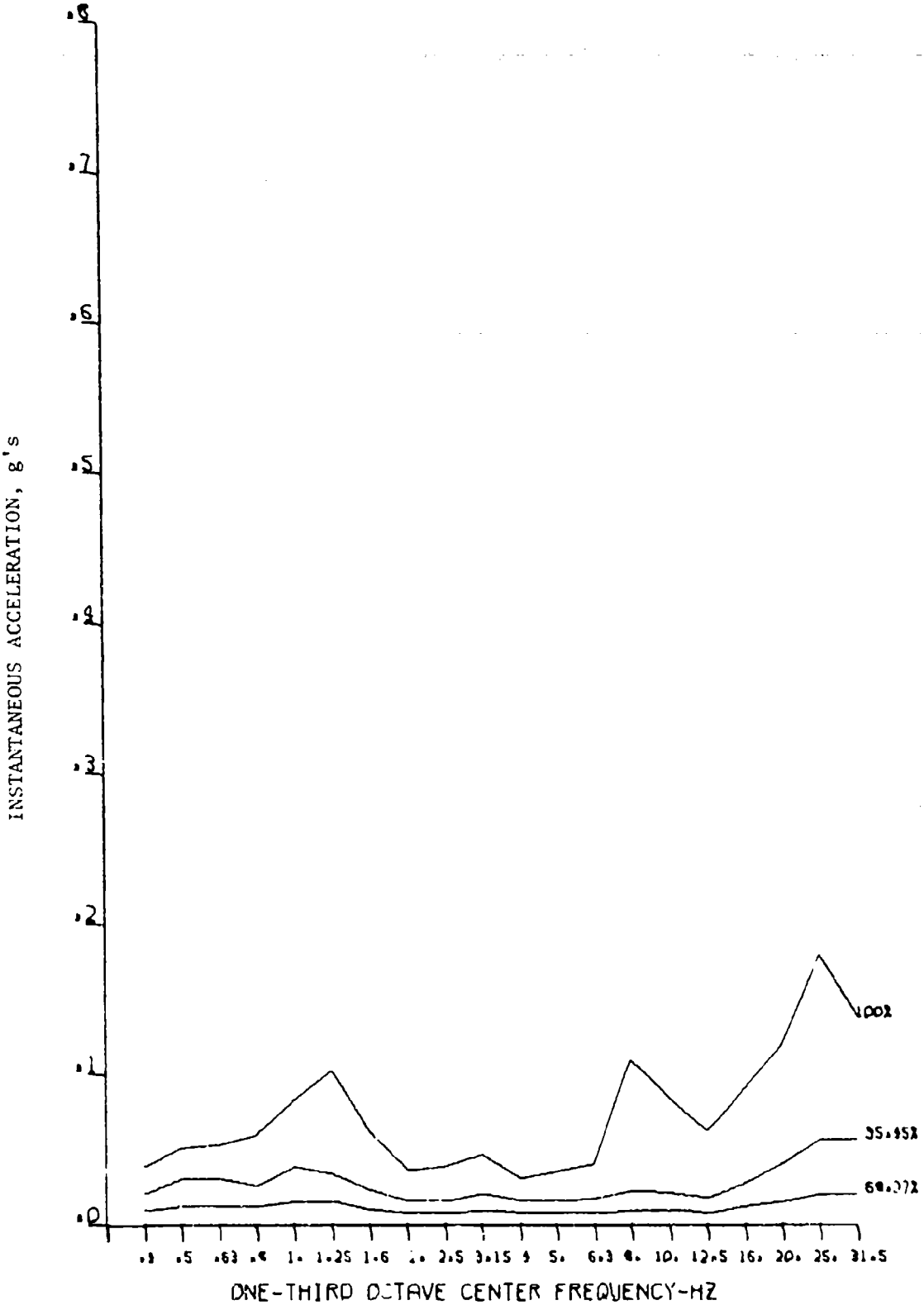

Figure 12. Vertical Taxiing Acceleration, Right Center Cargo Deck.

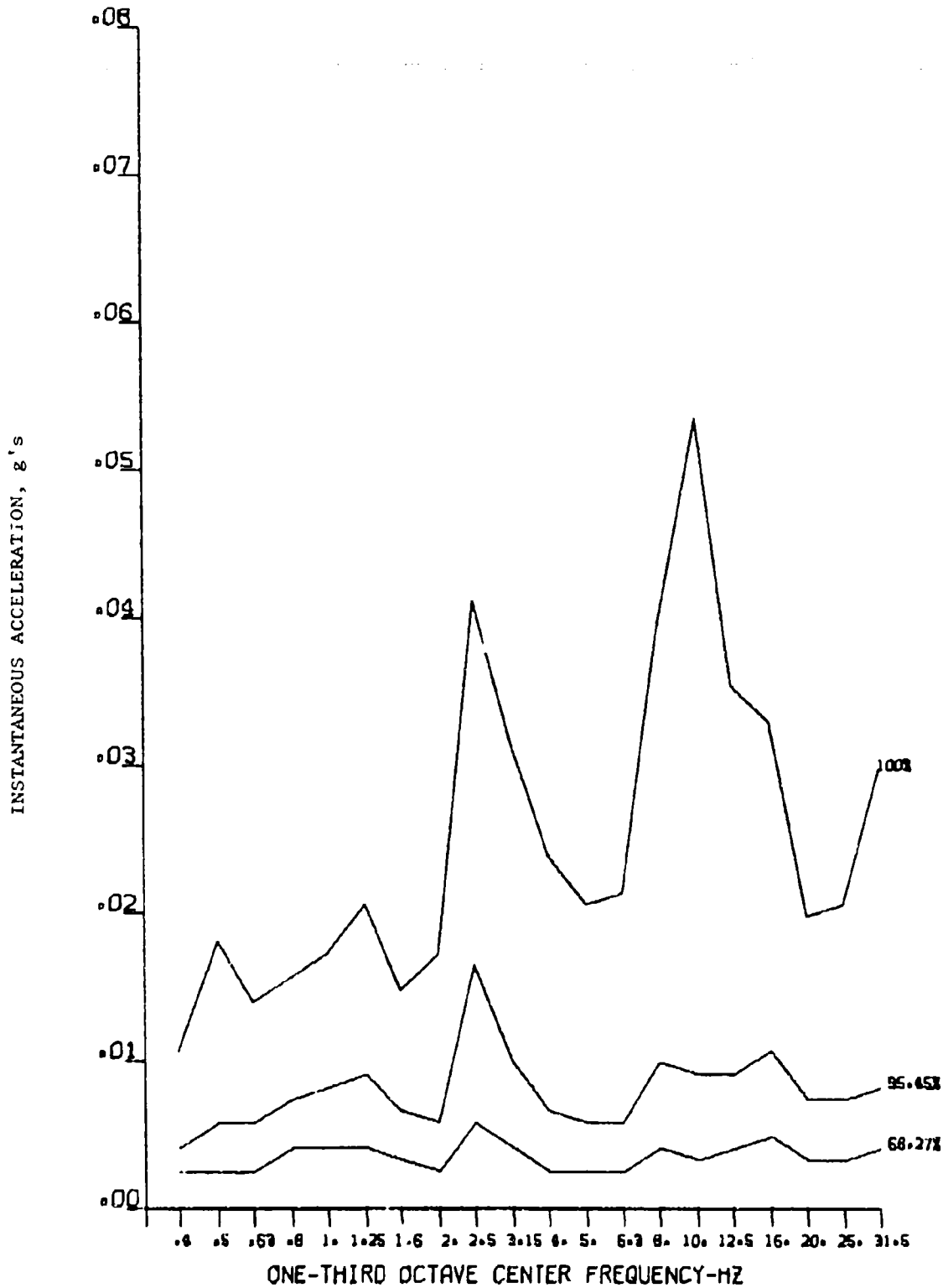

Figure 13. Longitudinal Taxiing Acceleration, Right Center Cargo Deck.

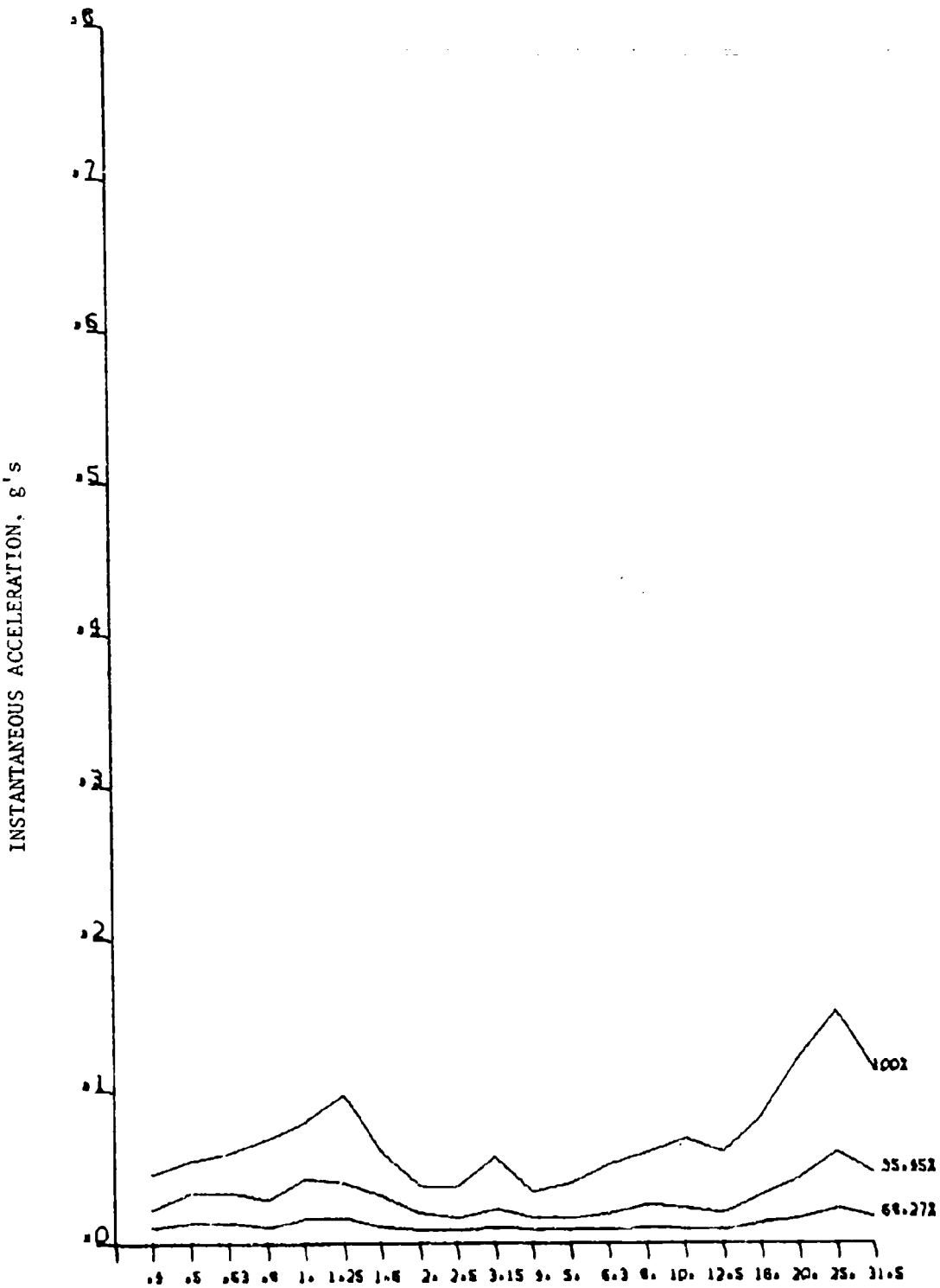

Figure 14. Vertical Taxiing Acceleration, Left Center Cargo Deck.

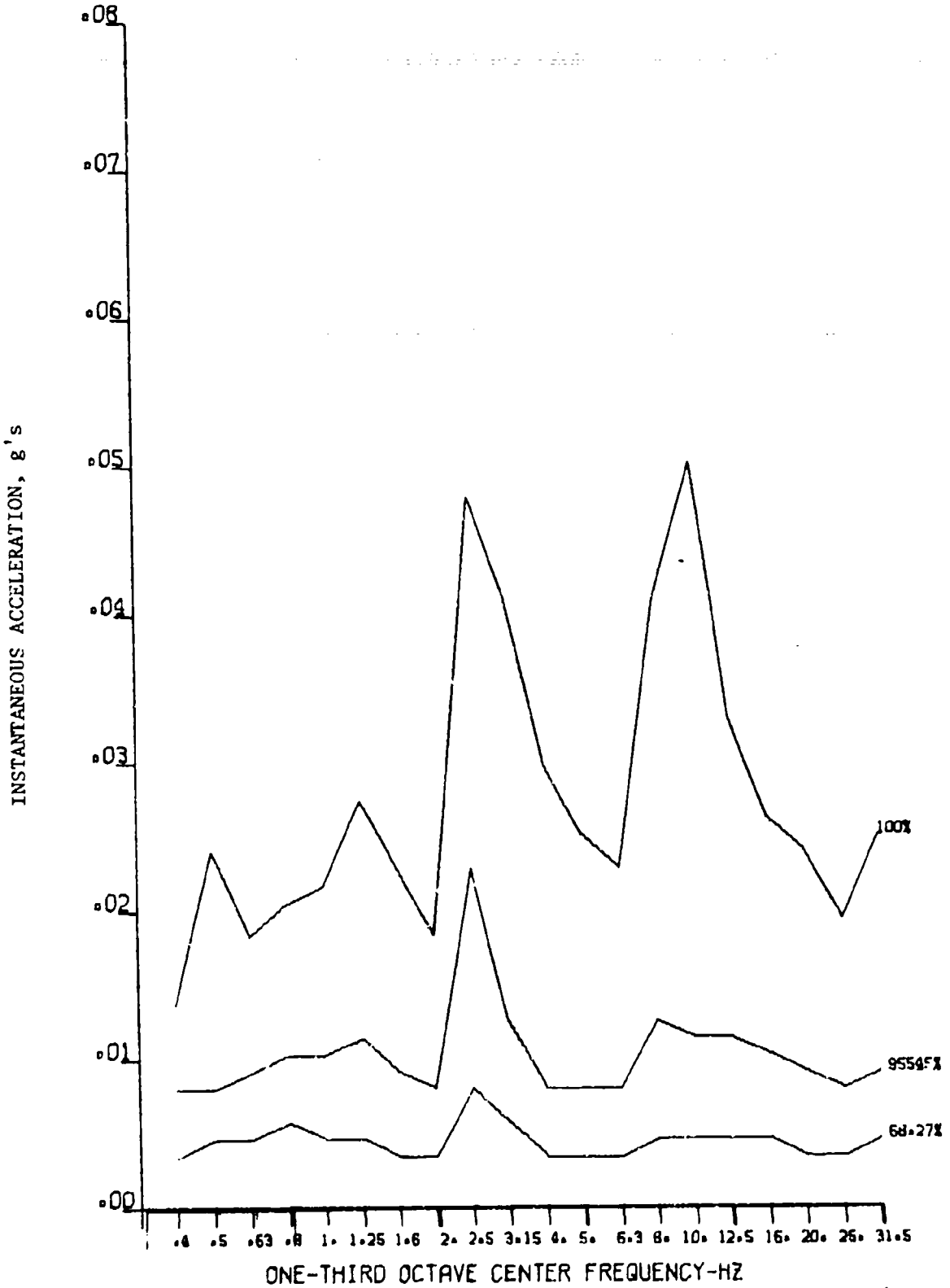

Figure 15. Longitudinal Taxiing Acceleration, Left Center Cargo Deck.

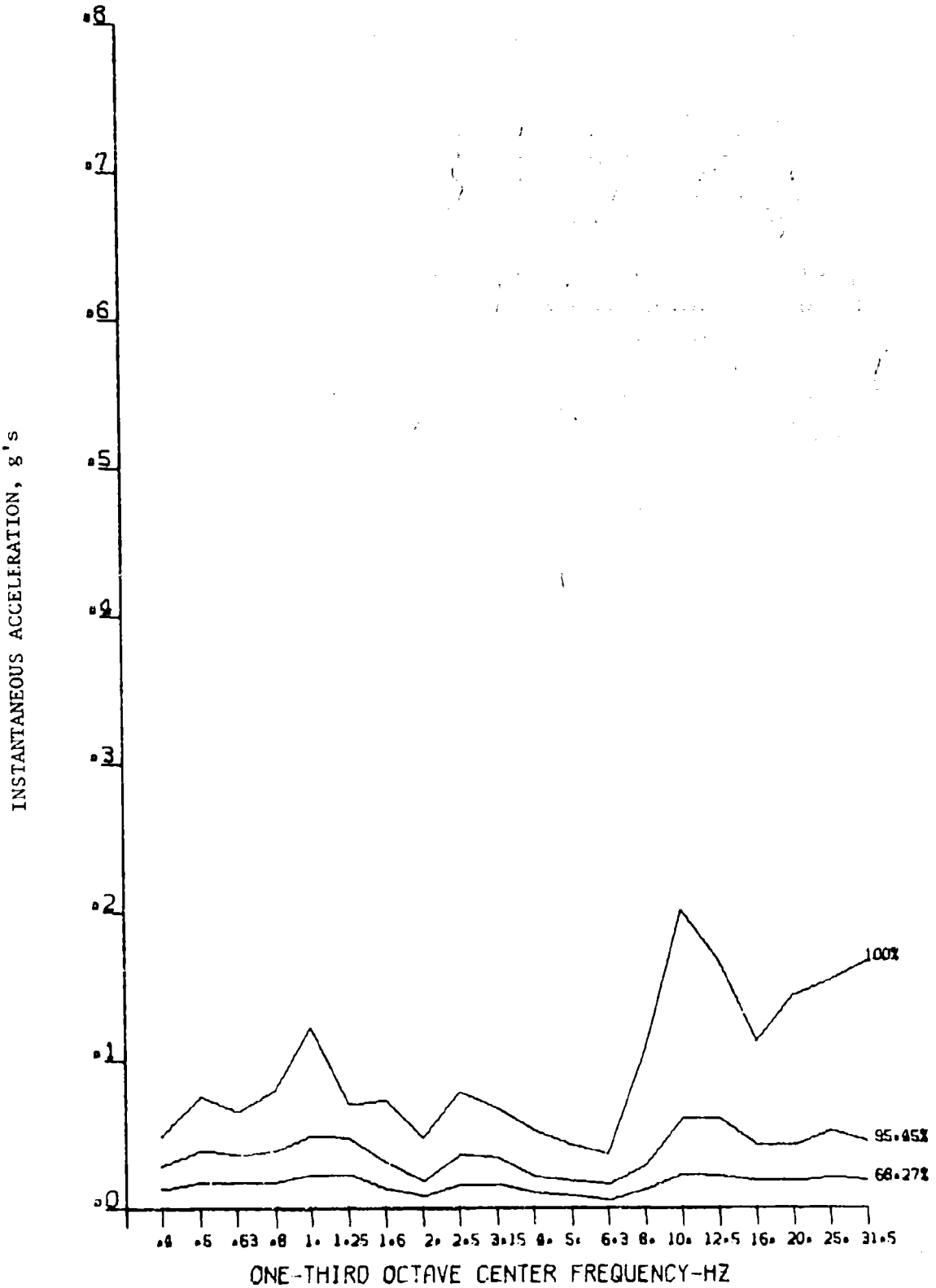

Figure 16. Vertical Taxiing Acceleration, Right Rear Cargo Deck.

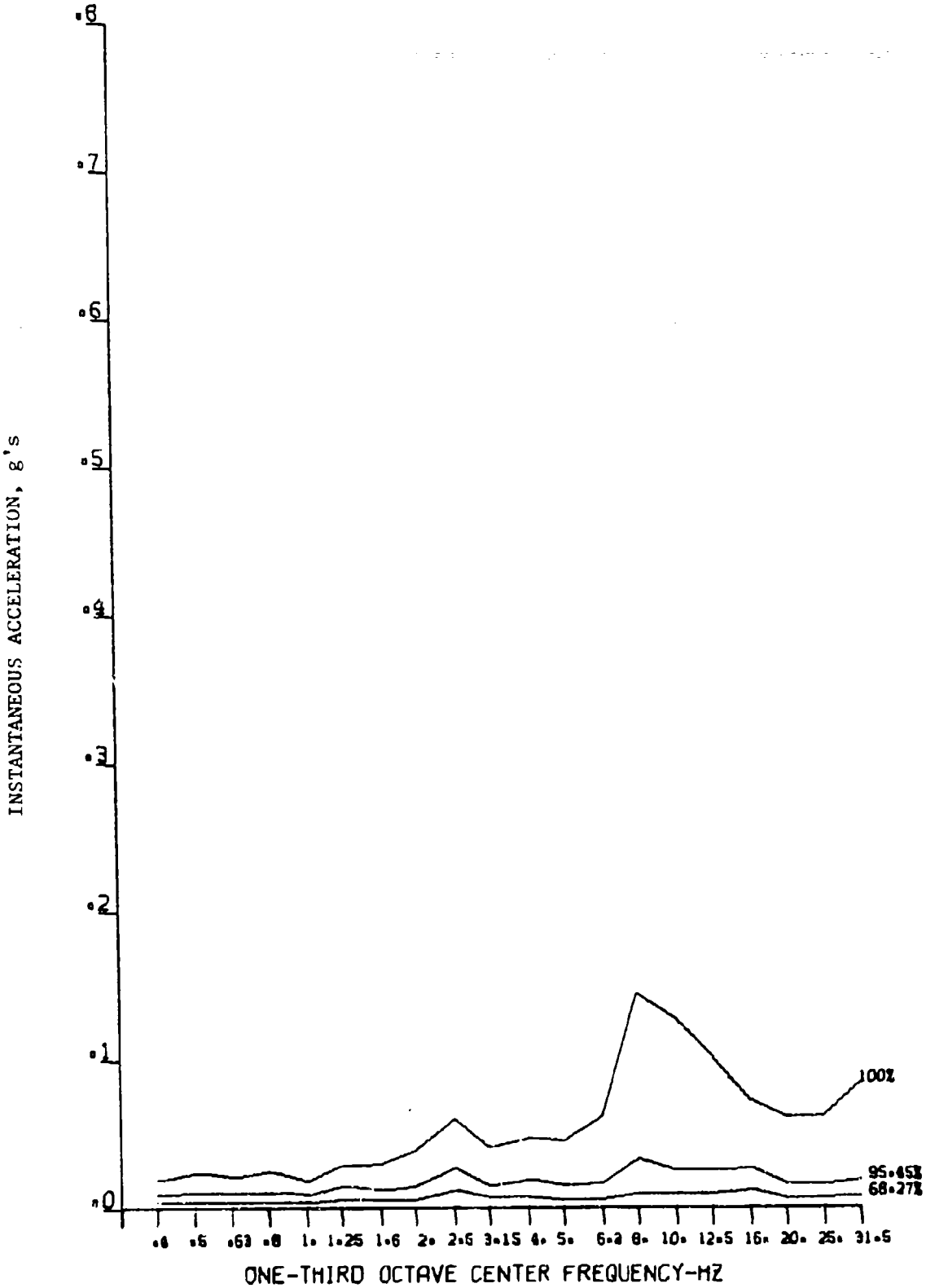

Figure 17. Lateral Taxiing Acceleration, Right Rear Cargo Deck.

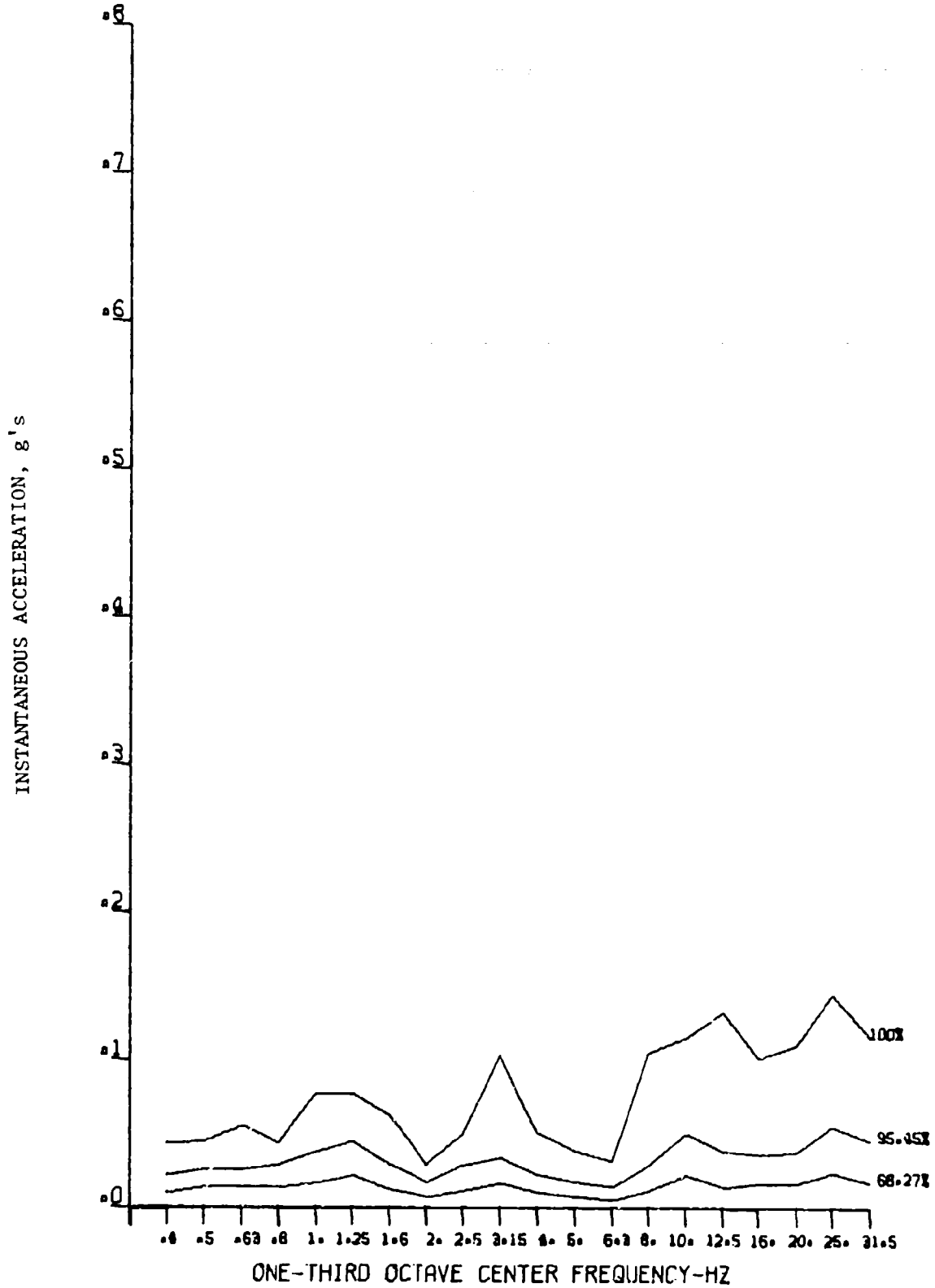

Figure 18. Vertical Taxiing Acceleration, Left Rear Cargo Deck.

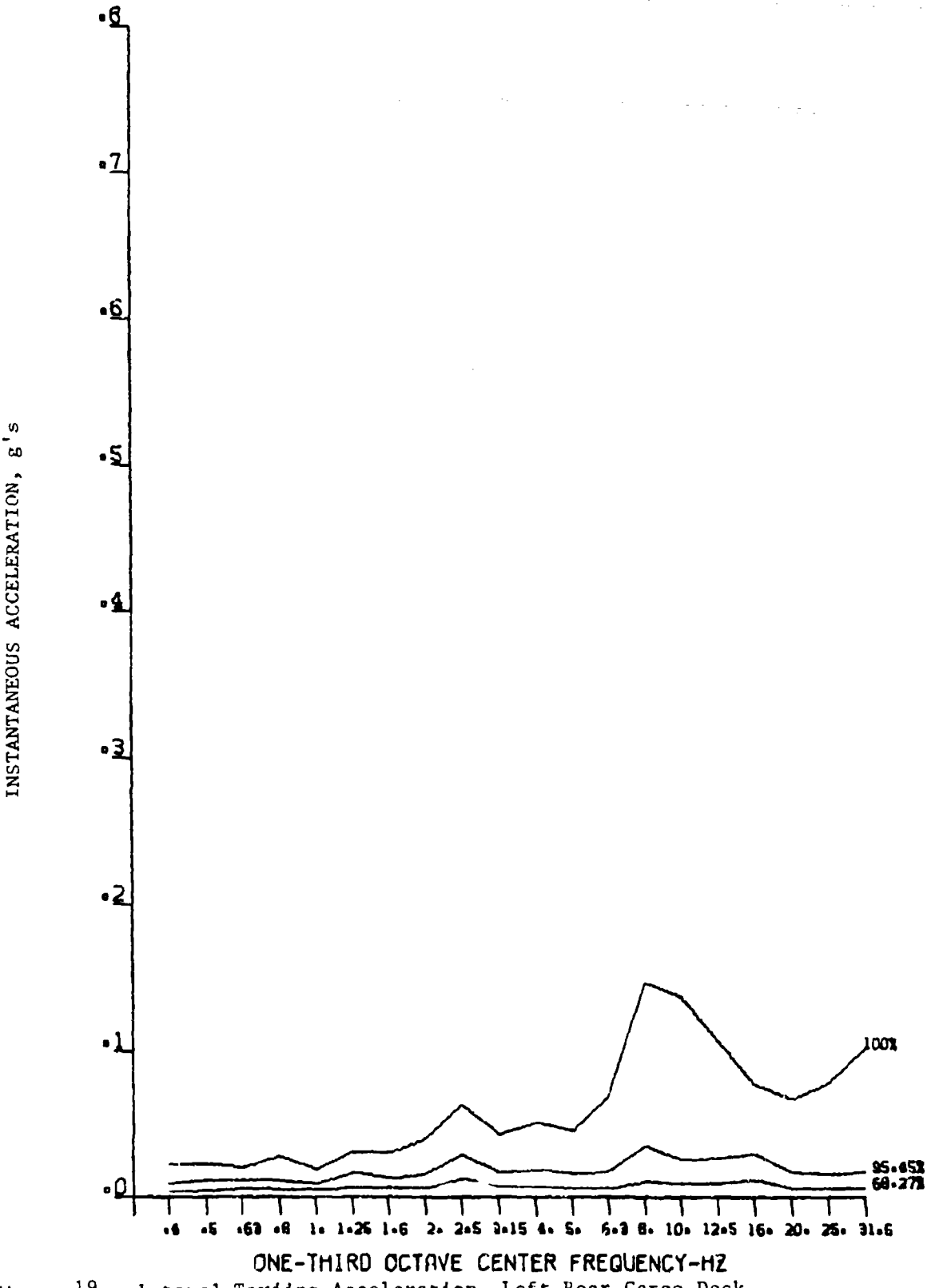

Figure 19. Lateral Taxiing Acceleration, Left Rear Cargo Deck.

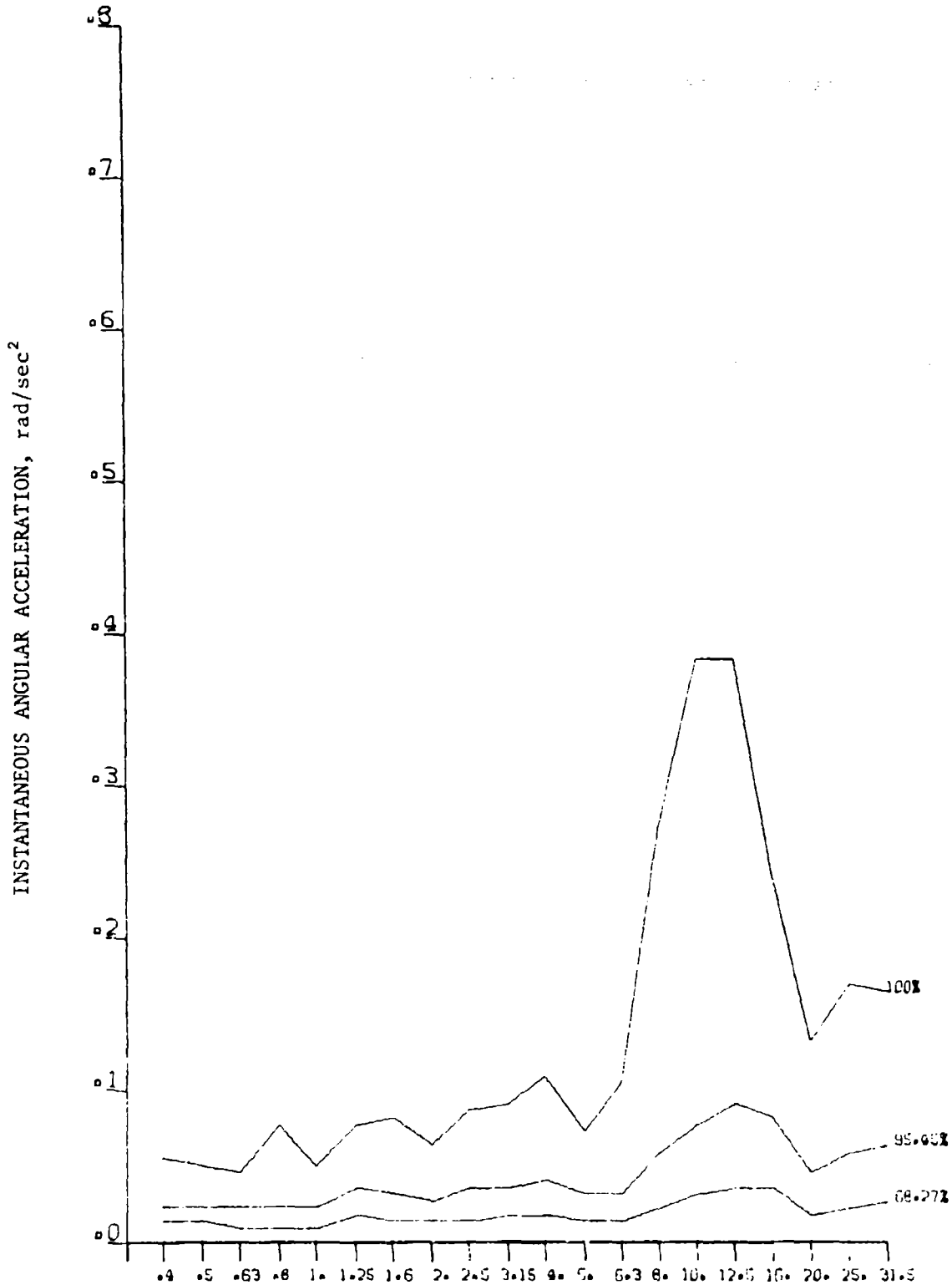

Figure 20. Roll Angular Acceleration During Taxiing.

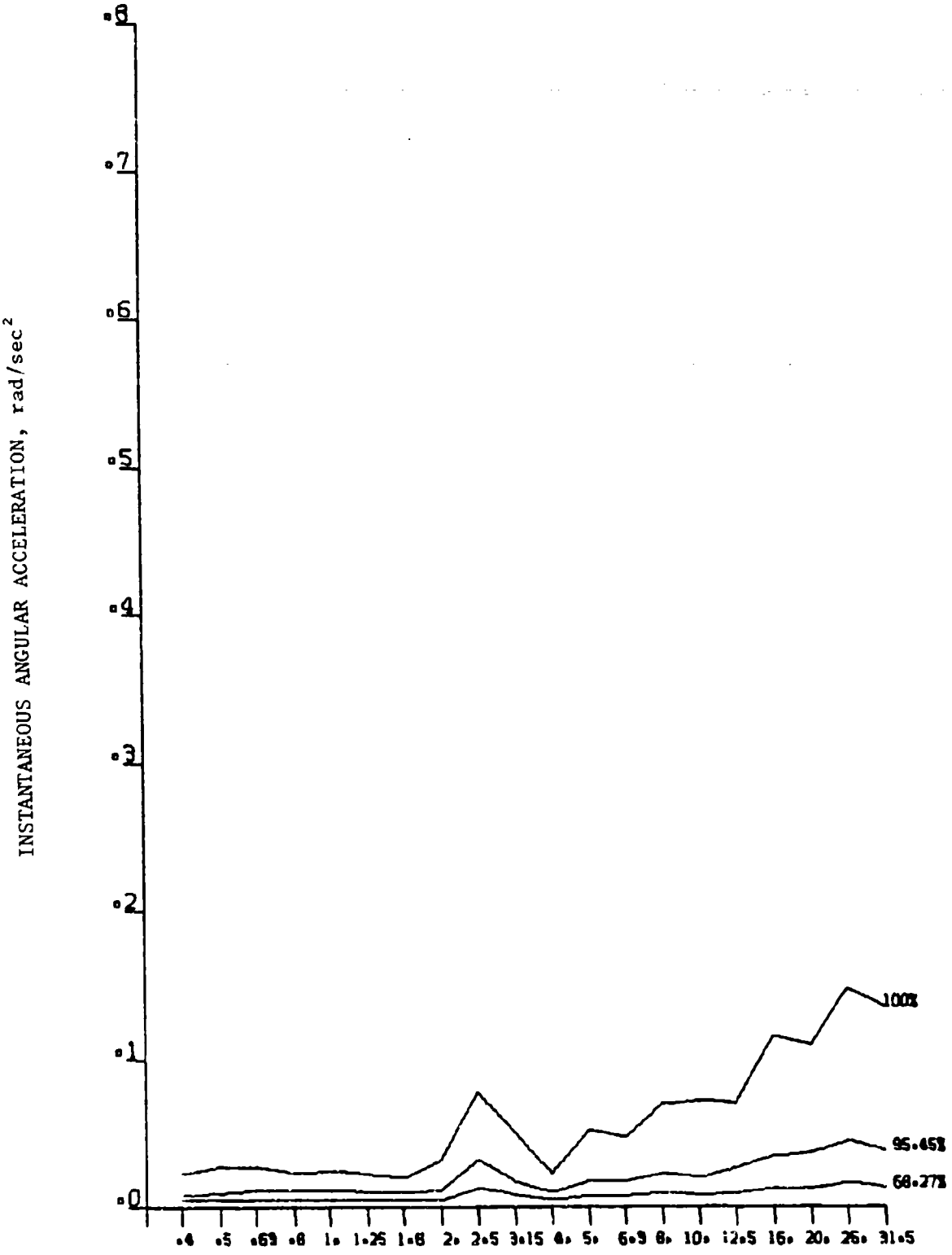

Figure 21. Pitch Angular Acceleration During Taxiing.

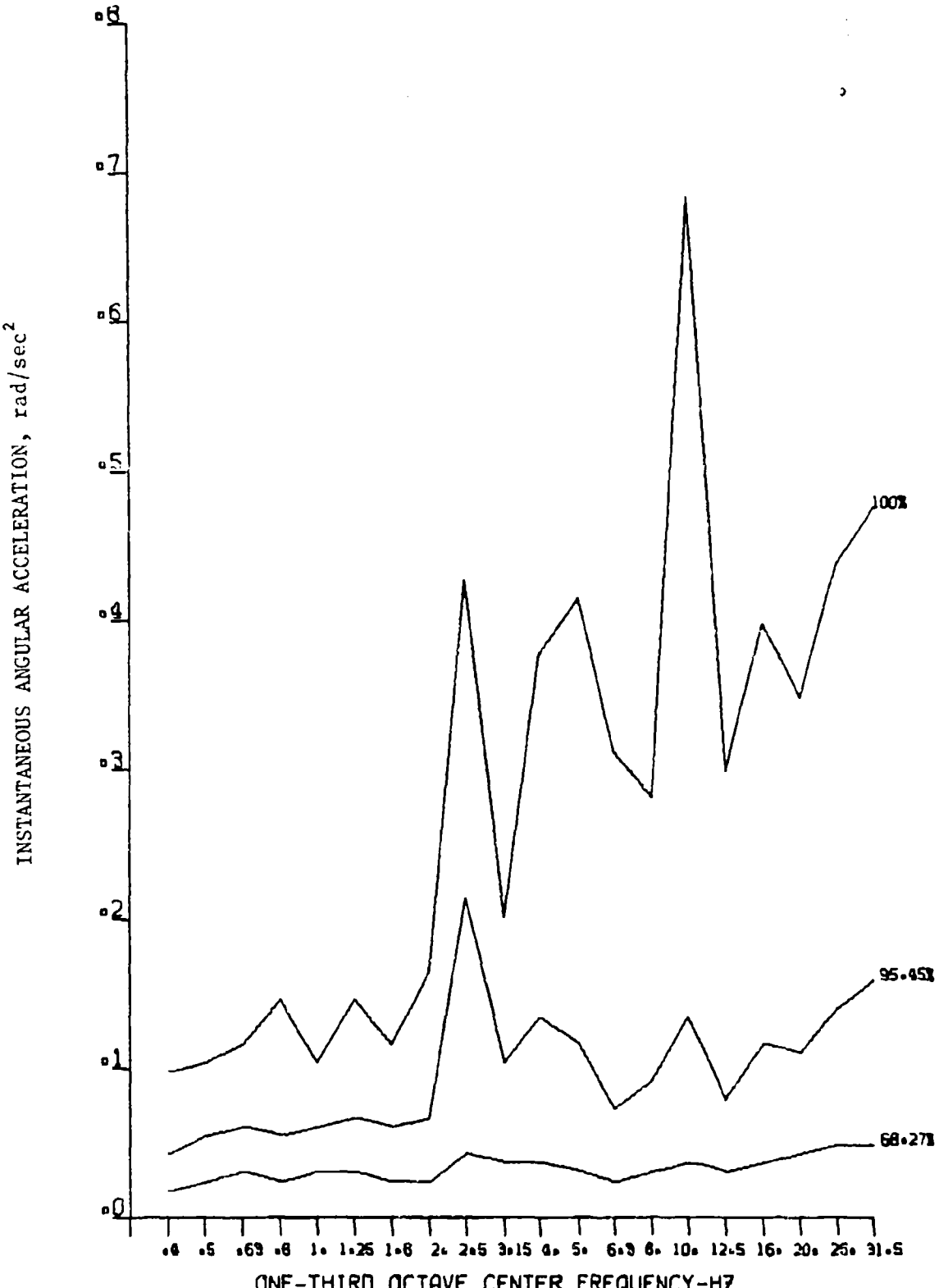

Figure 22. Yaw Angular Acceleration During Taxiing.

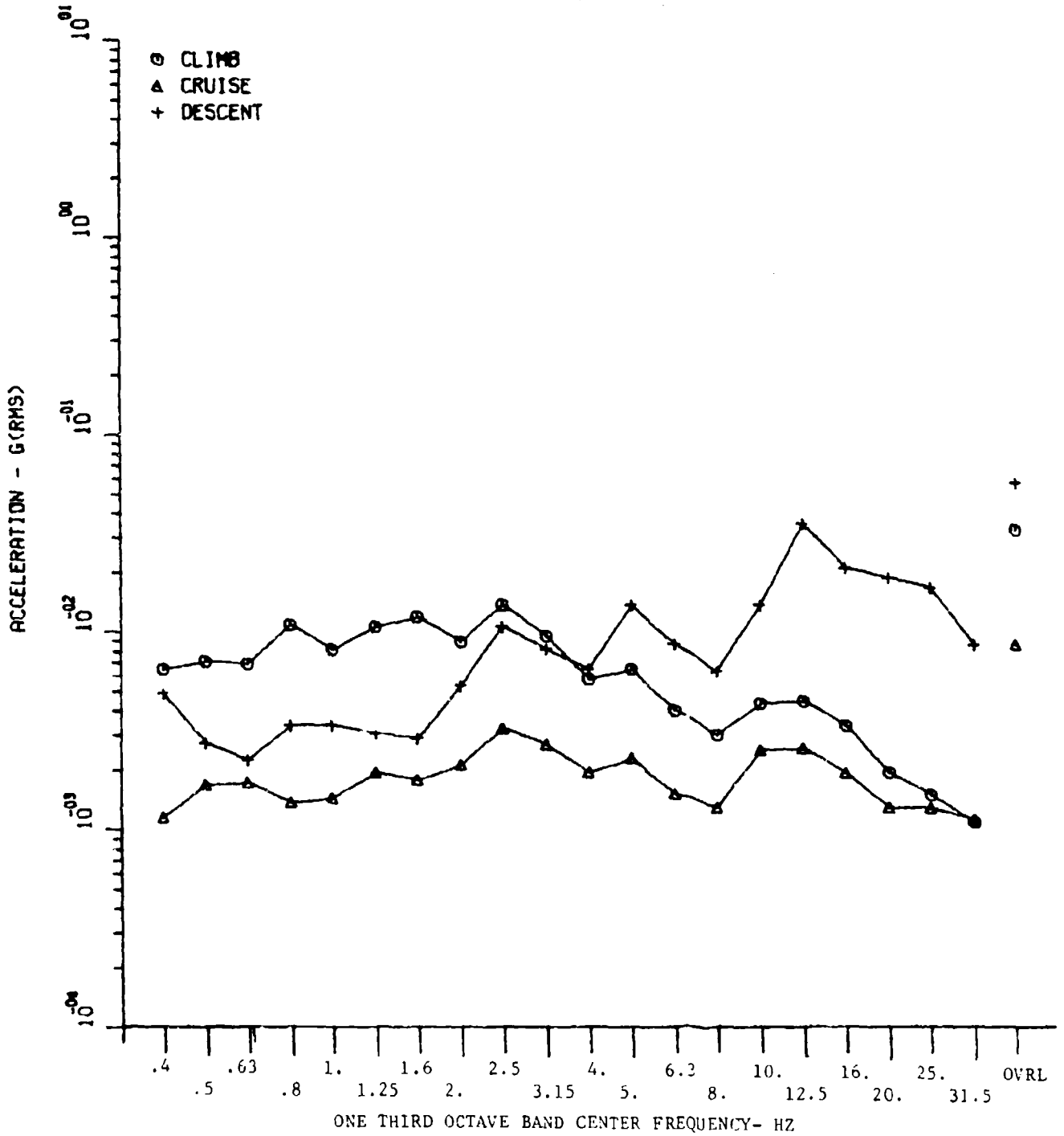

Figure 23a. Cruise, Climb, and Descent Vertical Acceleration, Right Front Cargo Deck - 0.4 to 31.5 Hz.

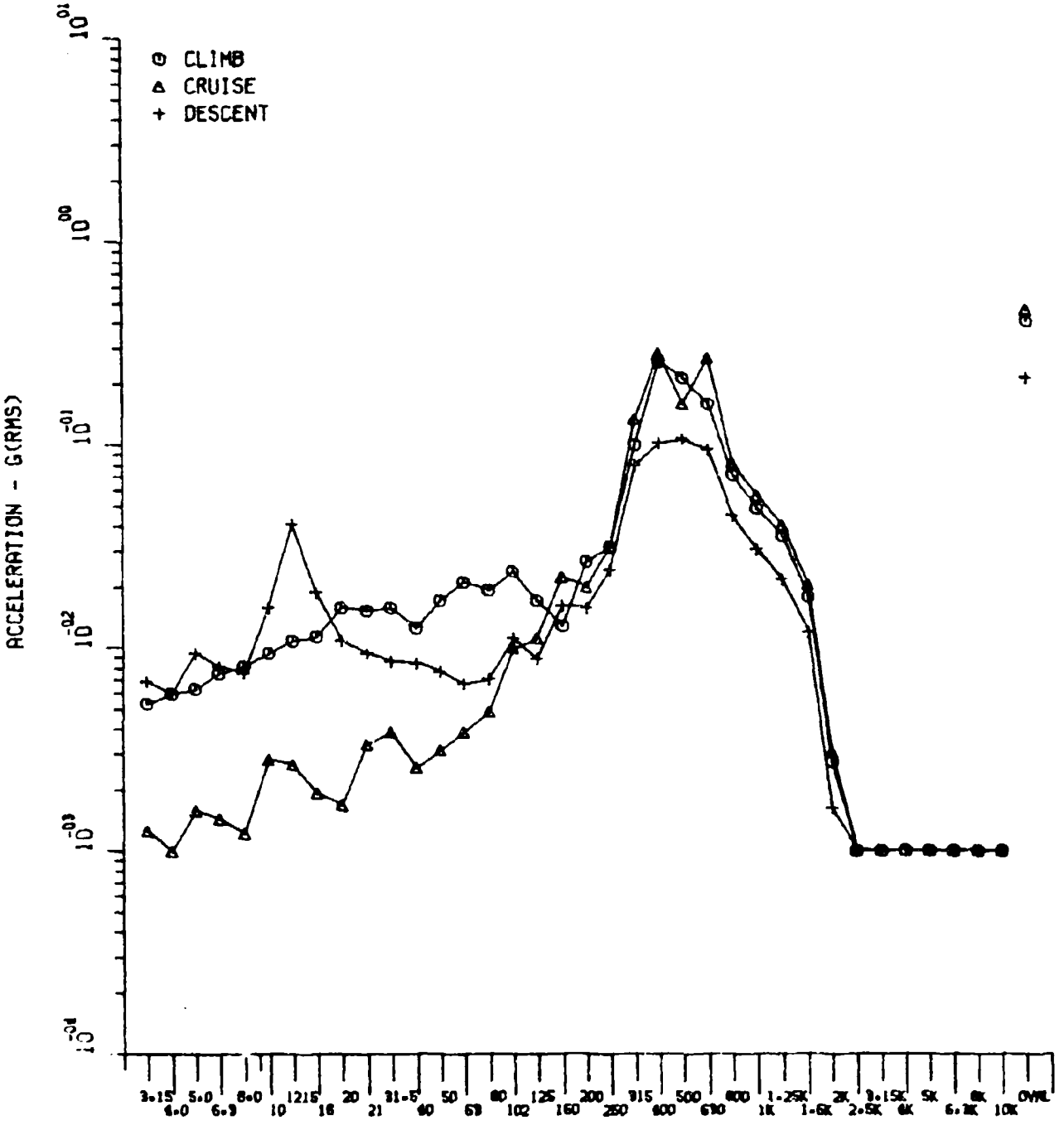

Figure 23b. Cruise, Climb, and Descent Vertical Acceleration, Right Front Cargo Deck - 3.15 Hz to 10KHz.

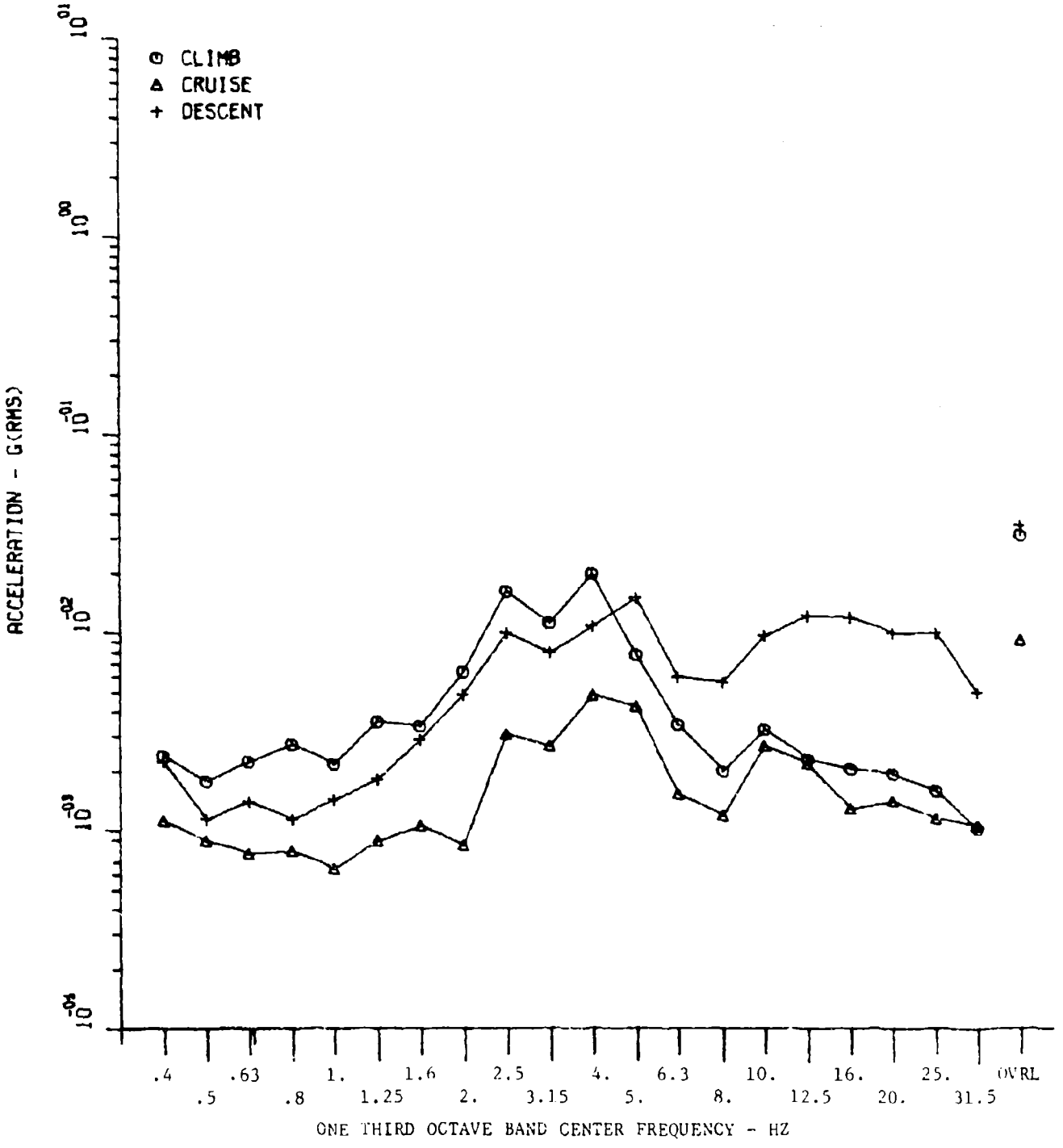

Figure 24a. Cruise, Climb, and Descent Lateral Acceleration, Right Front Cargo Deck - 0.4 to 31.5 Hz.

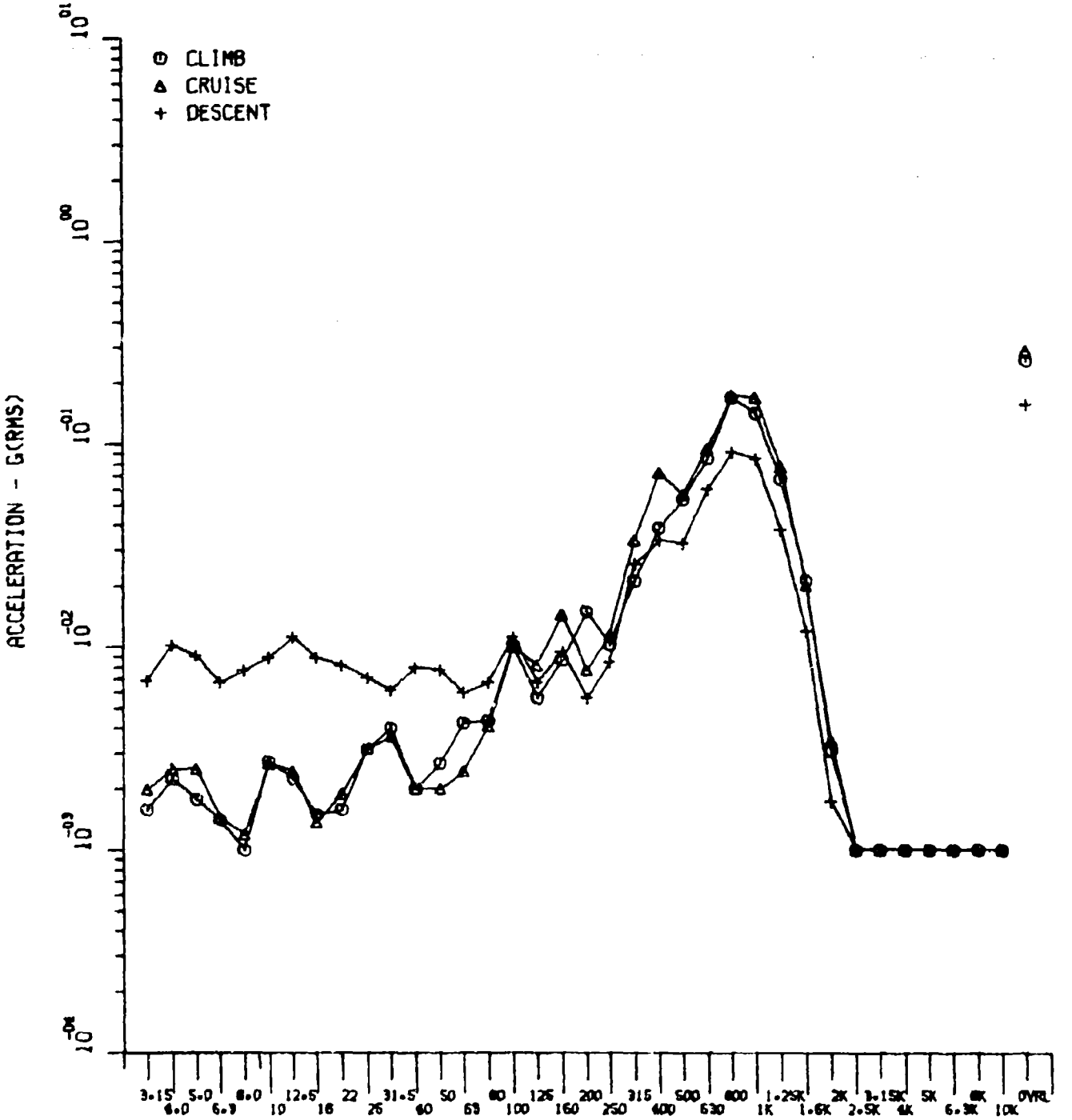

ONE THIRD OCTAVE BAND CENTER FREQUENCY - HZ

Figure 24b. Cruise, Climb, and Descent Lateral Acceleration, Right Front Cargo Deck - 3.15 Hz to 10KHz.

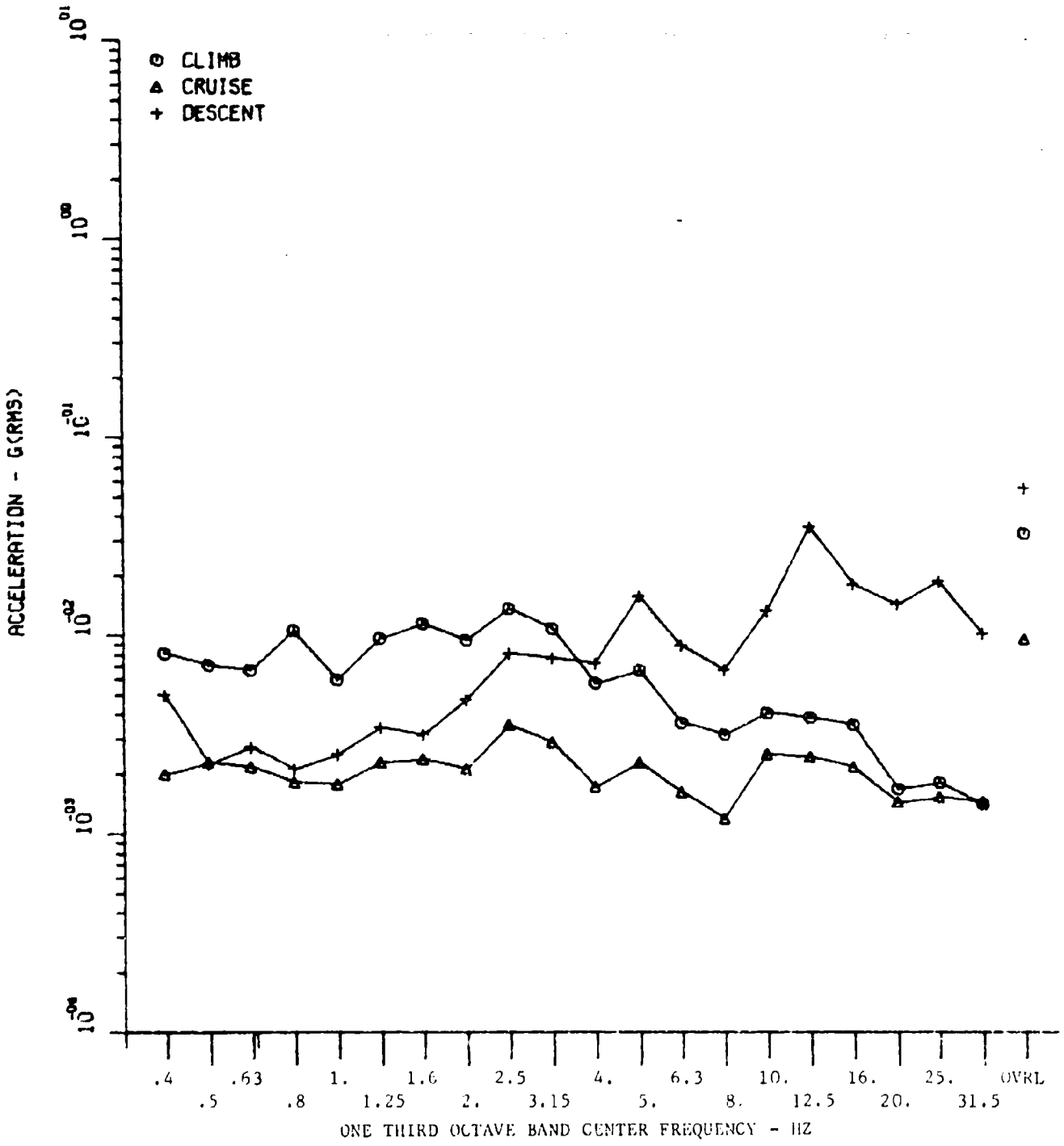

Figure 25a. Cruise, Climb, and Descent Vertical Acceleration, Left Front Cargo Deck - 0.4 to 31.5 Hz.

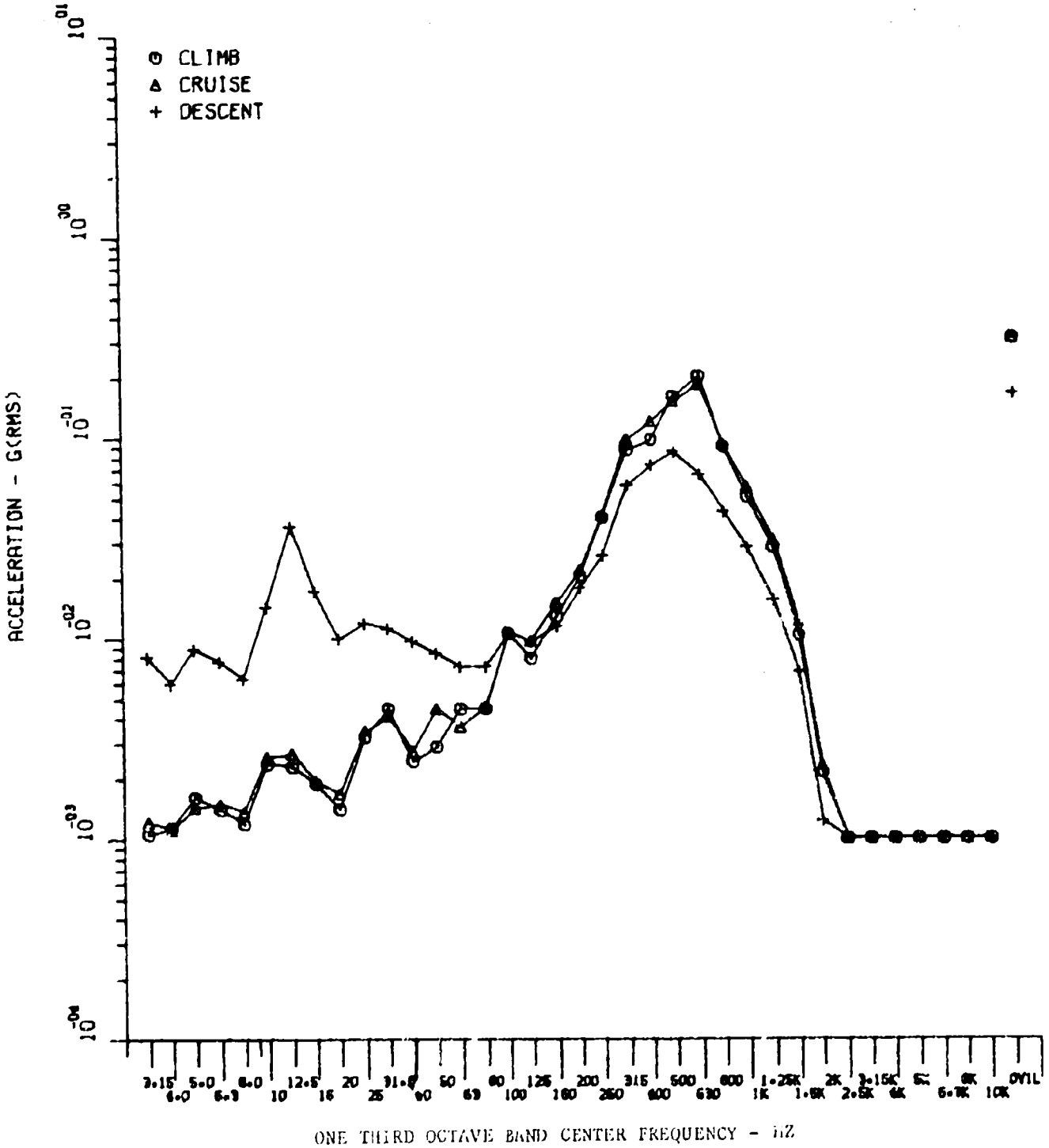

Figure 25b. Cruise, Climb, and Descent Vertical Acceleration, Left Front Cargo Deck - 3.15 Hz to 10KHz.

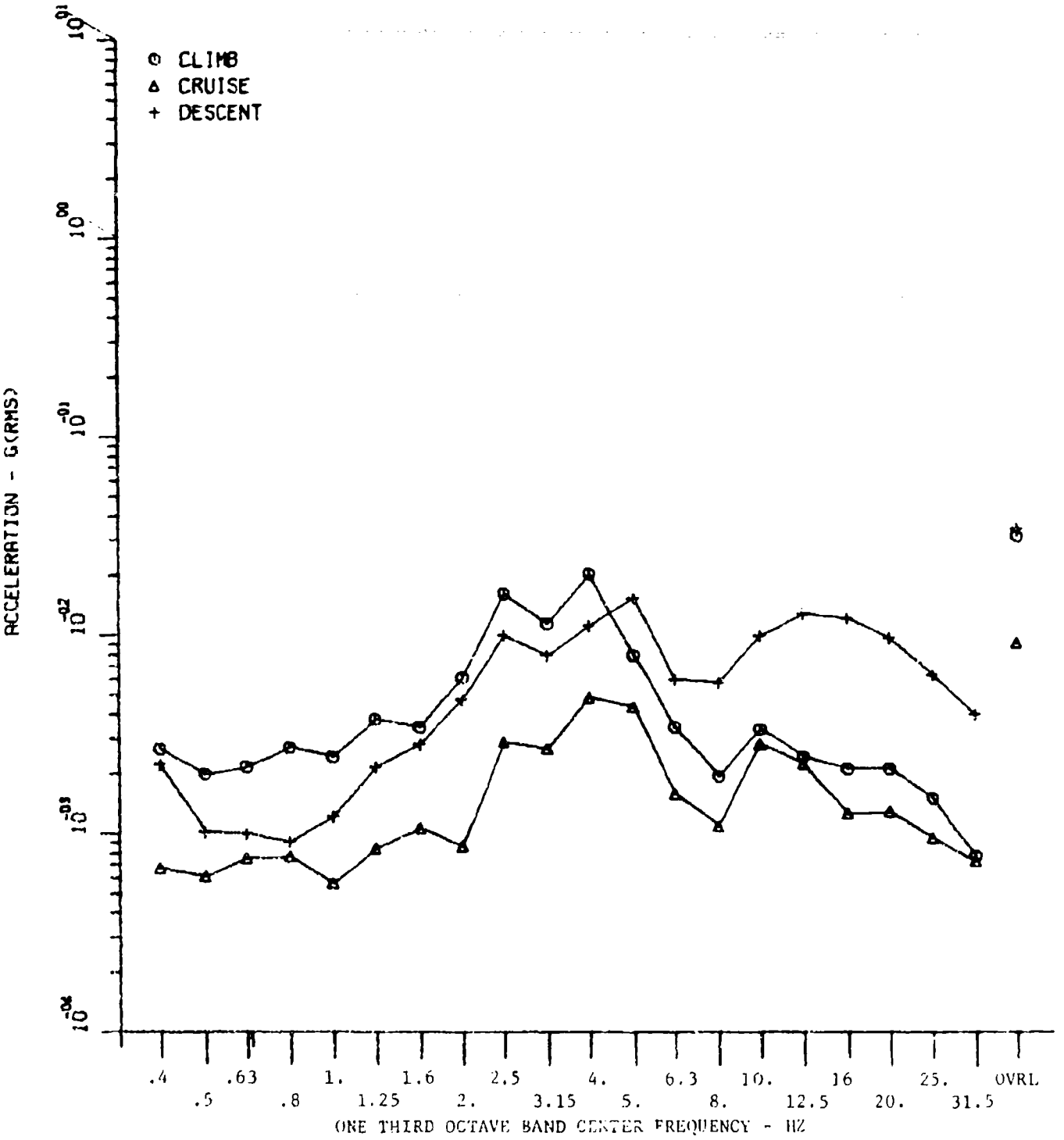

Figure 26a. Cruise, Climb, and Descent Lateral Acceleration, Left Front Cargo Deck - 0.4 to 31.5 Hz.

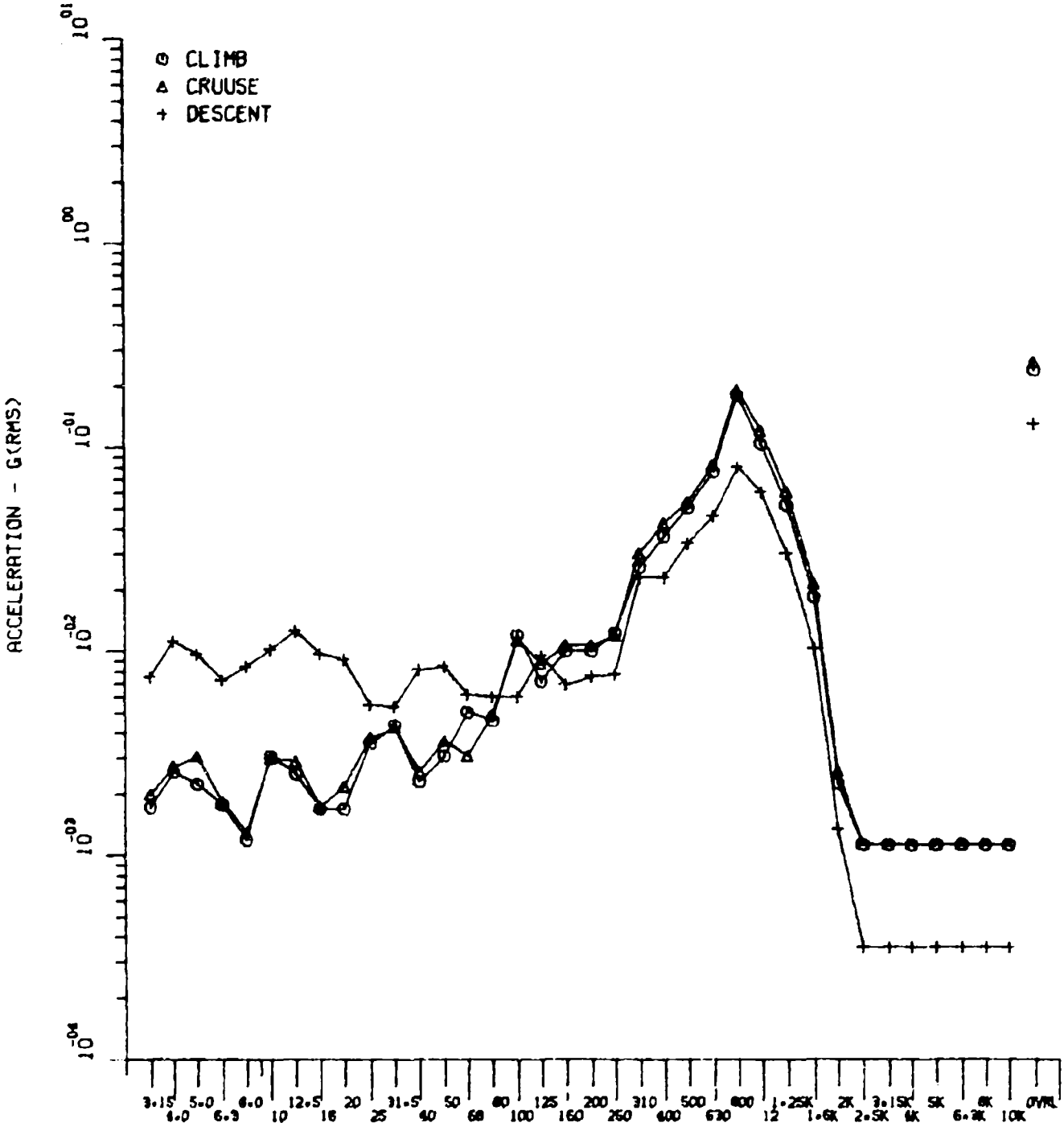

Figure 26b. Cruise, Climb, and Descent Lateral Acceleration, Left Front Cargo Deck - 3.15 Hz to 10KHz.

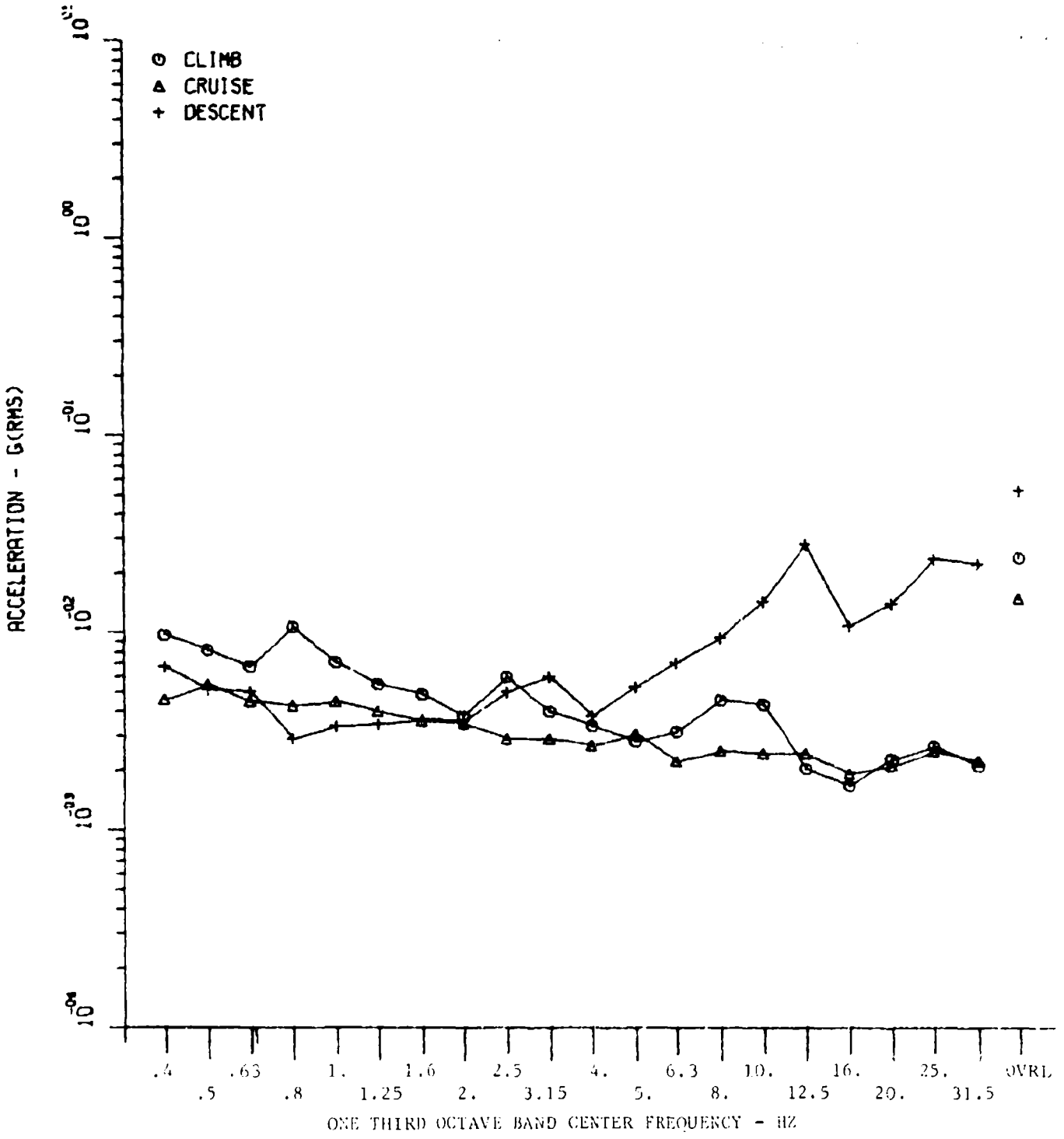

Figure 27a. Cruise, Climb, and Descent Vertical Acceleration, Right Center Cargo Deck - 0.4 to 31.5 Hz.

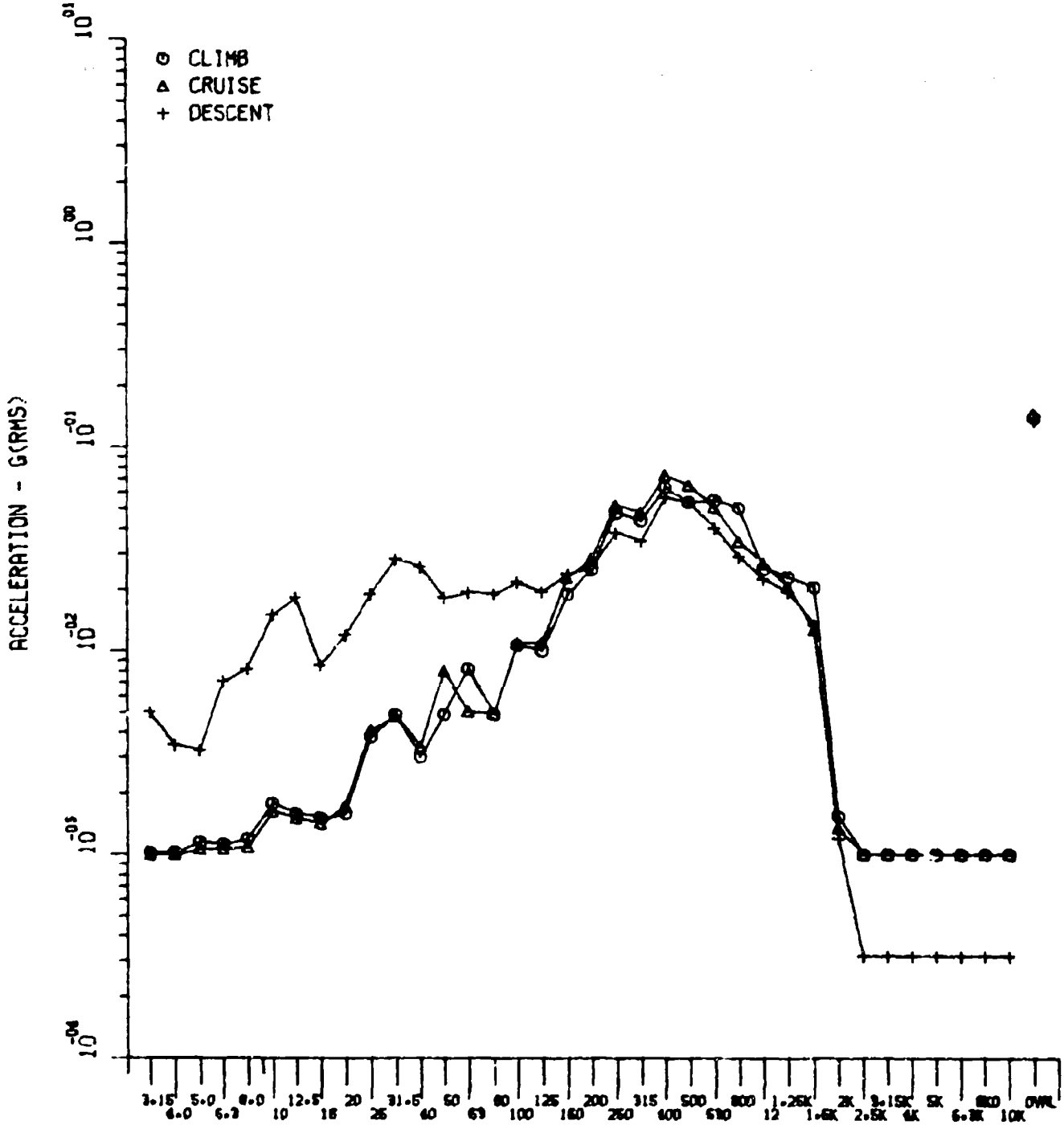

Figure 27b. Cruise, Climb, and Descent Vertical Acceleration, Right Center Cargo Deck - 3.15 Hz to 10KHz.

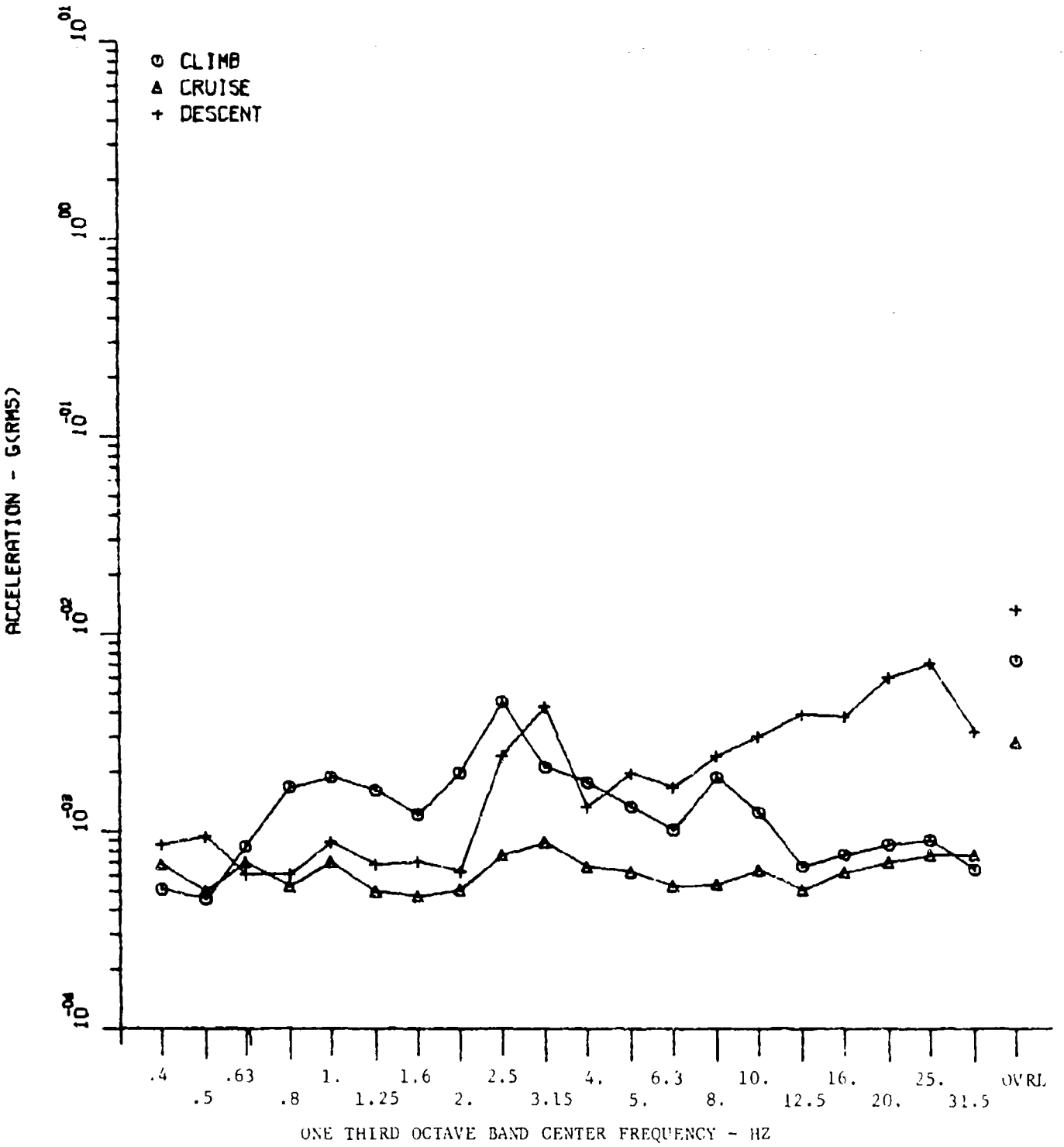

Figure 28a. Cruise, Climb, and Descent Longitudinal Acceleration, Right Center Cargo Deck - 0.4 to 31.5 Hz.

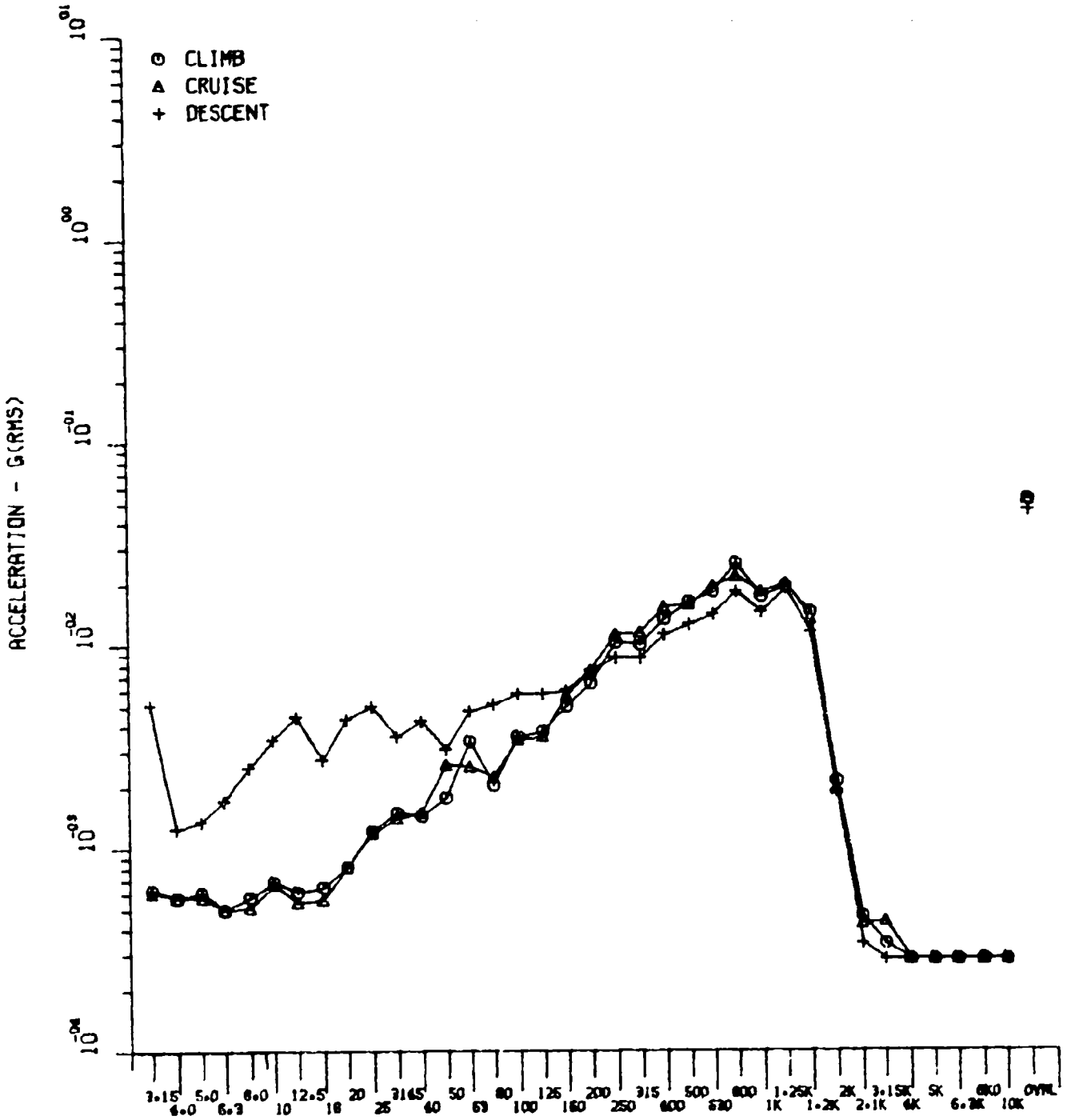

Figure 28b. Cruise, Climb, and Descent Longitudinal Acceleration, Right Center Cargo Deck - 3.15 Hz to 10KHz.

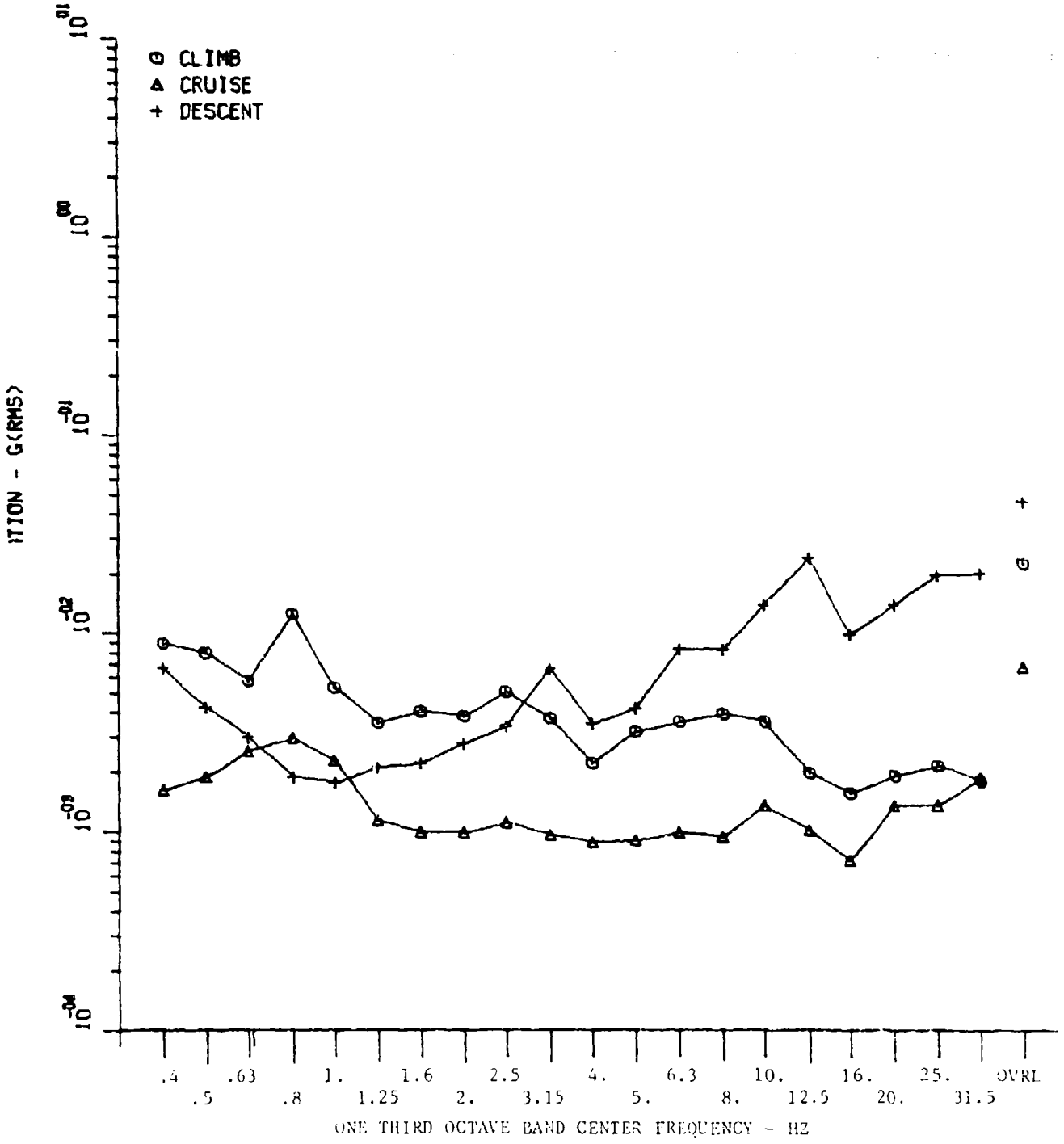

Figure 29a. Cruise, Climb, and Descent Vertical Acceleration, Left Center Cargo Deck - 0.4 to 31.5 Hz.

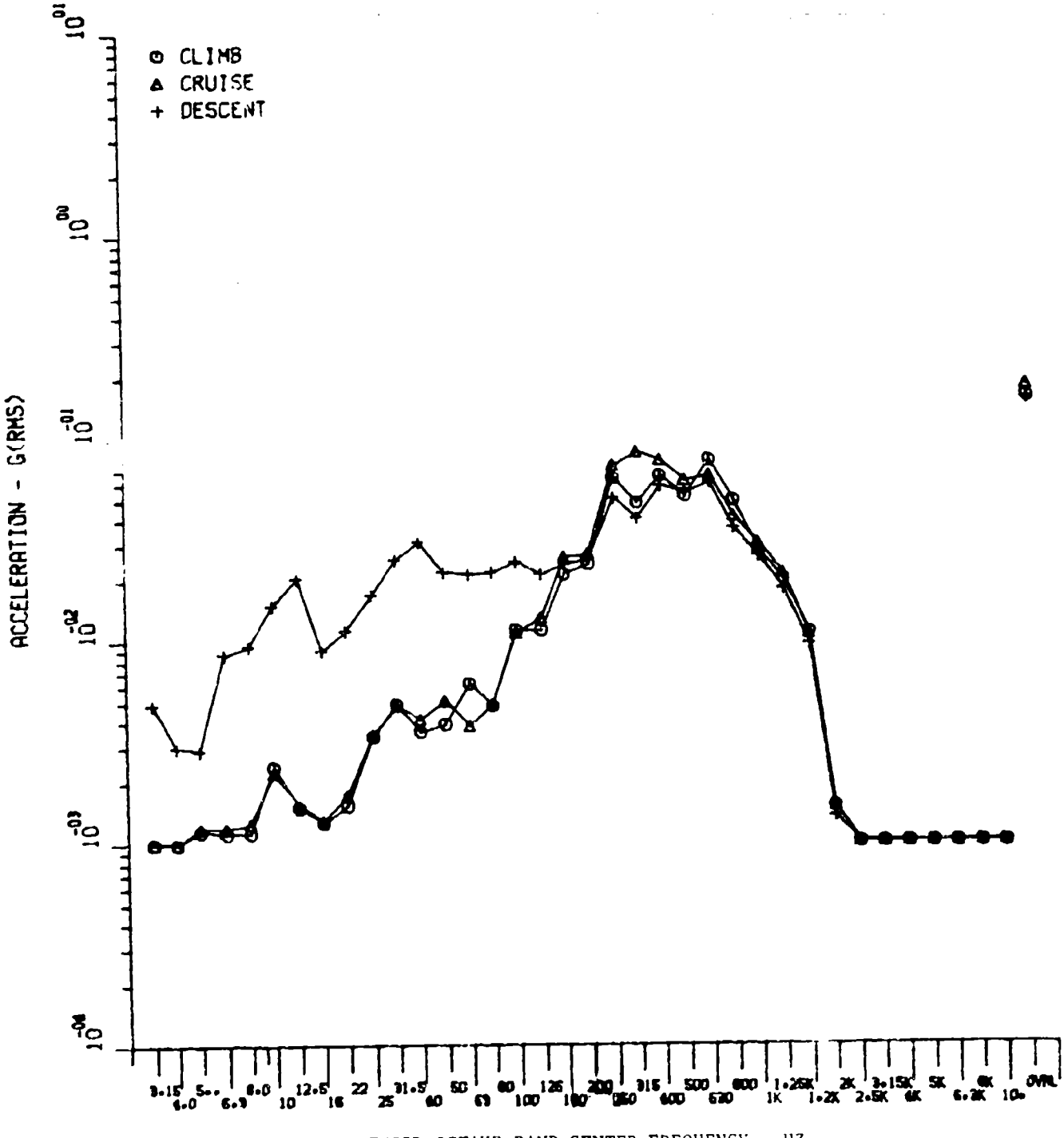

Figure 29b. Cruise, Climb, and Descent Vertical Acceleration, Left Center Cargo Deck - 3.15 Hz to 10KHz.

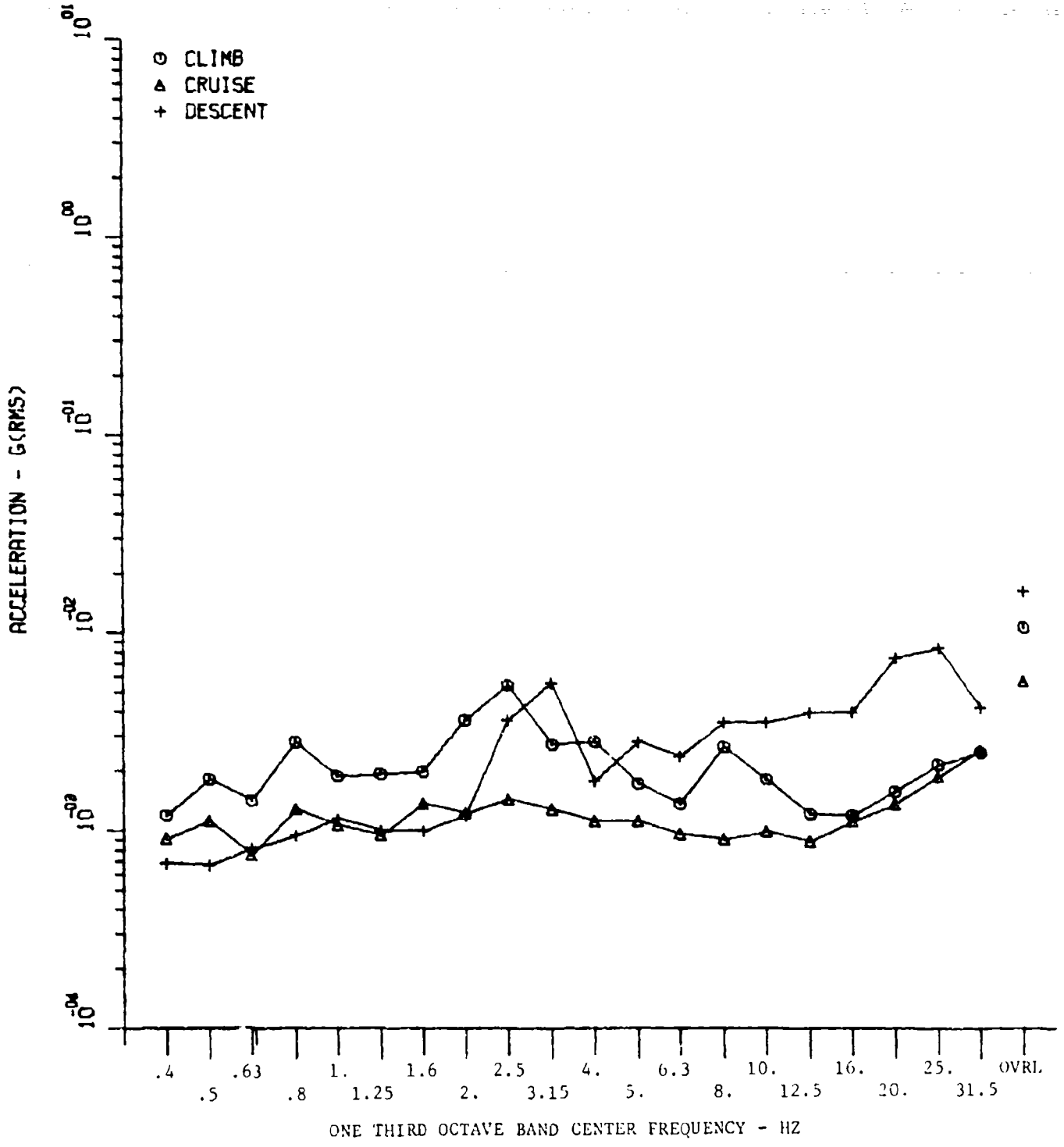

Figure 30a. Cruise, Climb, and Descent Longitudinal Acceleration, Left Center Cargo Deck - 0.4 to 31.5 Hz.

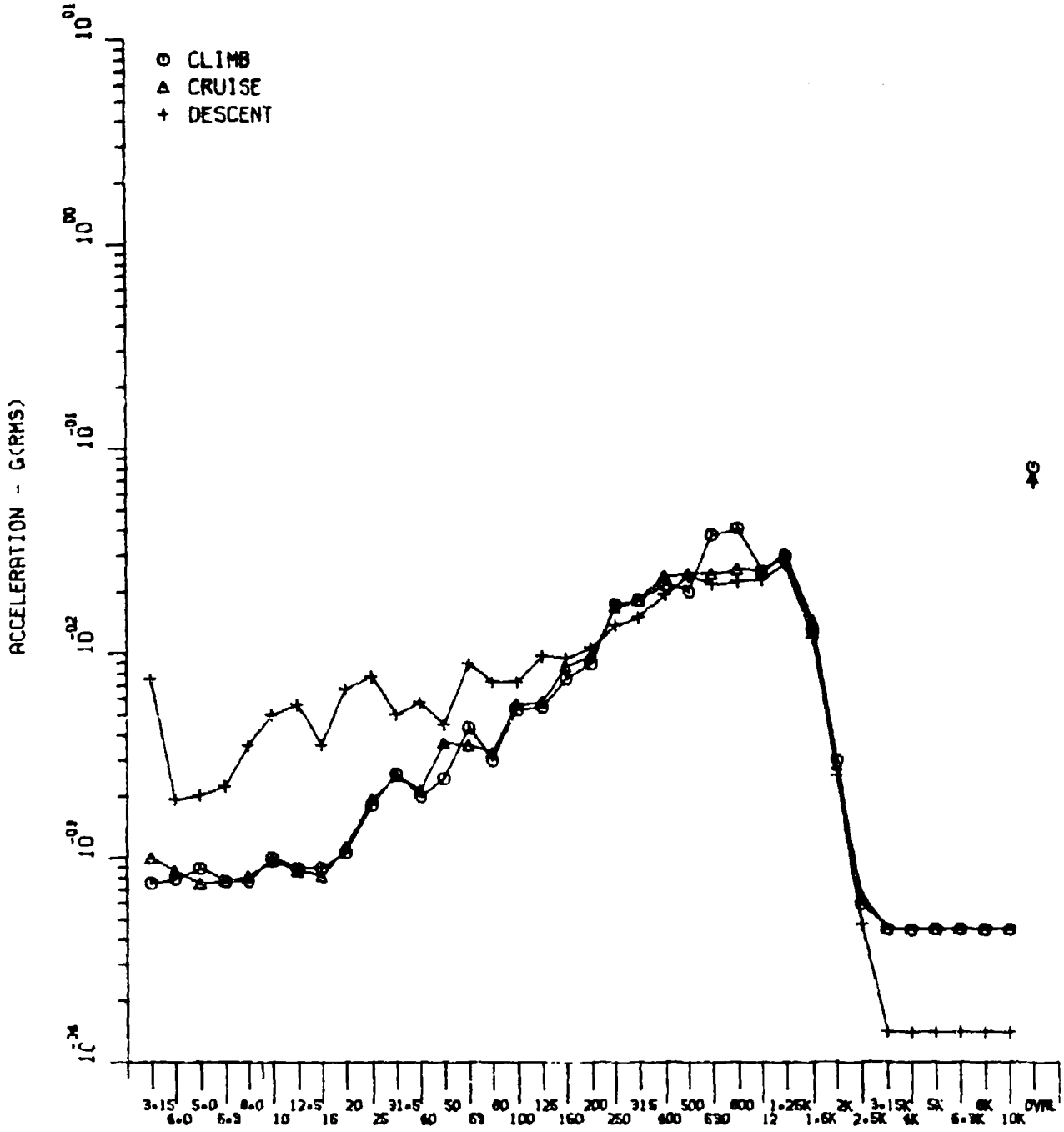

Figure 30b. Cruise, Climb, and Descent Longitudinal Acceleration, Left Center Cargo Deck - 3.15 Hz to 10KHz.

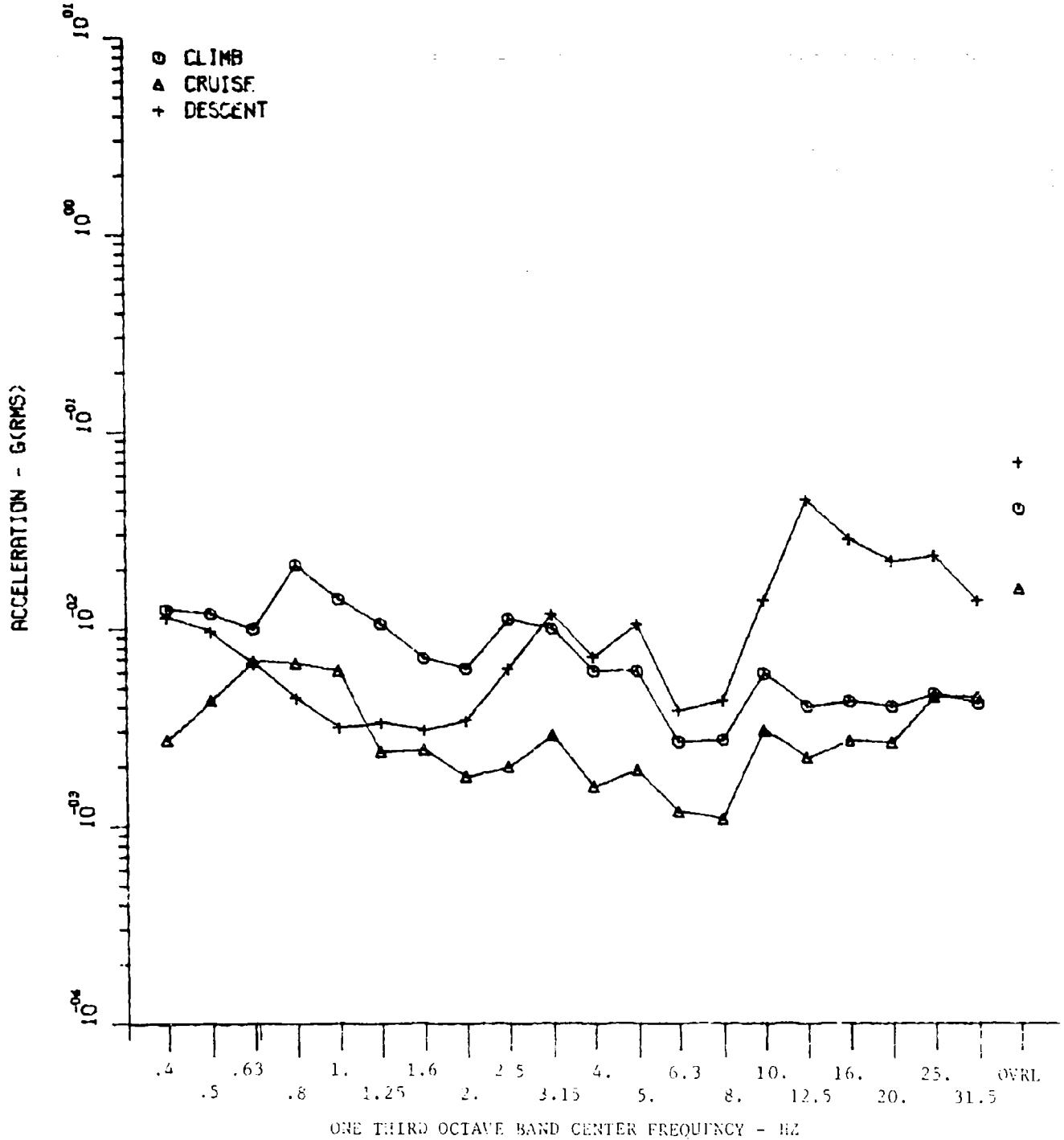

Figure 31a. Cruise, Climb, and Descent Vertical Acceleration, Right Rear Cargo Deck - 0.4 to 31.5 Hz.

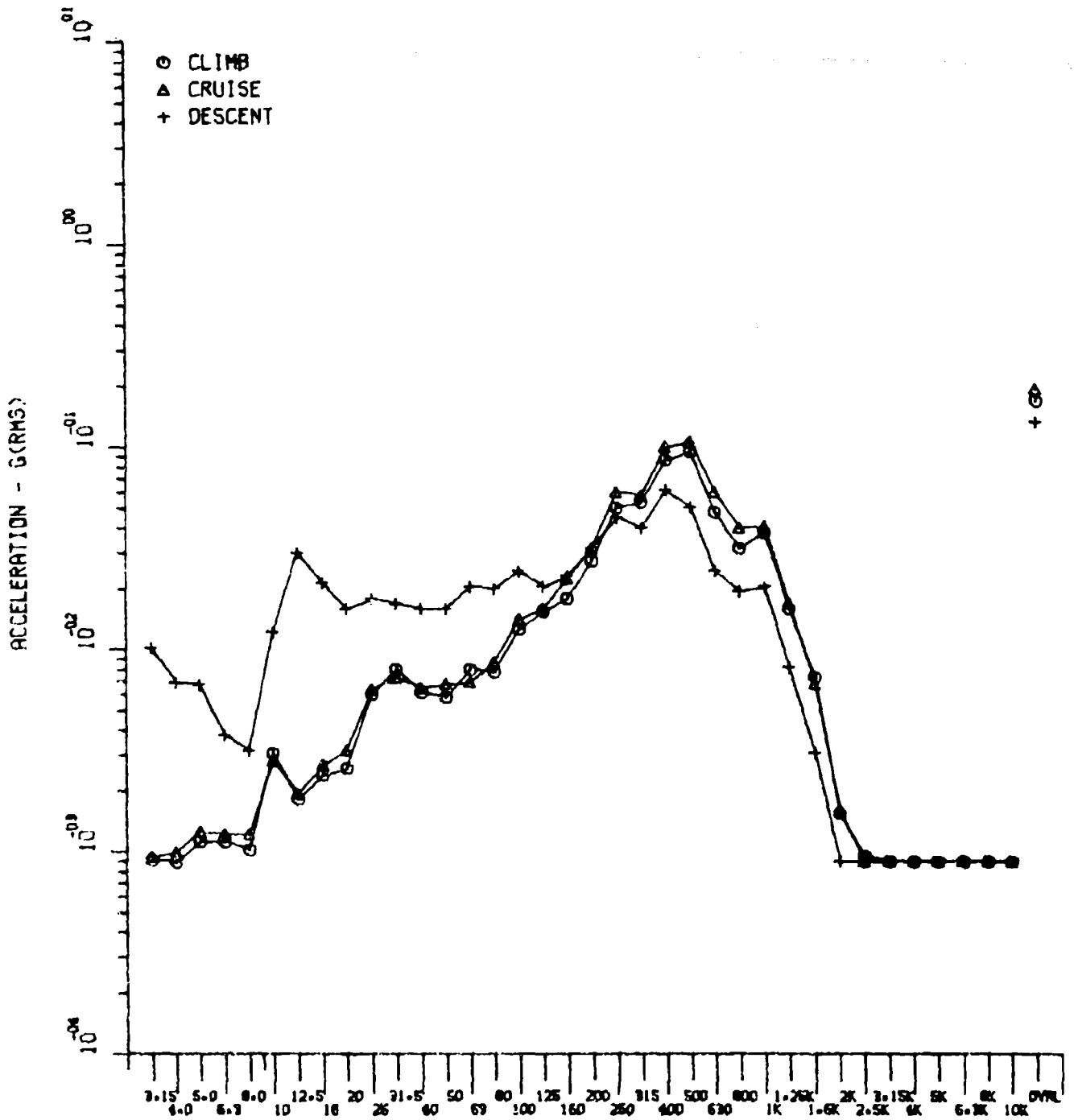

Figure 31b. Cruise, Climb, and Descent Vertical Acceleration, Right Center Cargo Deck - 3.15 Hz to 10KHz.

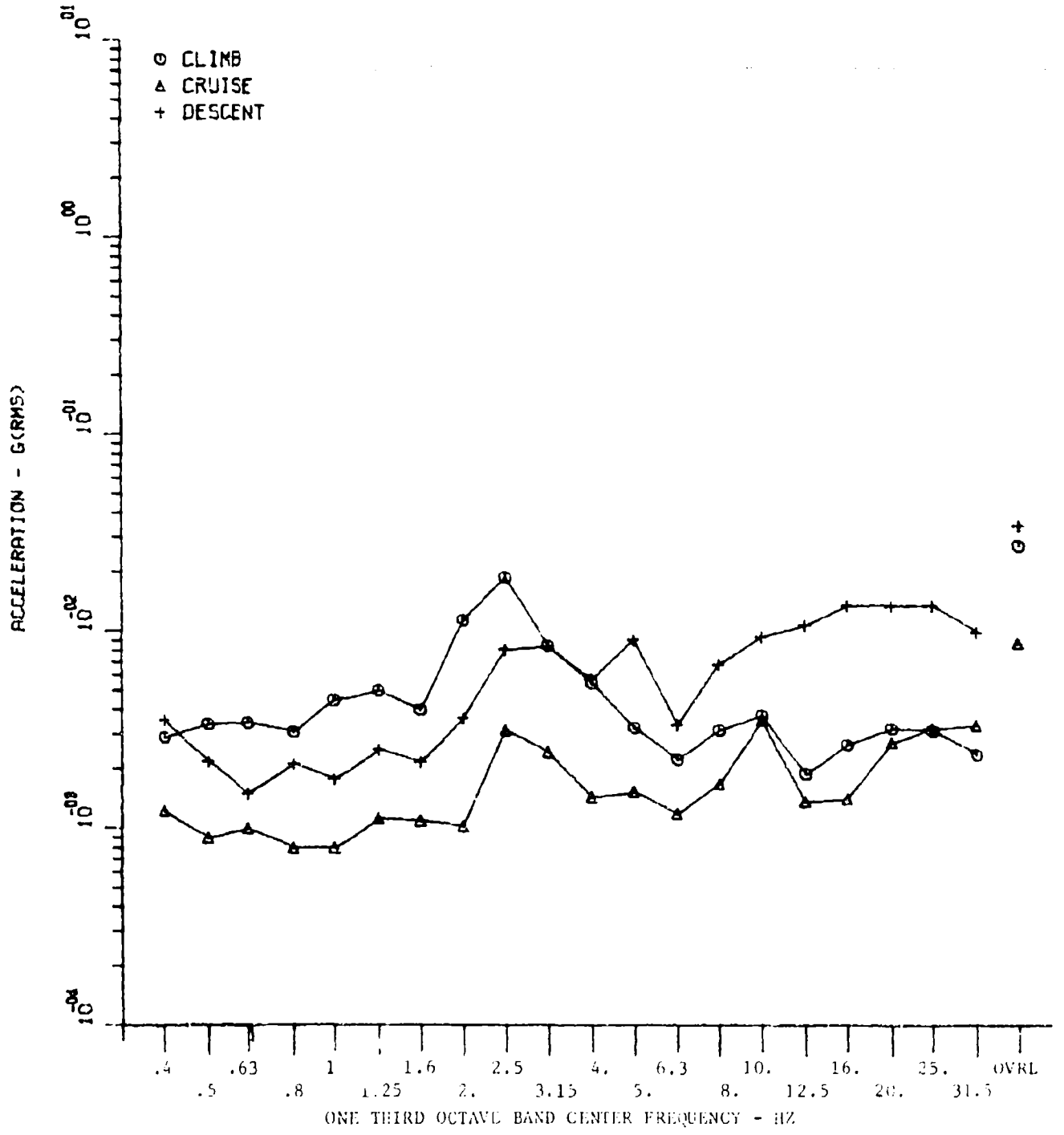

Figure 32a. Cruise, Climb, and Descent Lateral Acceleration, Right Rear Cargo Deck - 0.4 to 31.5 Hz.

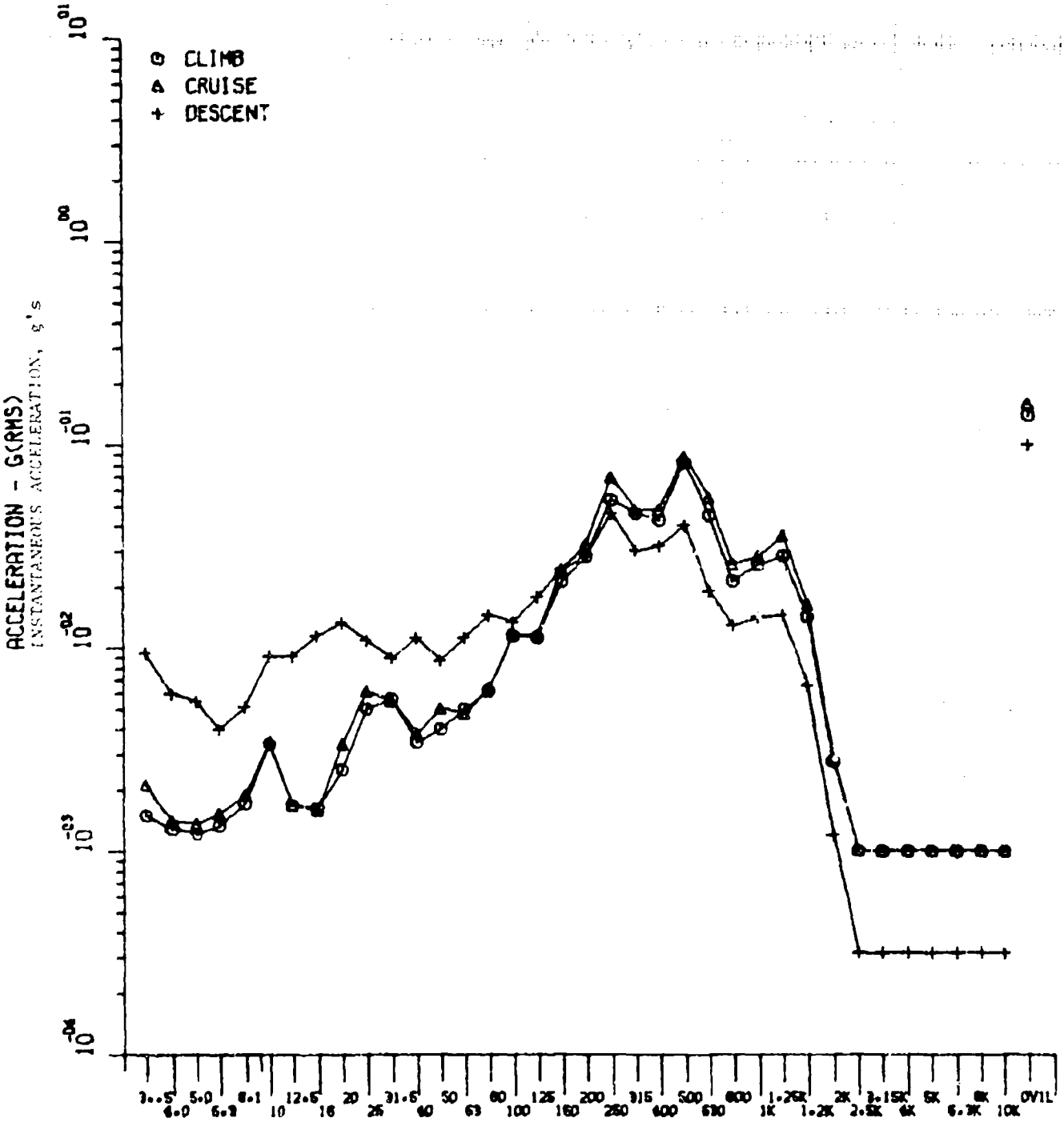

Figure 32b. Cruise, Climb, and Descent Lateral Acceleration, Right Rear Cargo Deck - 3.15 Hz to 10KHz.

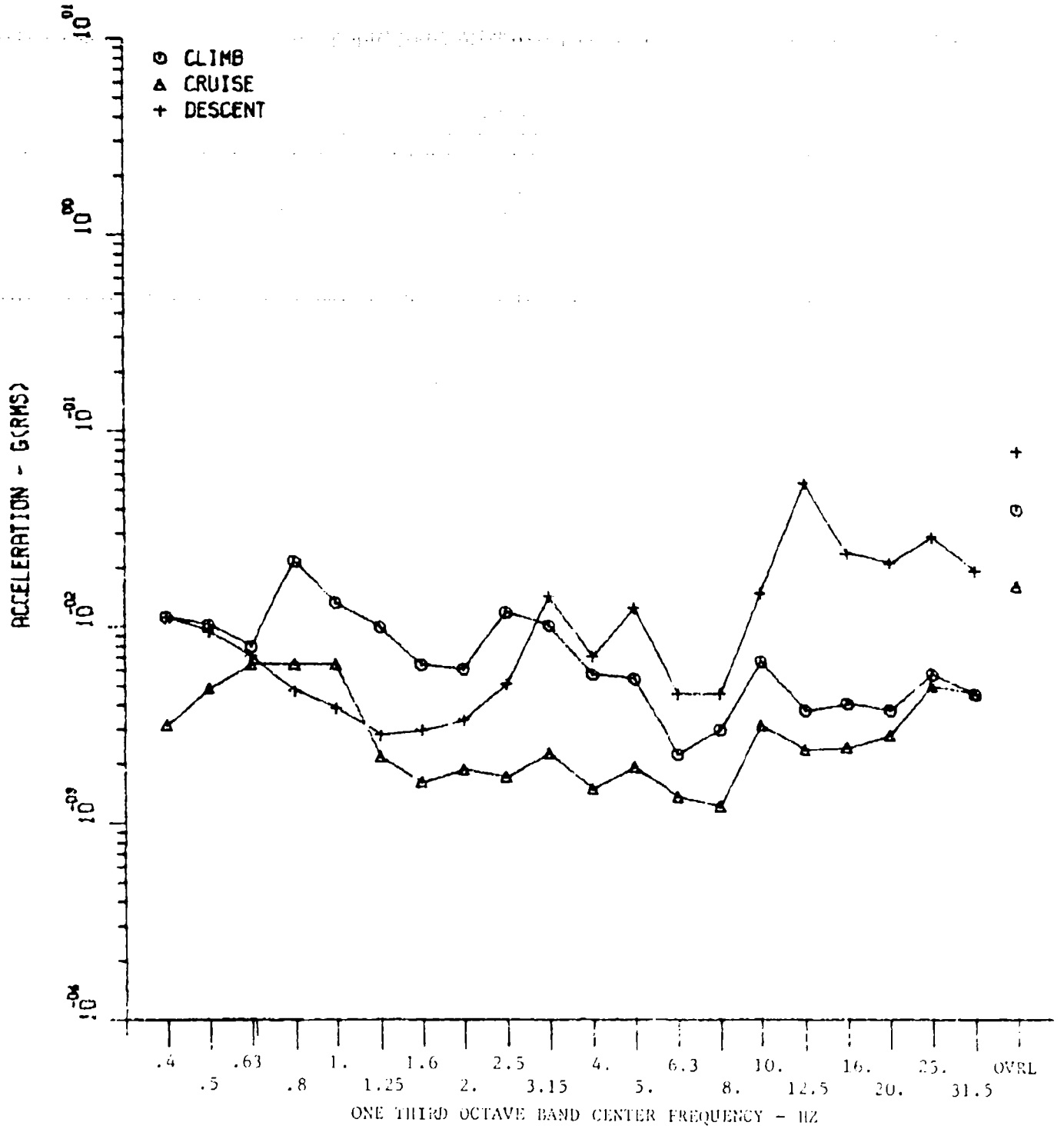

Figure 33a. Cruise, Climb, and Descent Vertical Acceleration, Left Rear Cargo Deck - 0.4 to 31.5 Hz.

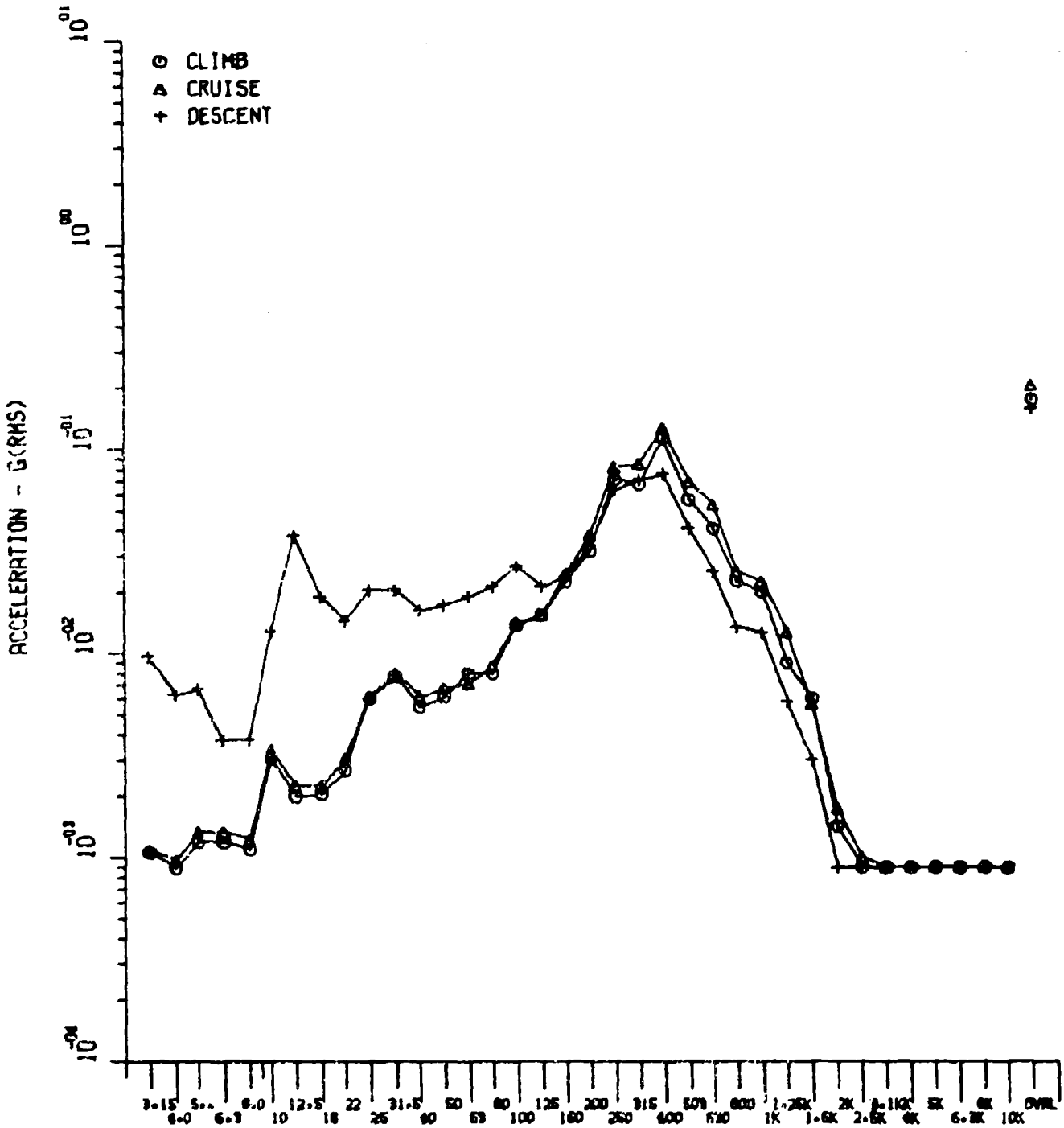

Figure 33b. Cruise, Climb, and Descent Vertical Acceleration, Left Rear Cargo Deck - 3.15 Hz to 10KHz.

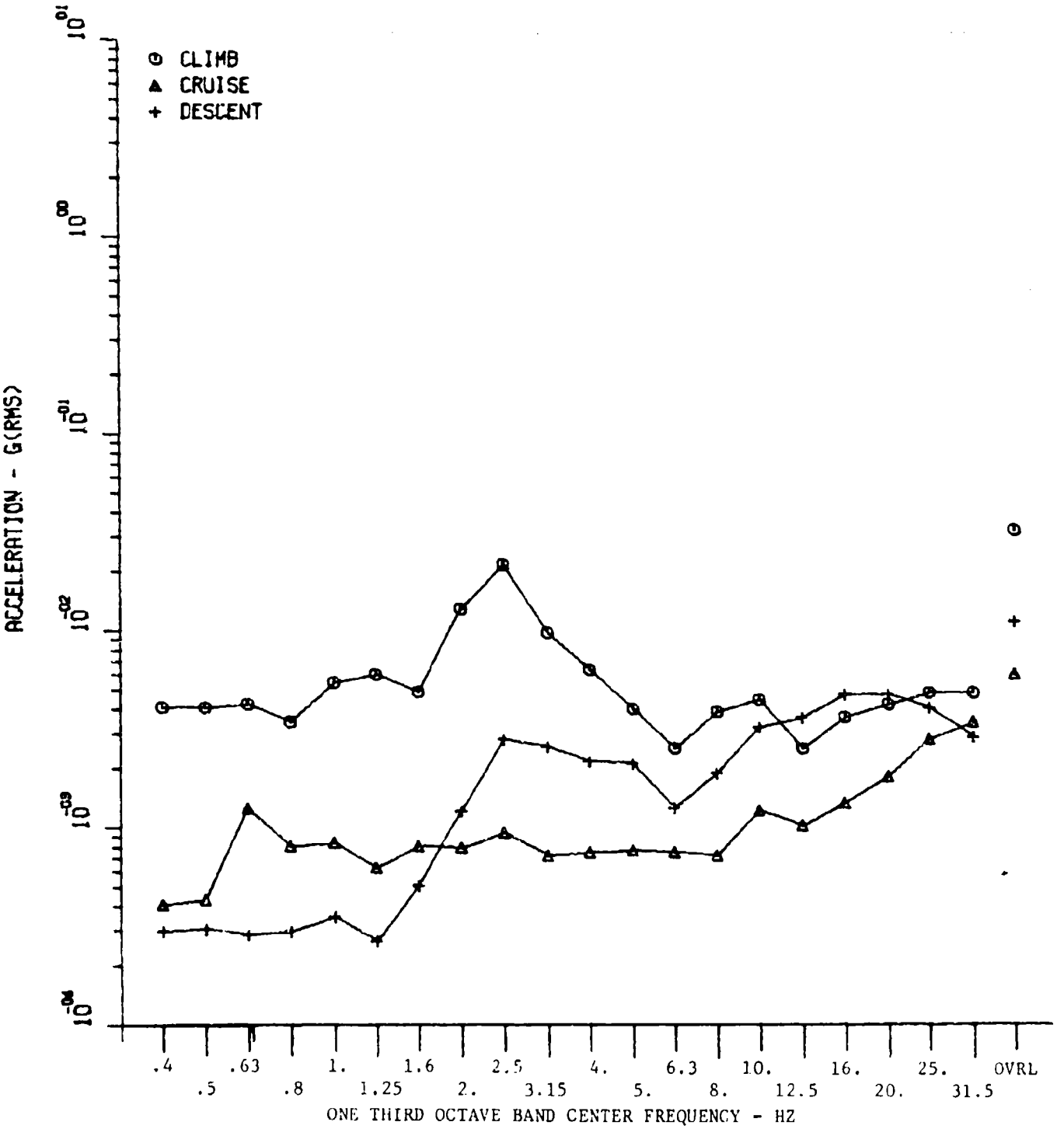

Figure 34a. Cruise, Climb, and Descent Lateral Acceleration, Left Rear Cargo Deck - 0.4 to 31.5 Hz.

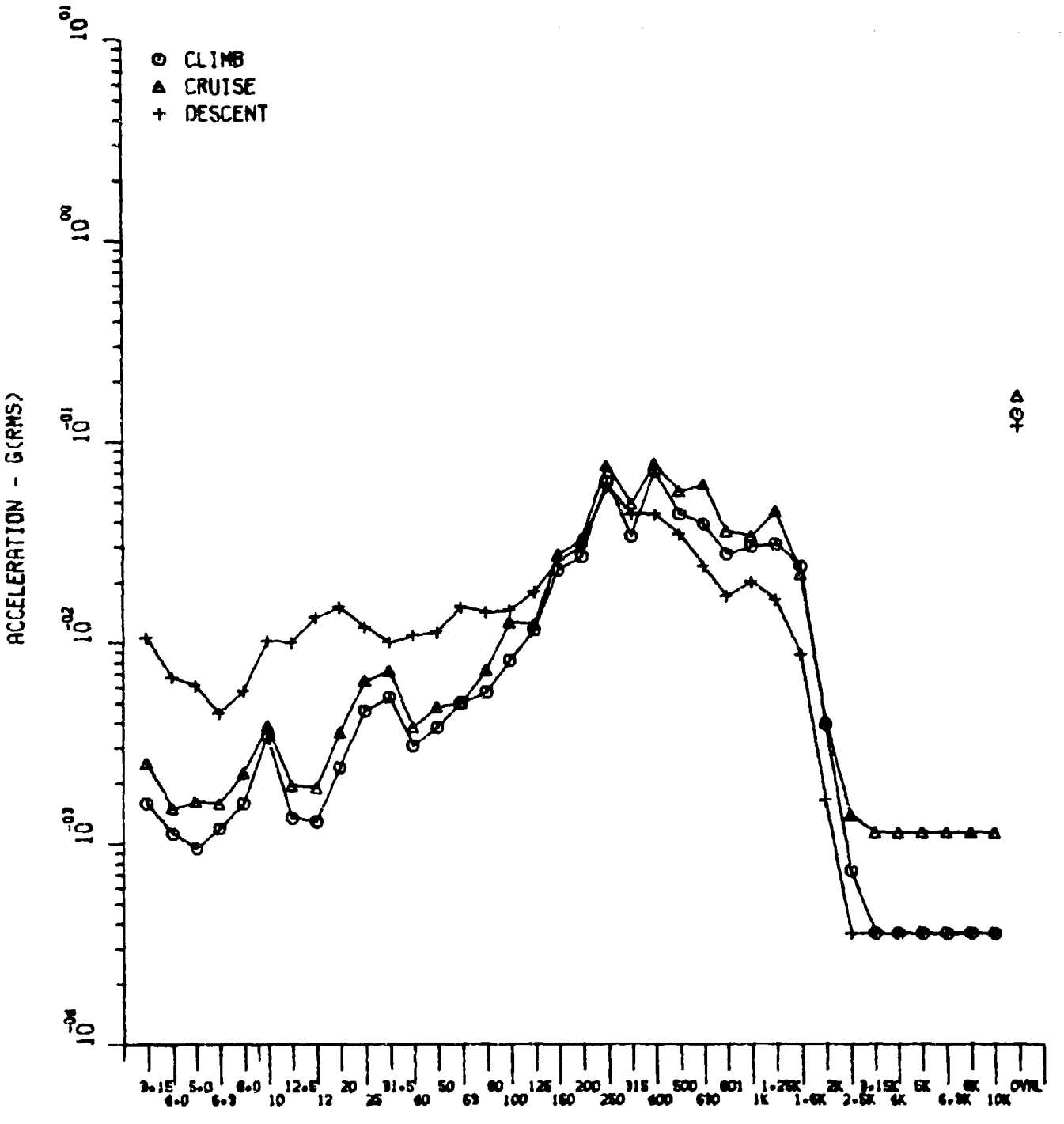

Figure 34b. Cruise, Climb, and Descent Lateral Acceleration, Left Rear Cargo Deck - 3.15 Hz to 10KHz.

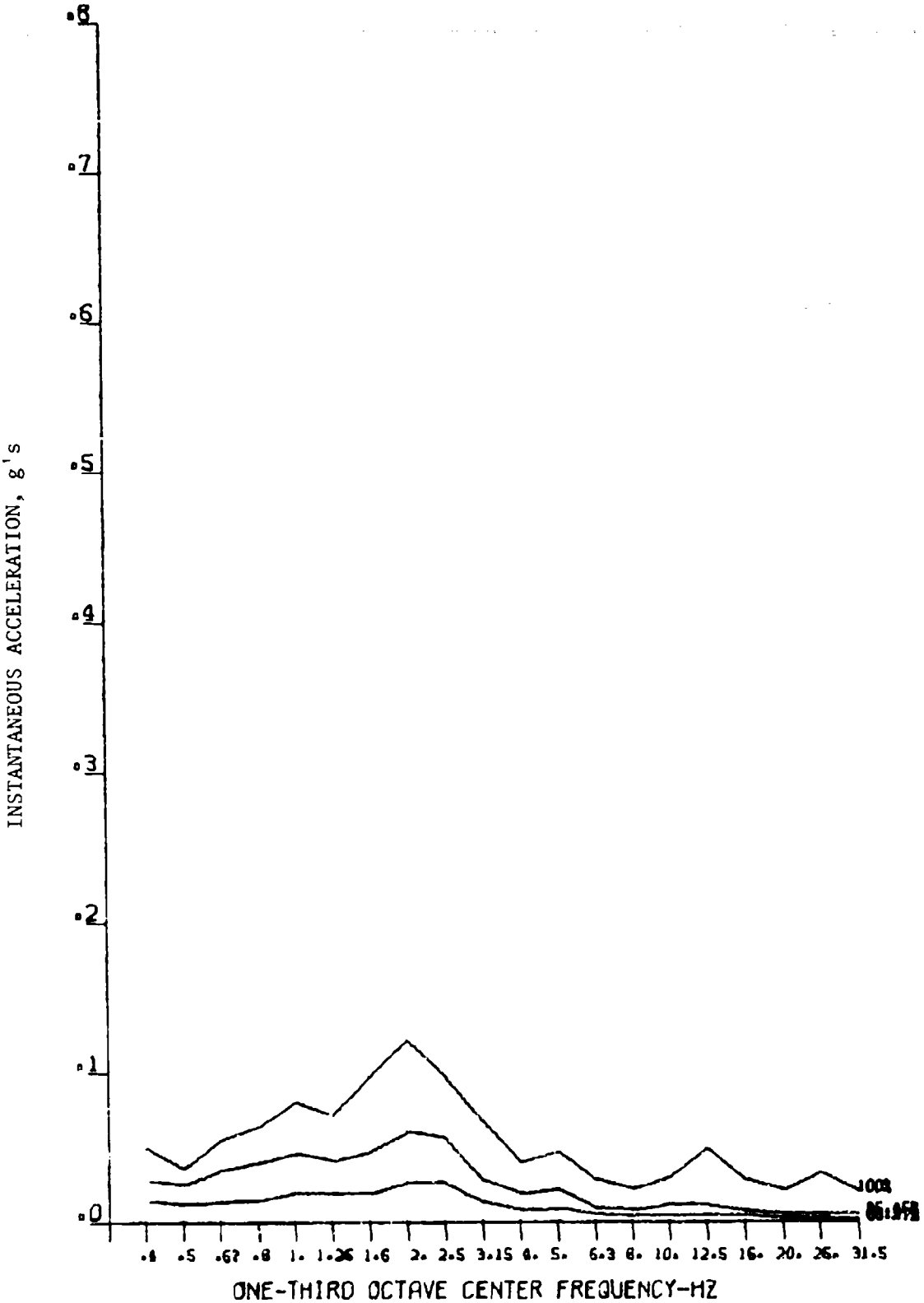

Figure 35. Vertical Terrain-Following Acceleration, Right Front Cargo Deck.

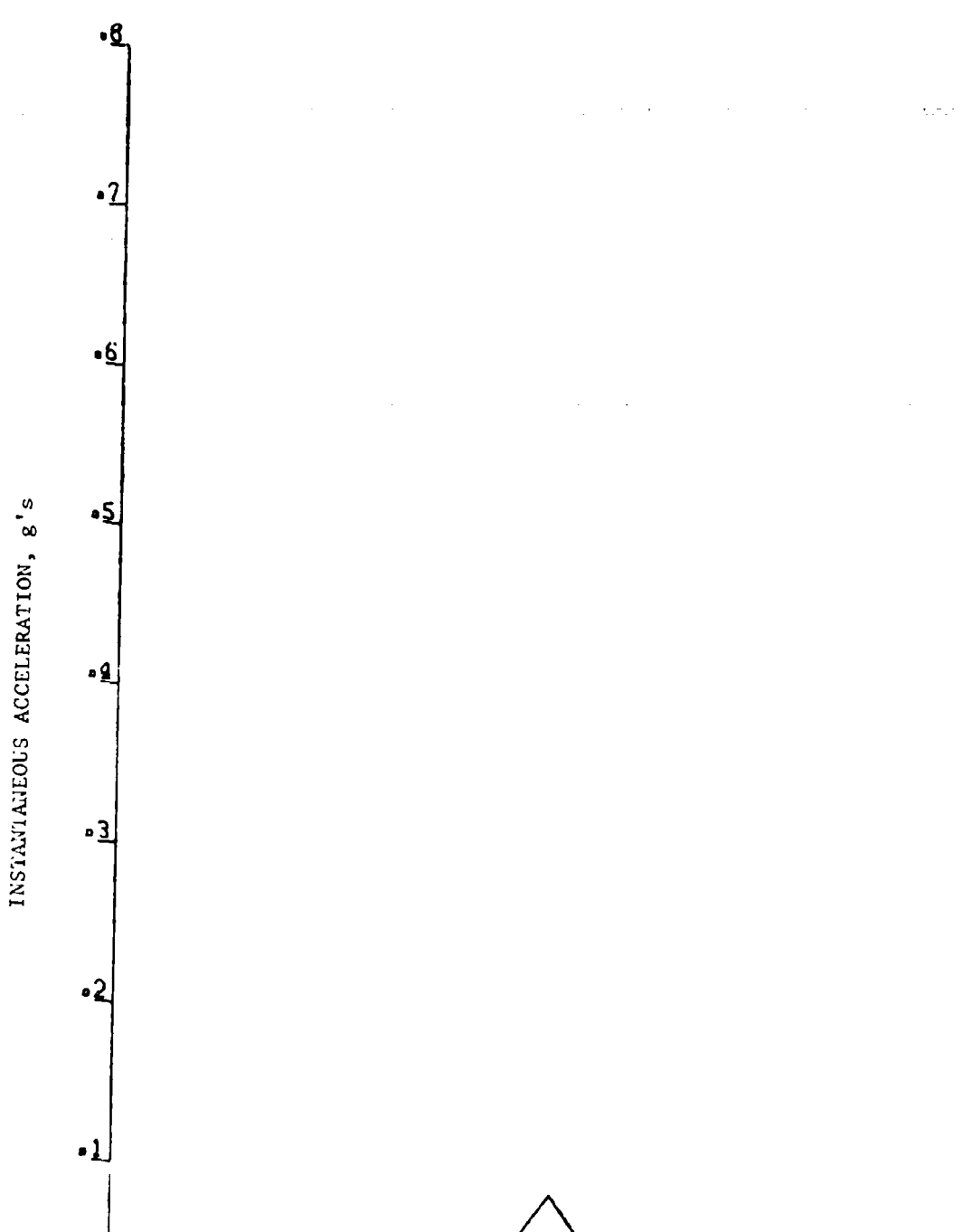

Figure 36. Lateral Terrain-Following Acceleration, Right Front Cargo Deck.

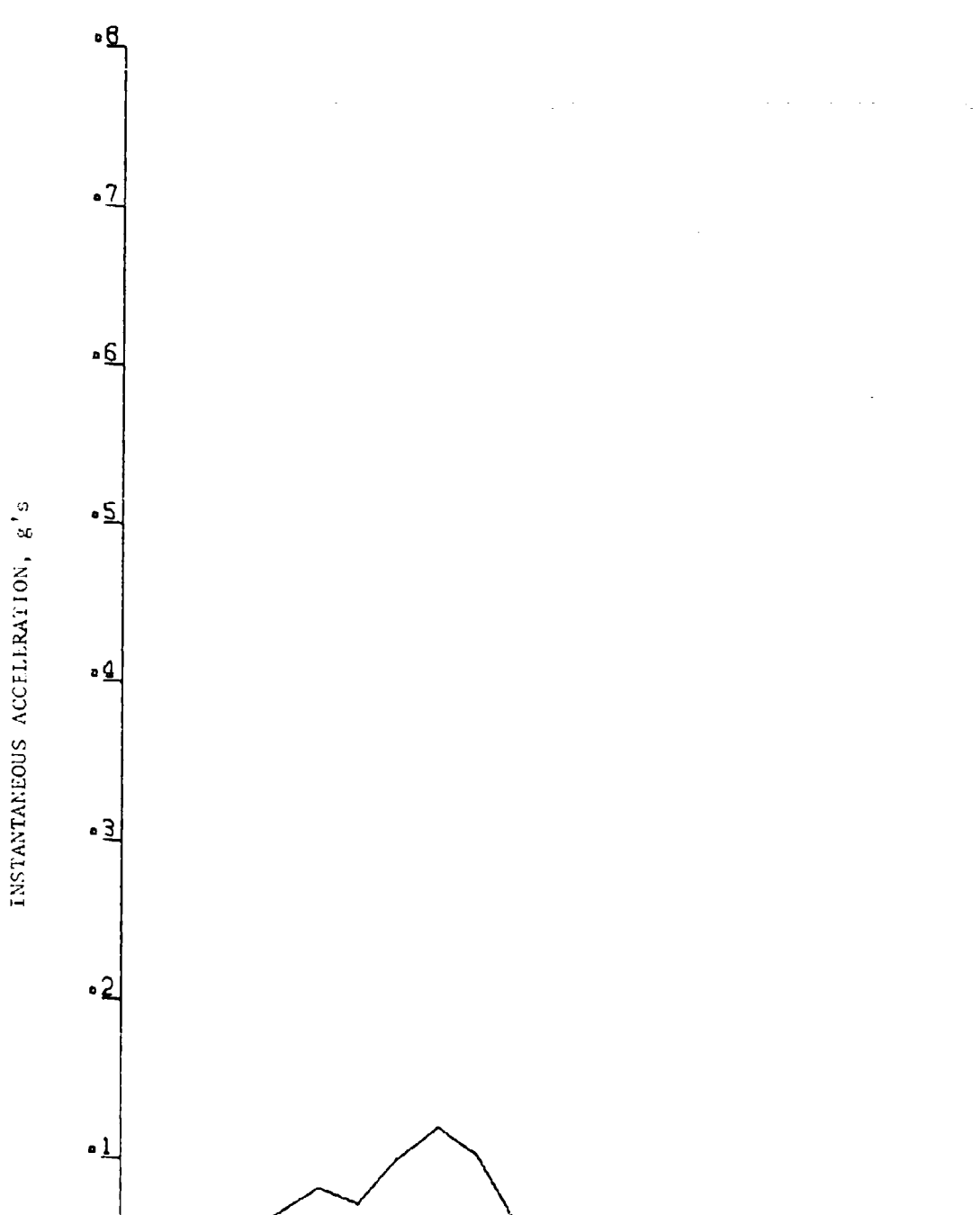

Figure 37. Vertical Terrain-Following Acceleration, Left Front Cargo Deck.

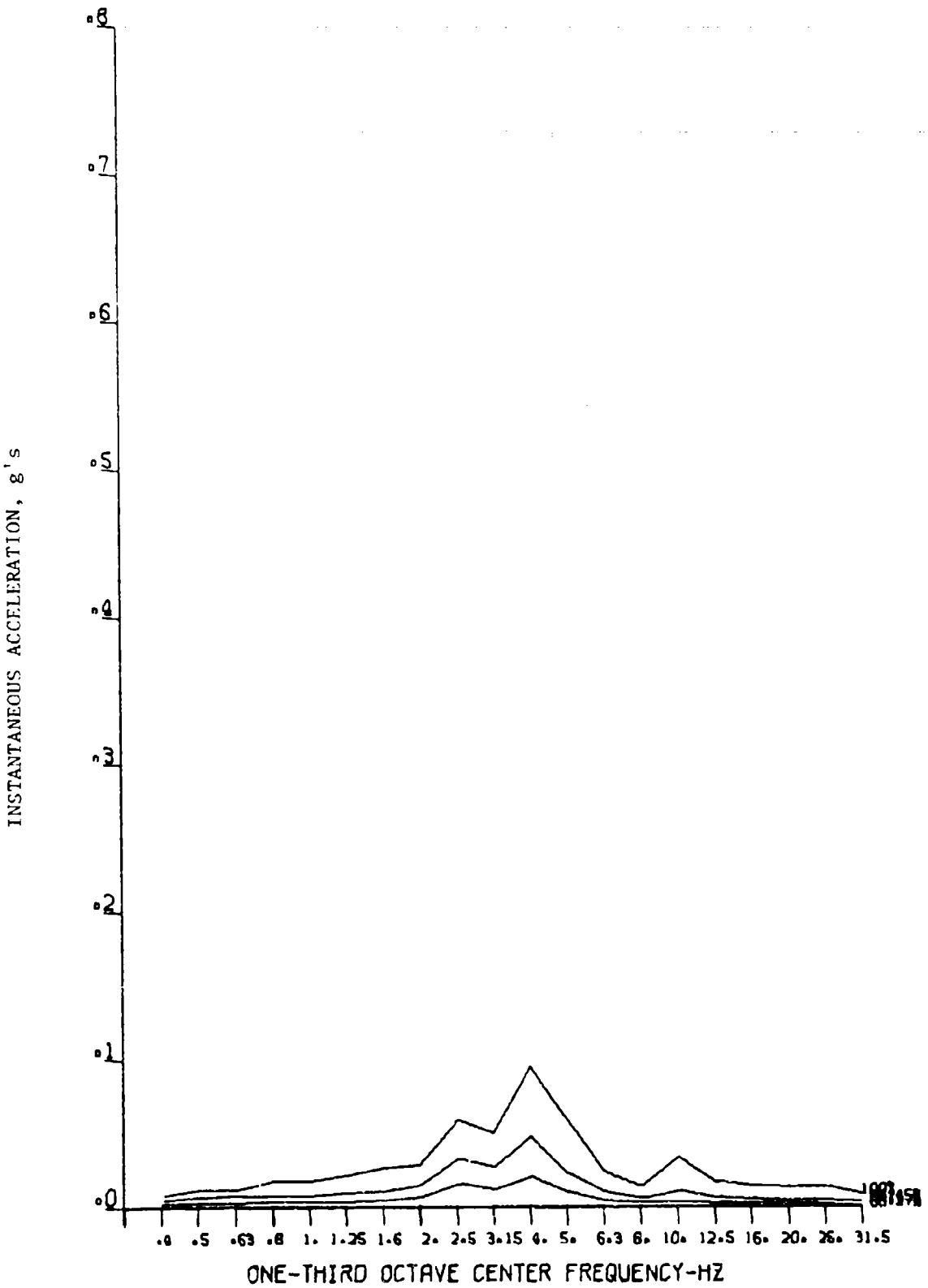

Figure 38. Lateral Terrain-Following Acceleration, Left Front Cargo Deck.

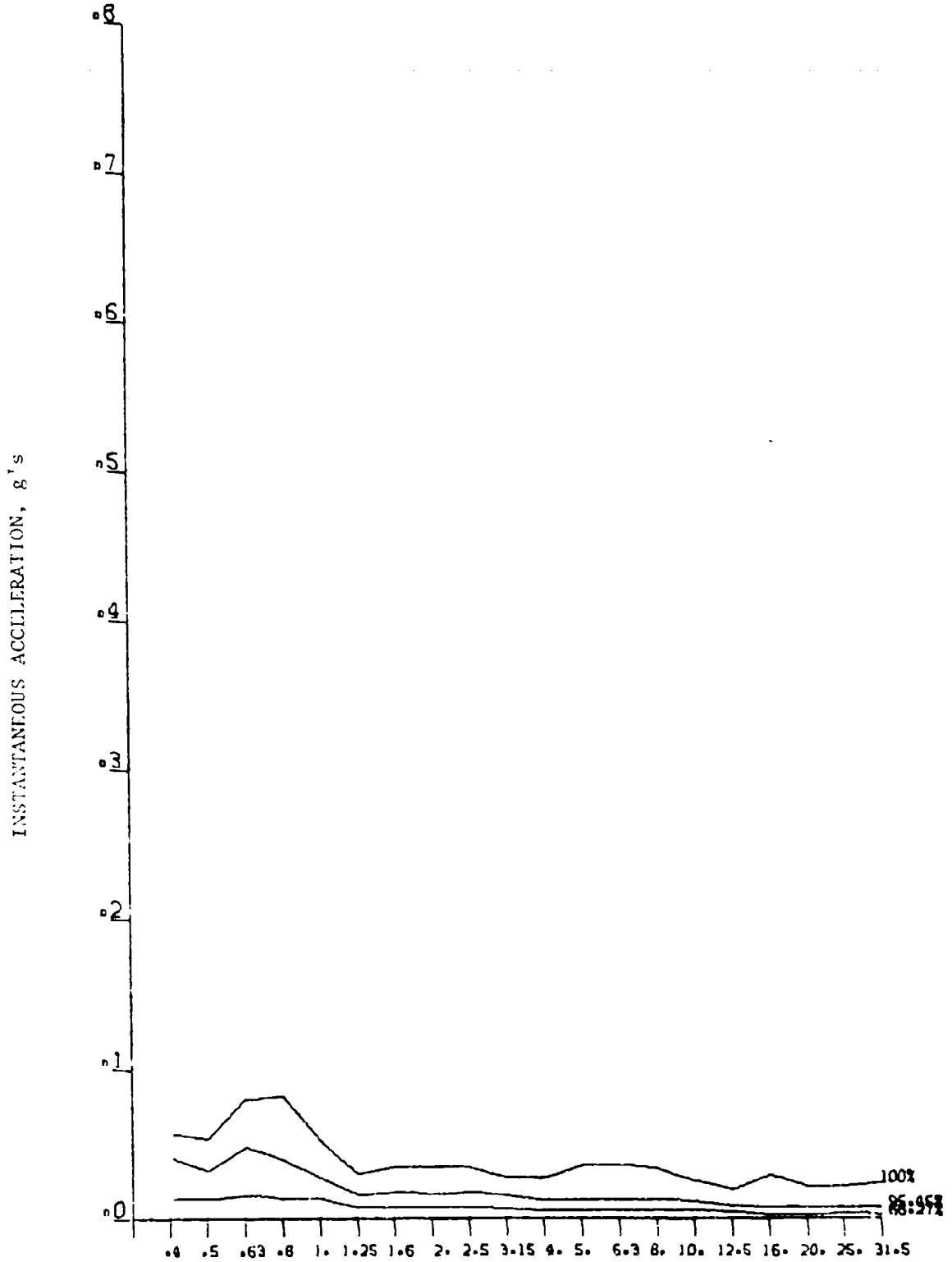

Figure 39. Vertical Terrain-Following Acceleration. Right Center Cargo Deck.

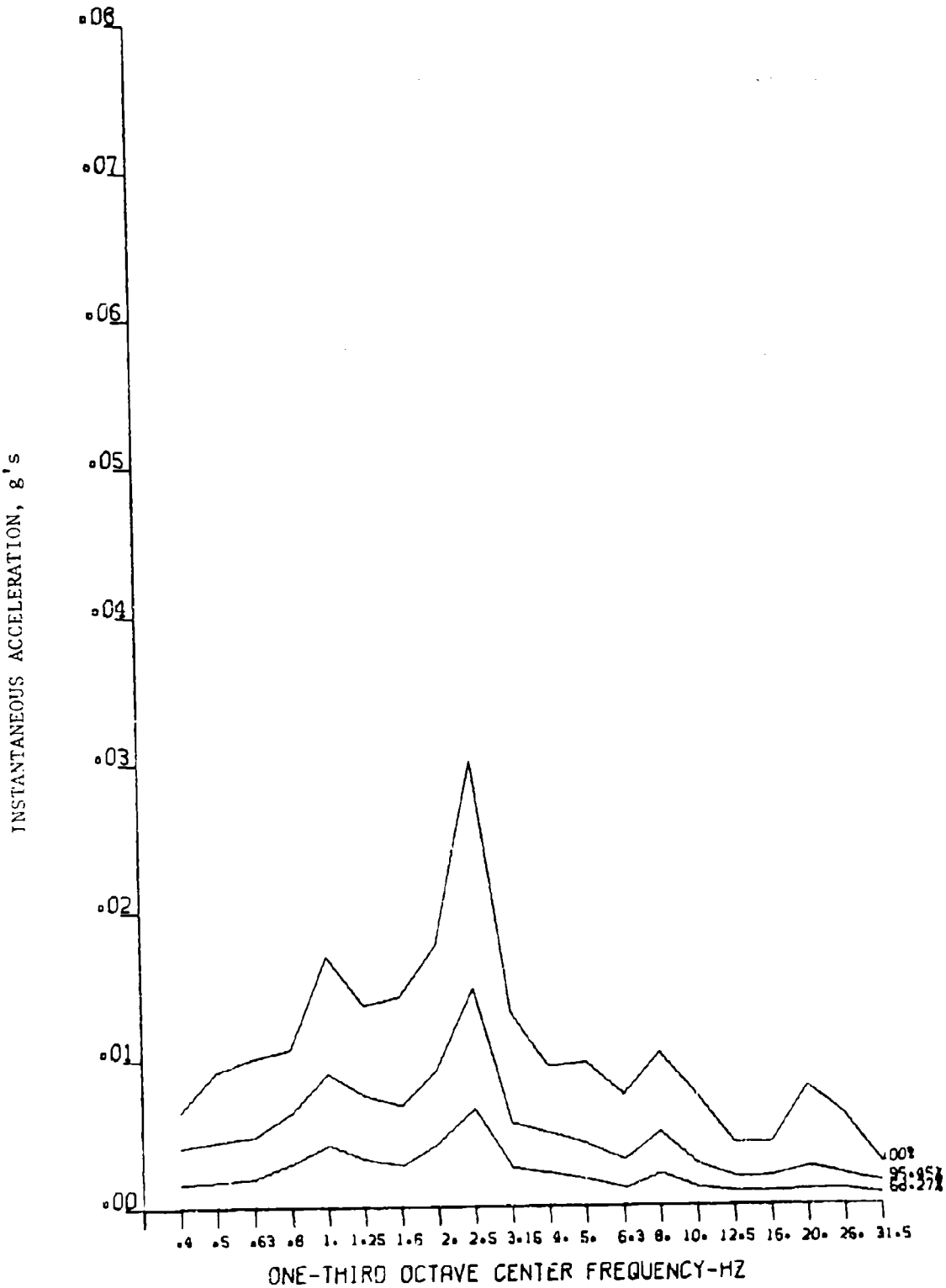

Figure 40. Longitudinal Terrain-Following Acceleration, Right Center Cargo Deck.

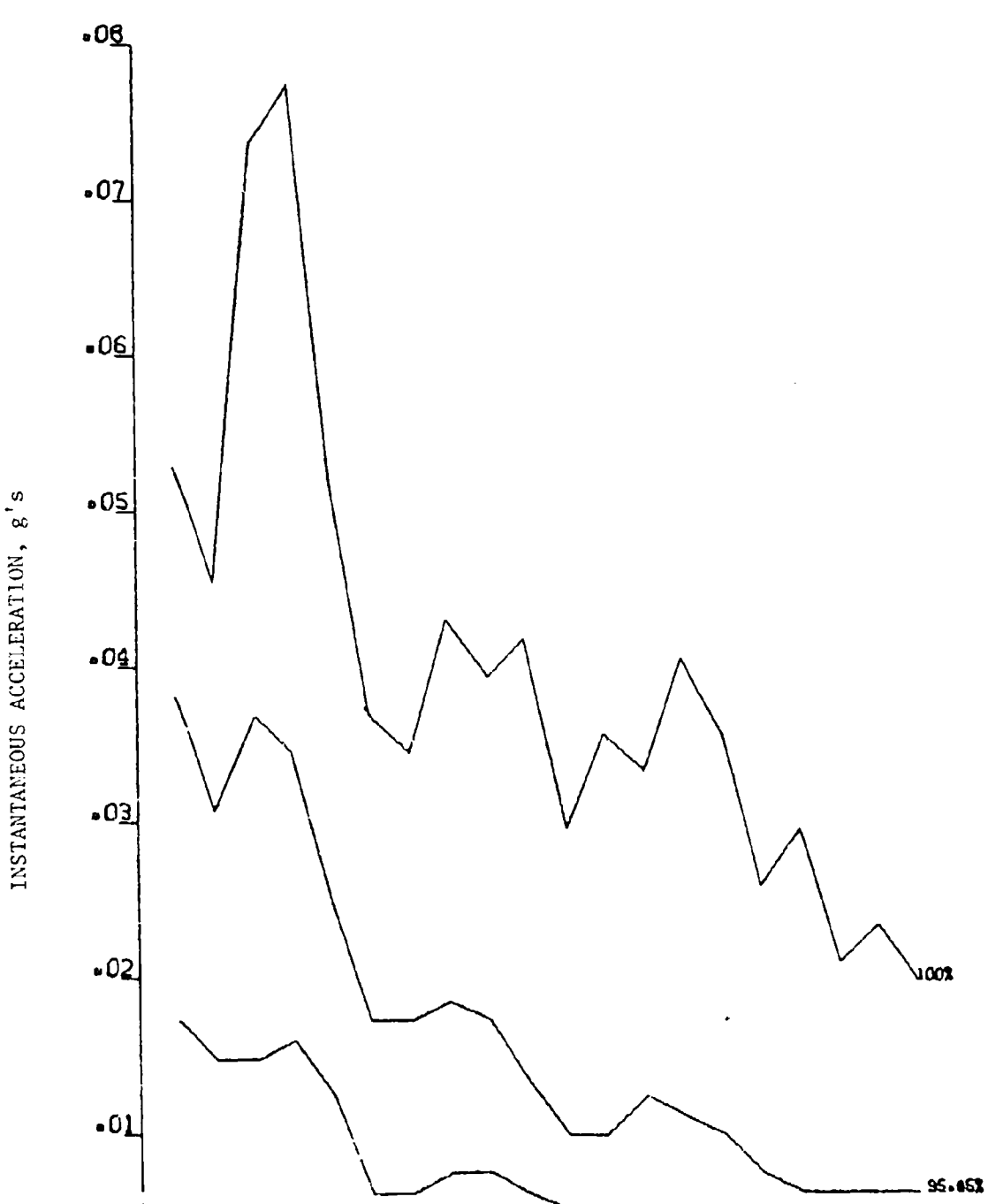

Figure 41. Vertical Terrain-Following Acceleration, Left Center Cargo Deck.

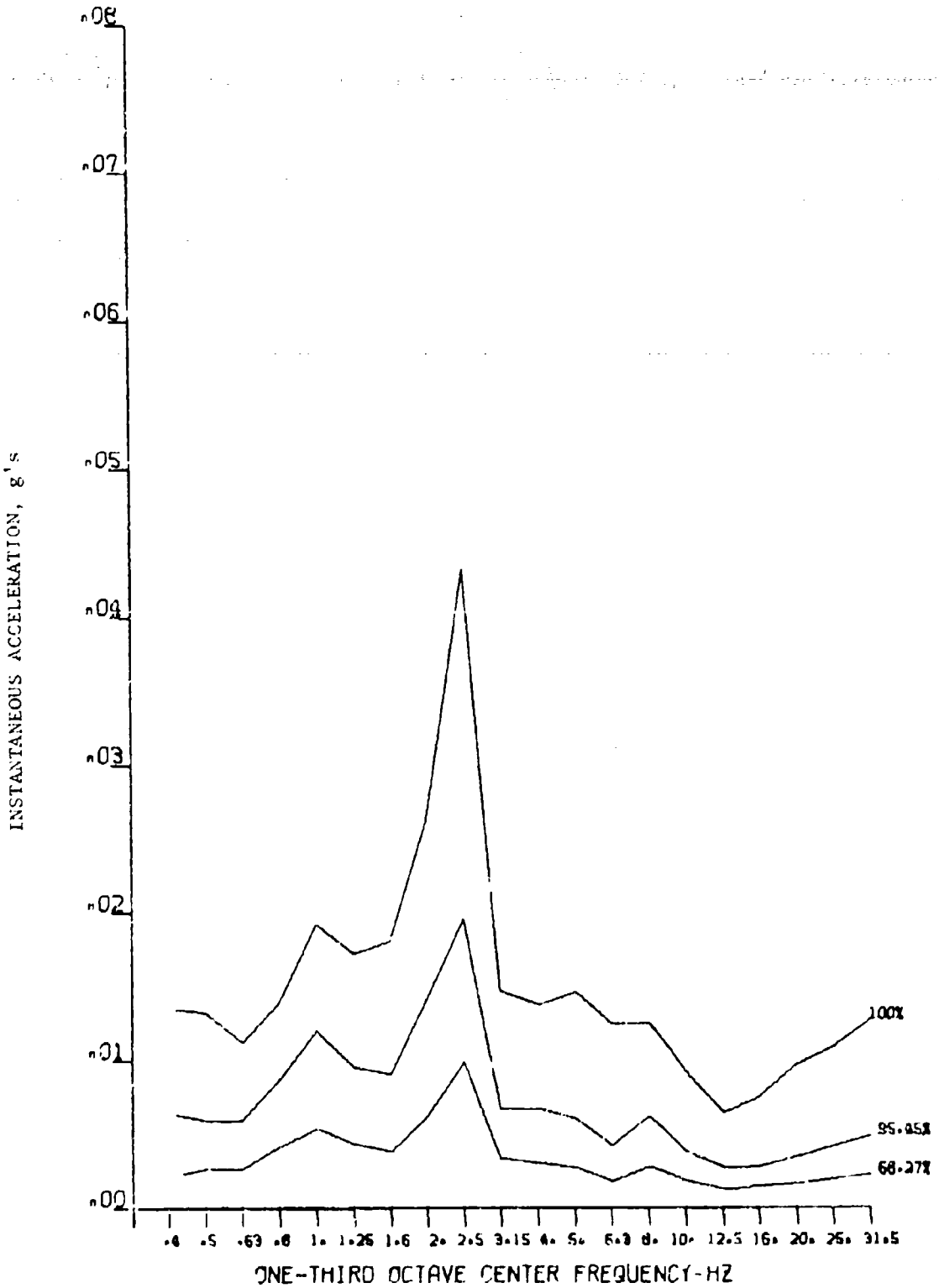

Figure 42. Longitudinal Terrain-Following Acceleration, Left Center Cargo Deck.

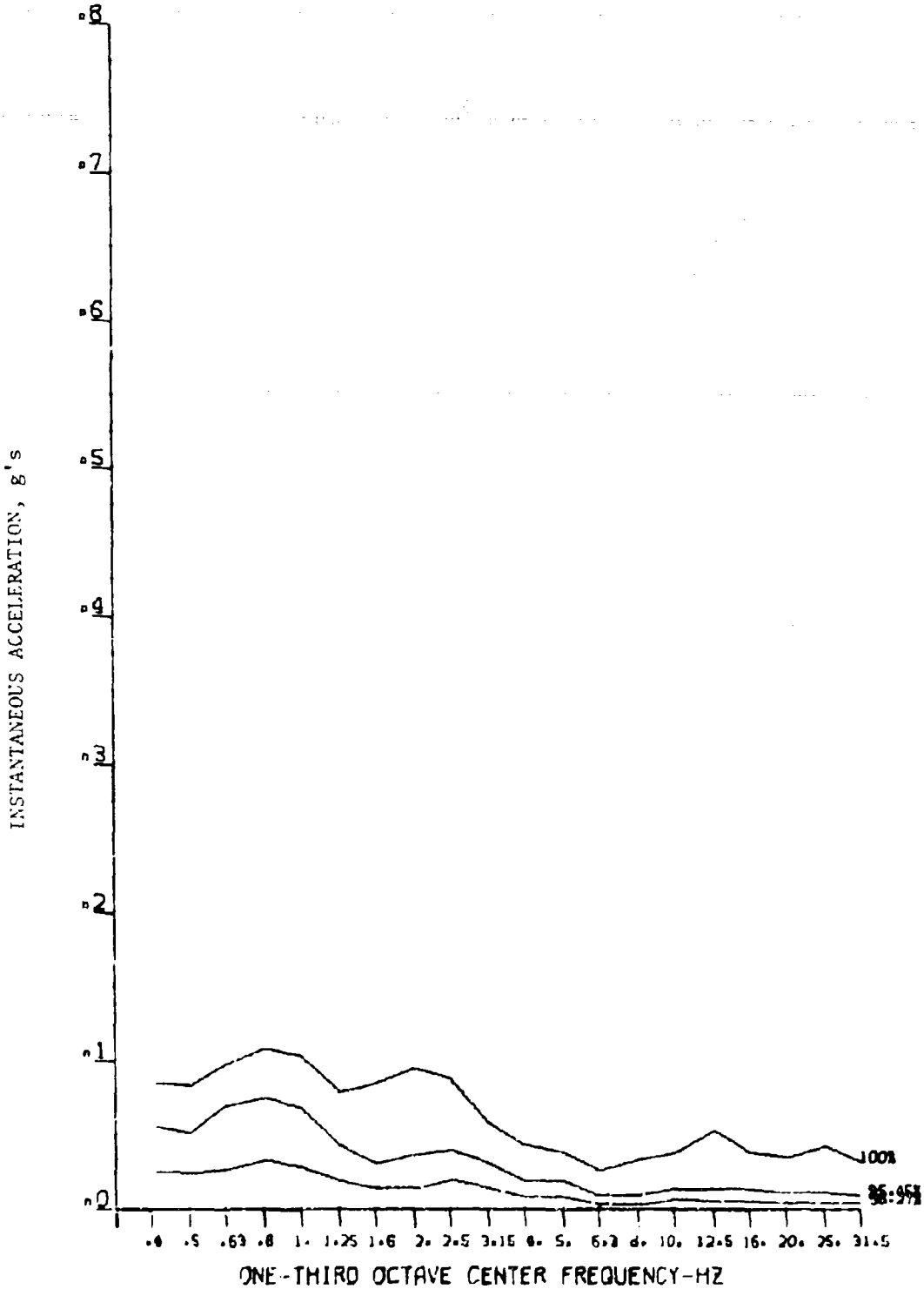

Figure 43. Vertical Terrain-Following Acceleration, Right Rear Cargo Deck.

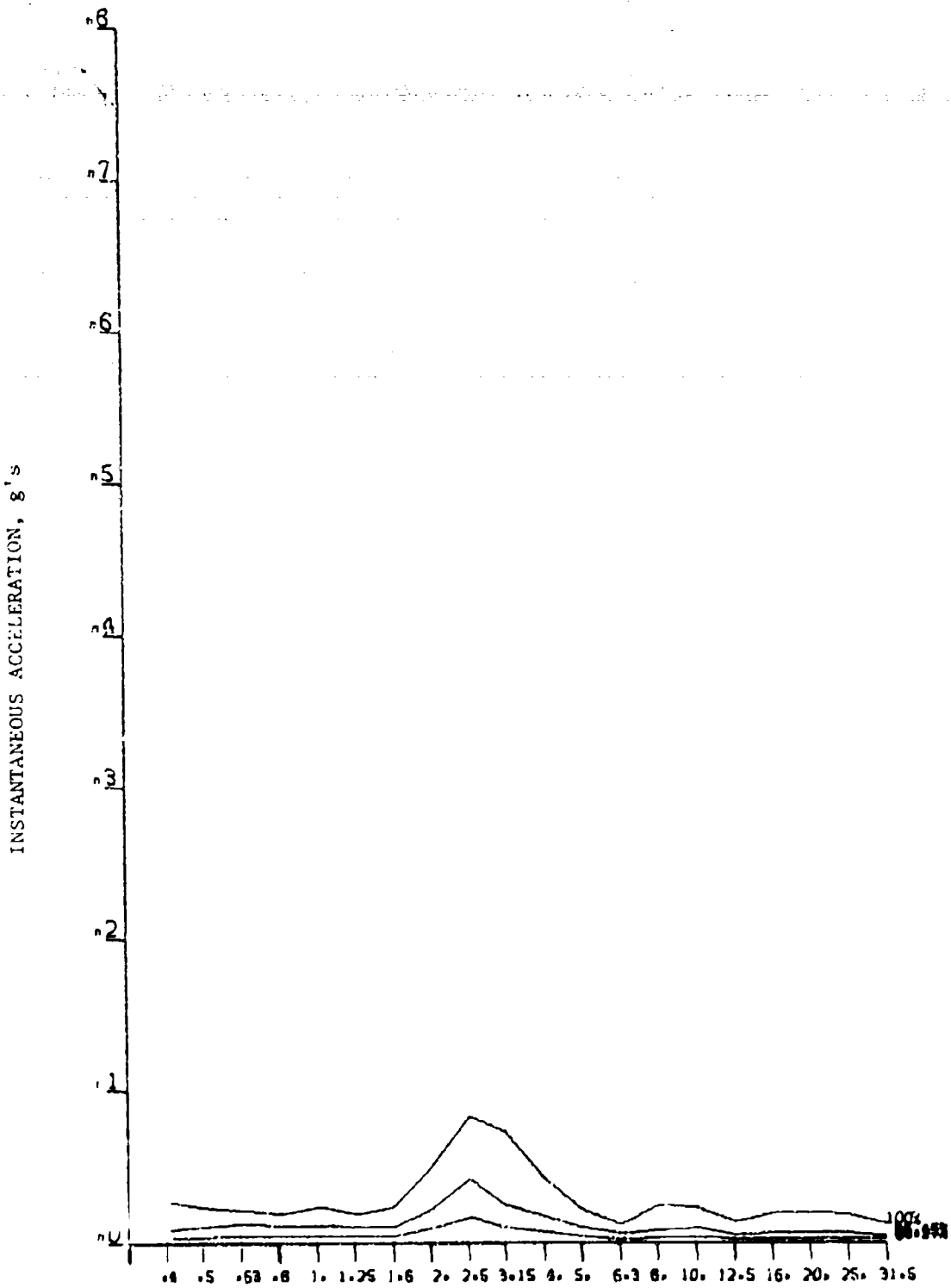

Figure 44. Lateral Terrain-Following Acceleration, Right Rear Cargo Deck.

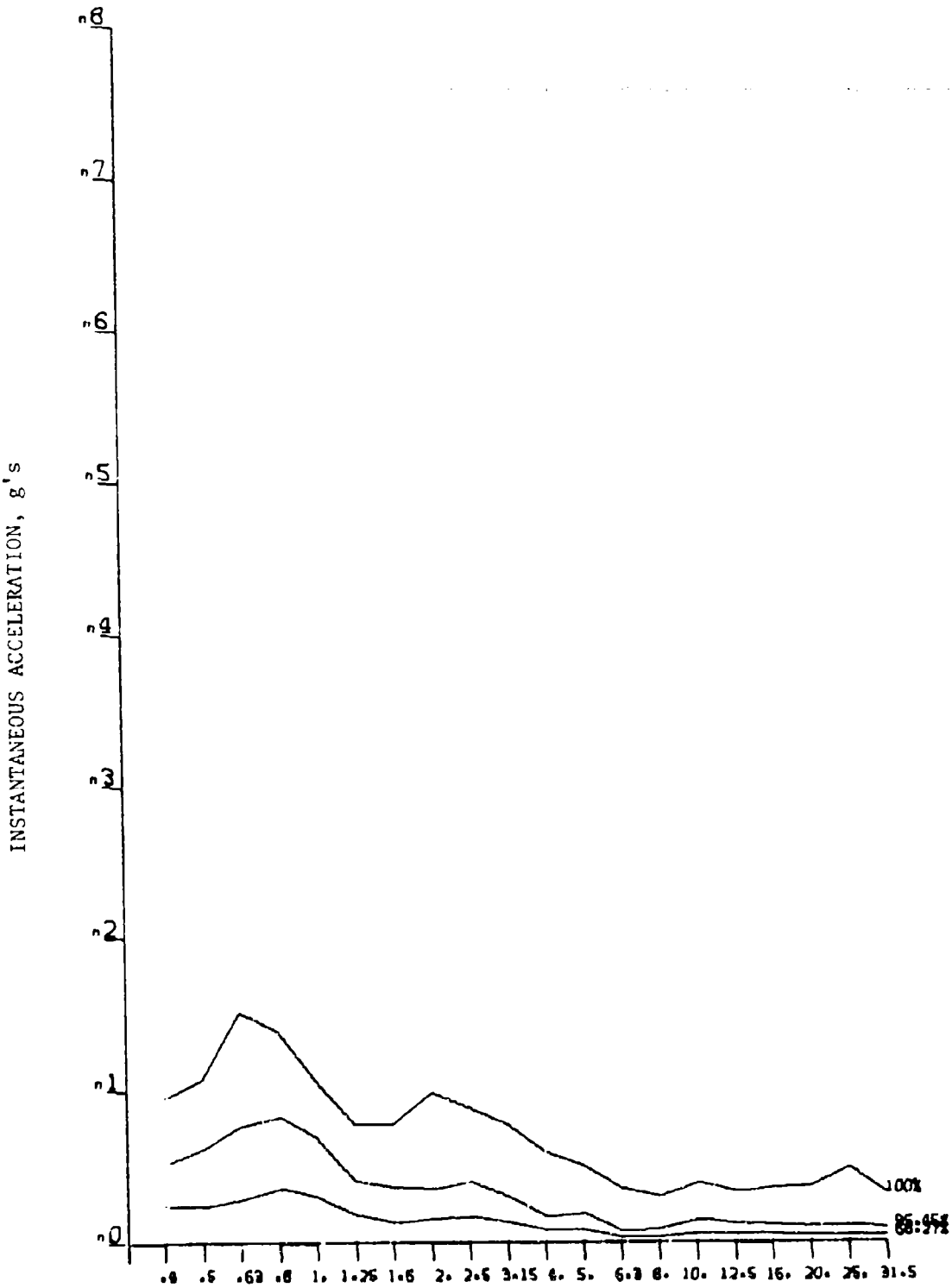

Figure 45. Vertical Terrain-Following Acceleration, Left Rear Cargo Deck.

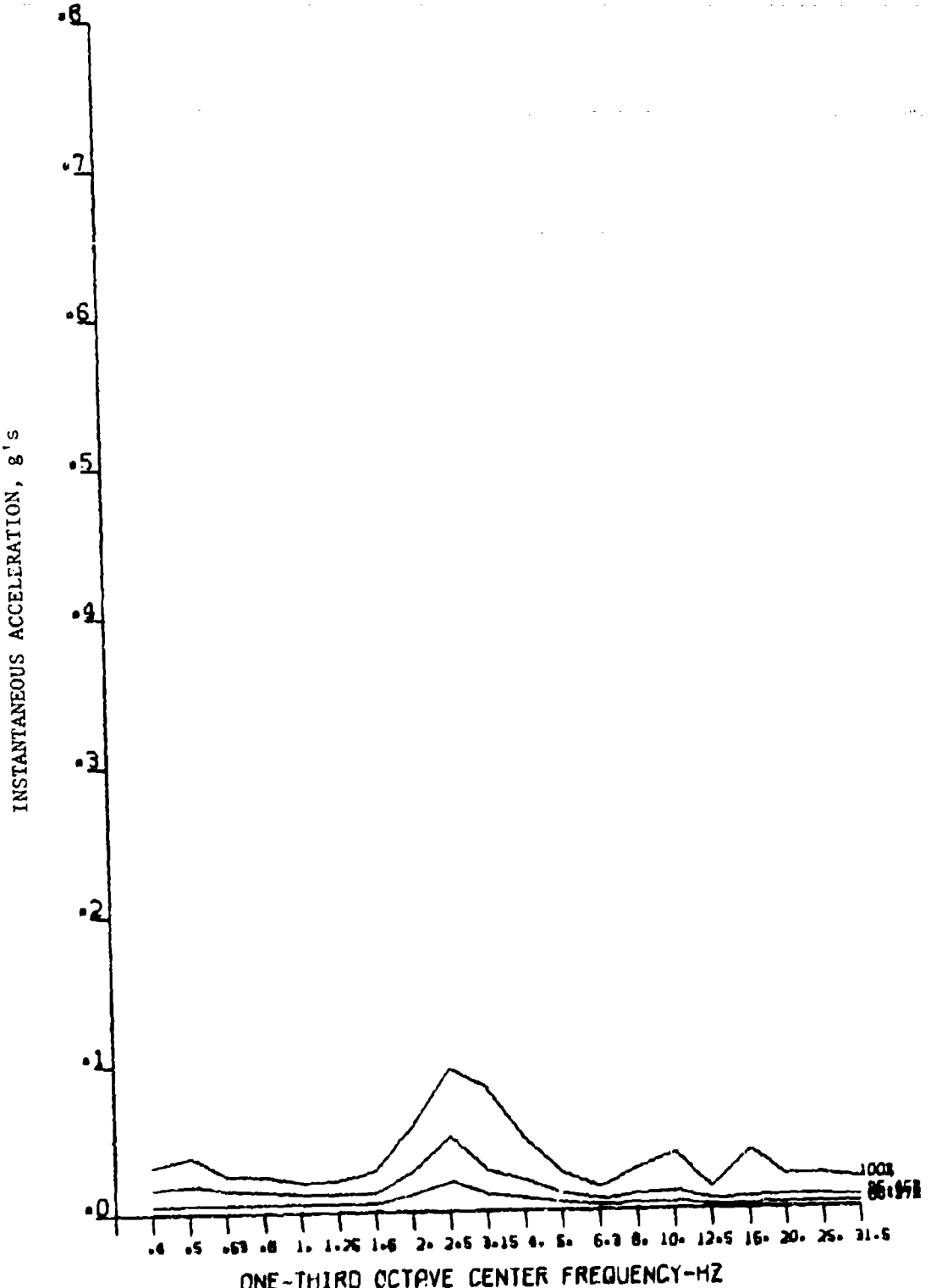

Figure 46. Lateral Terrain-Following Acceleration, Left Rear Cargo Deck.

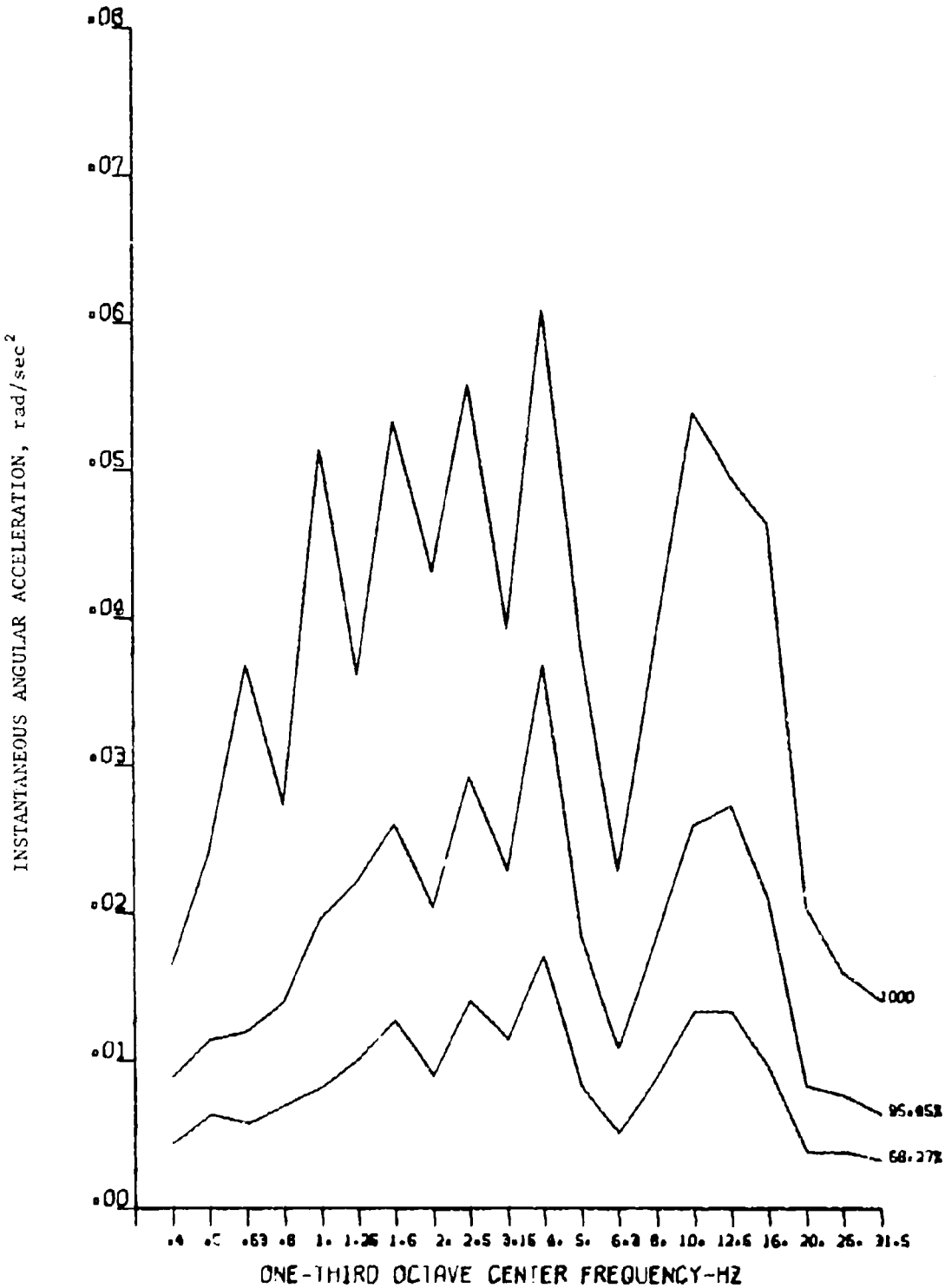

Figure 47. Roll Angular Acceleration During Terrain Following.

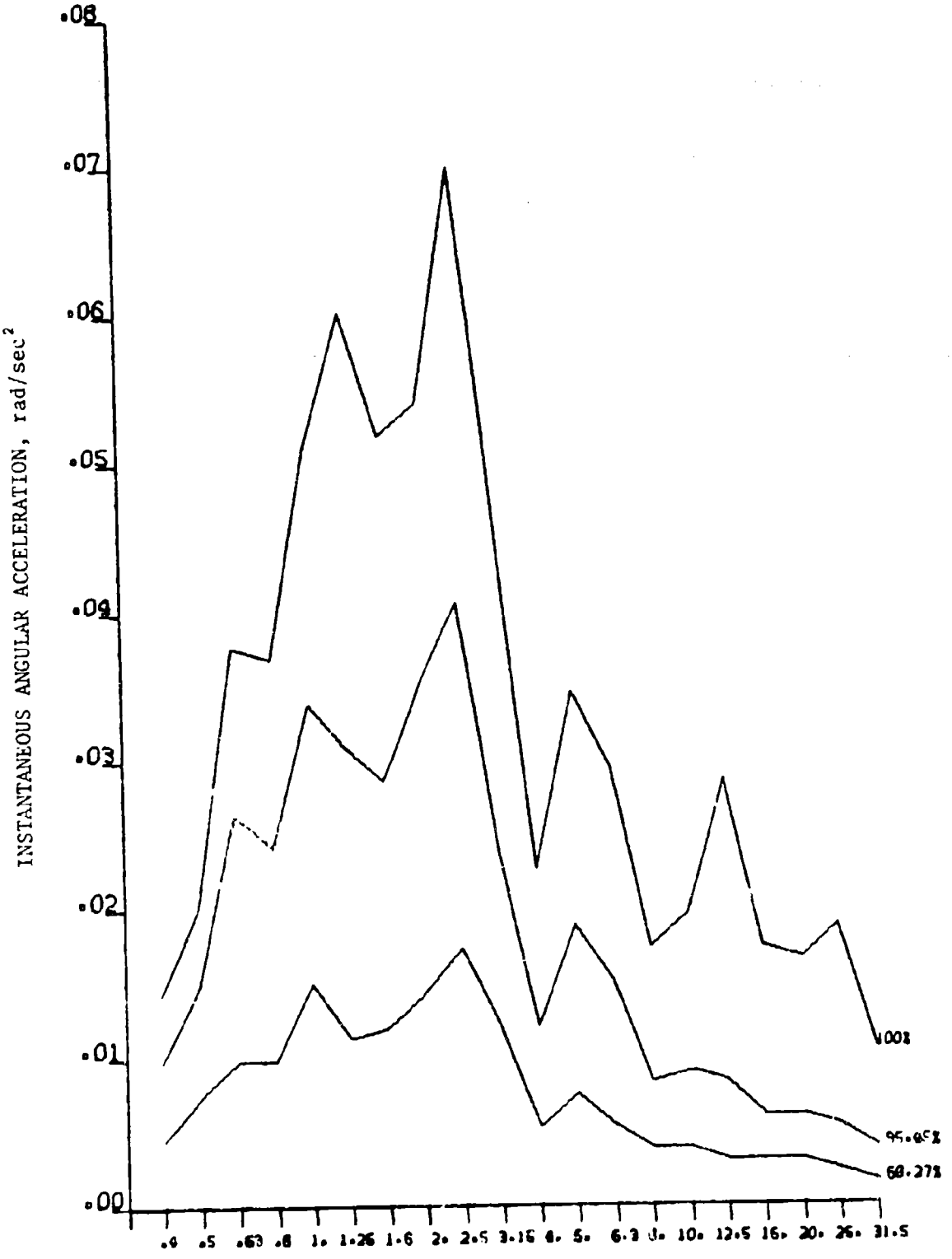

Figure 48. Pitch Angular Acceleration During Terrain Following.

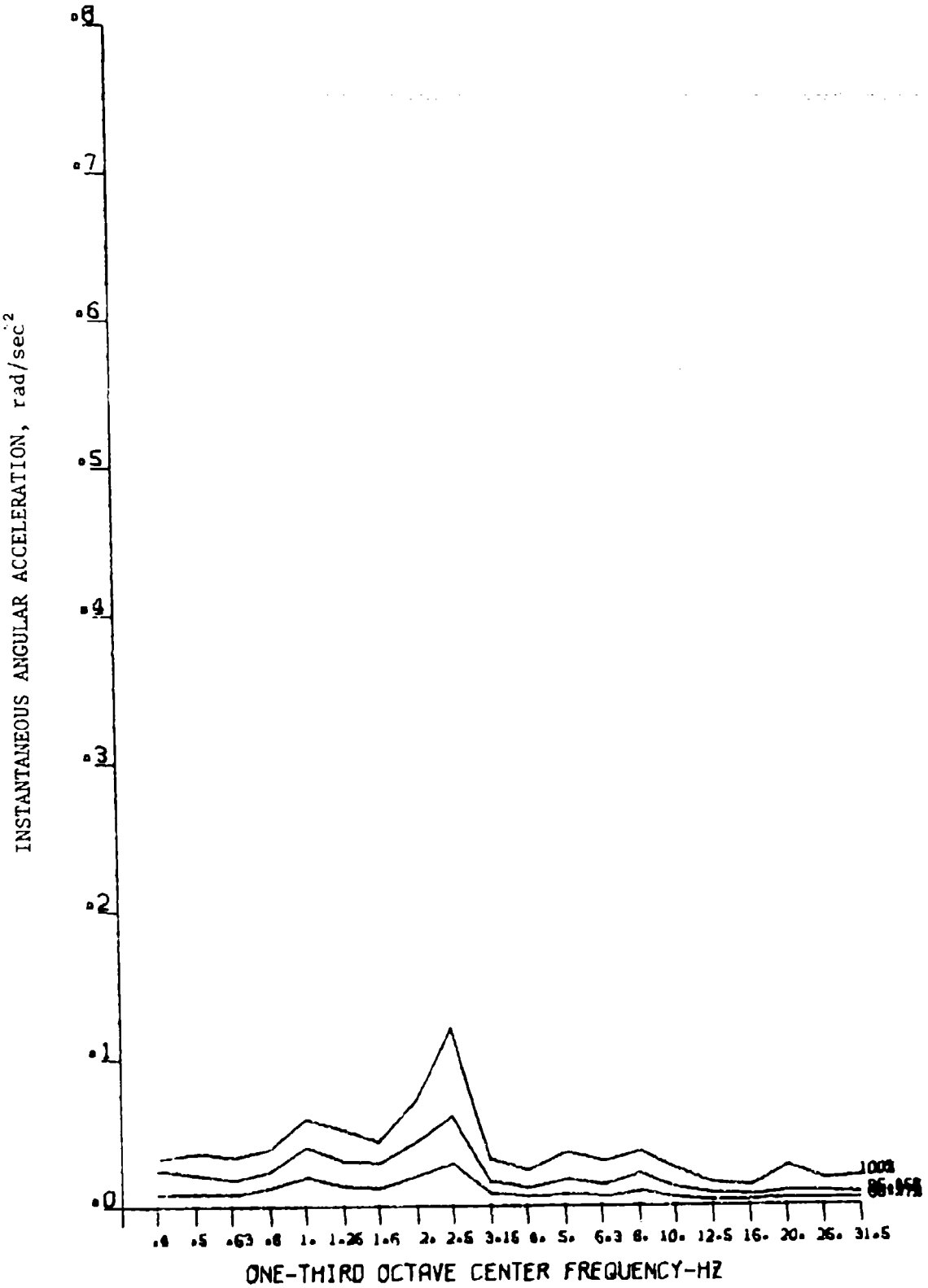

Figure 49. Yaw Angular Acceleration During Terrain Following.

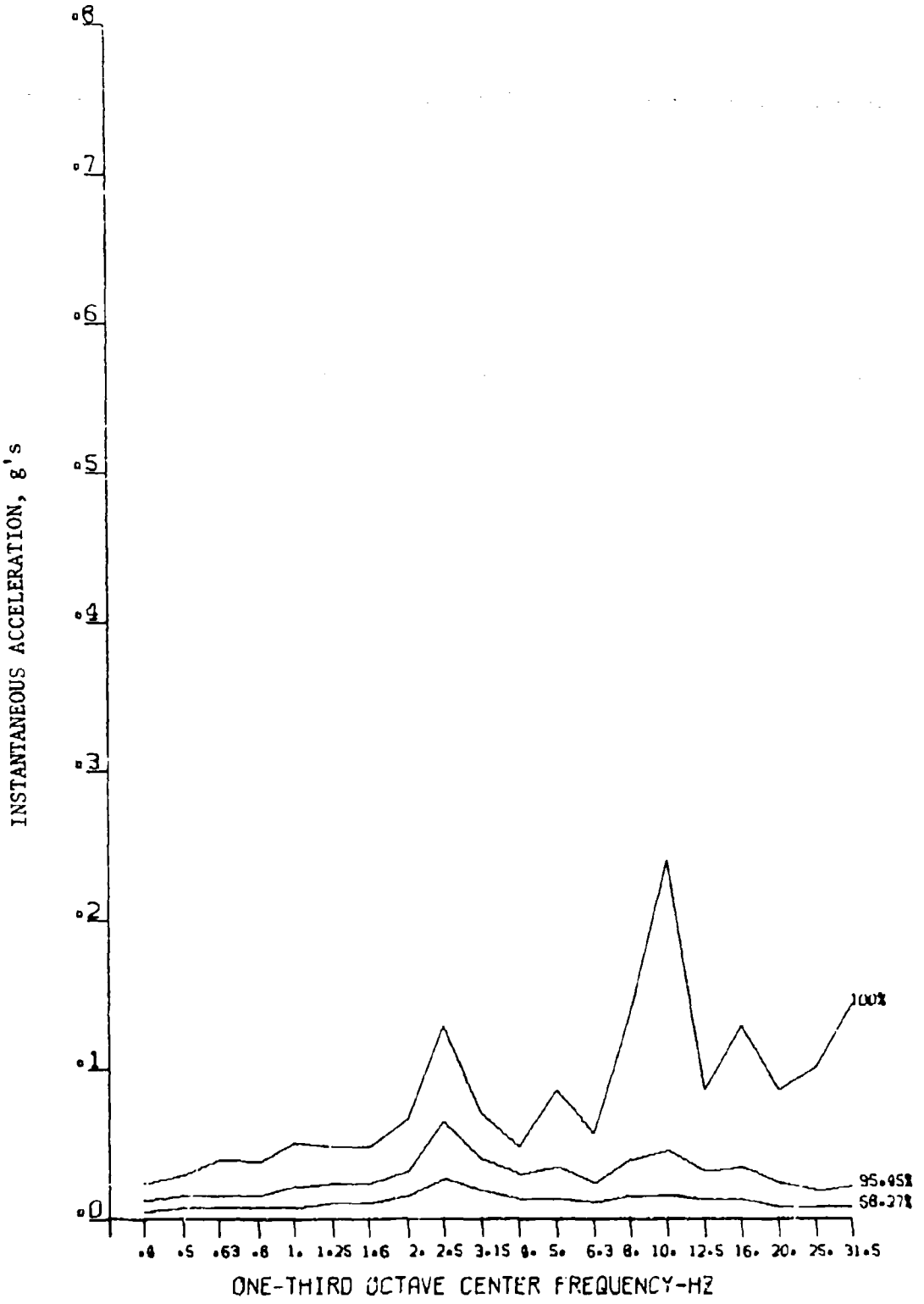

Figure 50. Vertical Landing Acceleration, Right Front Cargo Deck.

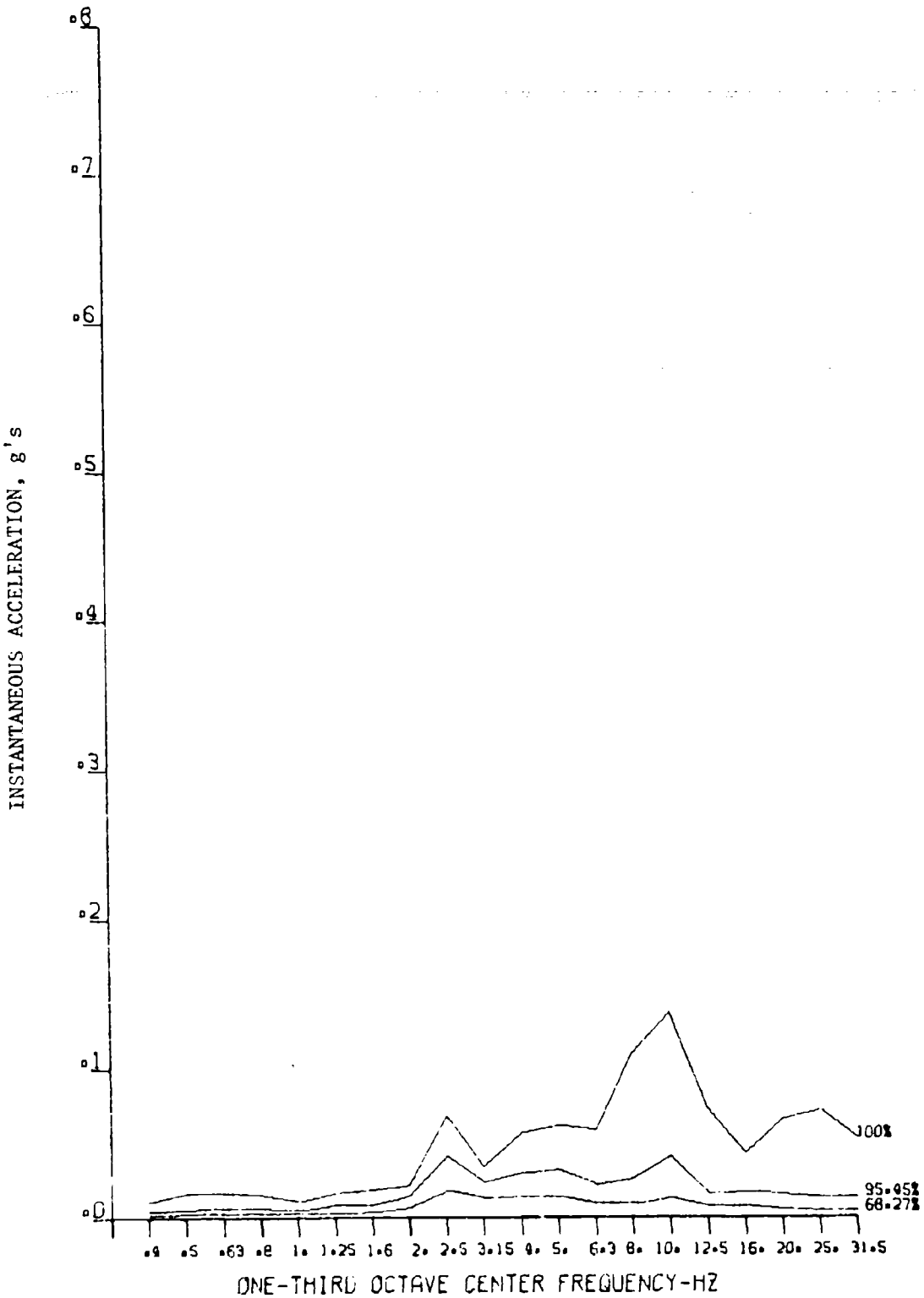

Figure 51. Lateral Landing Acceleration, Right Front Cargo Deck.

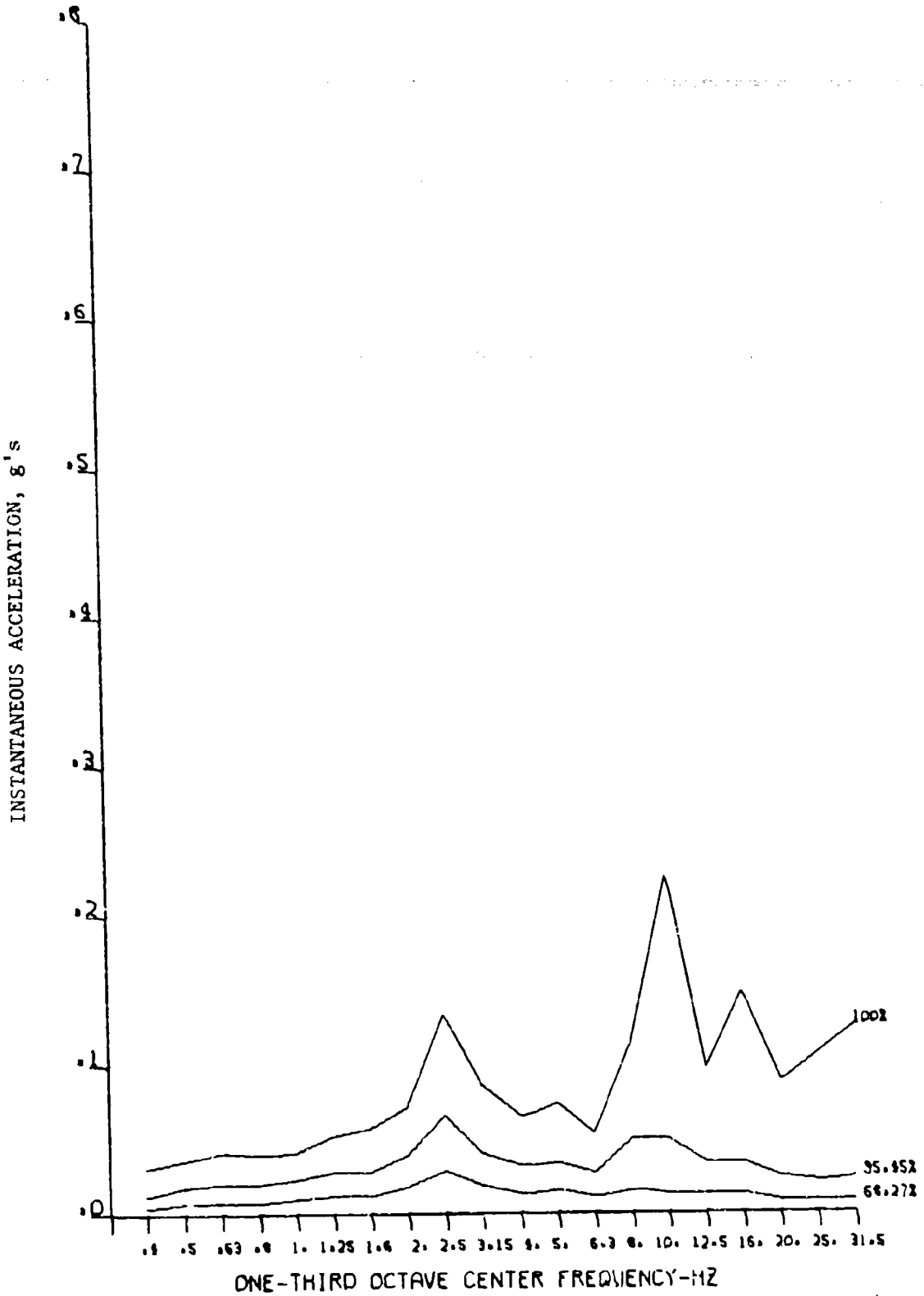

Figure 52. Vertical Landing Acceleration, Left Front Cargo Deck.

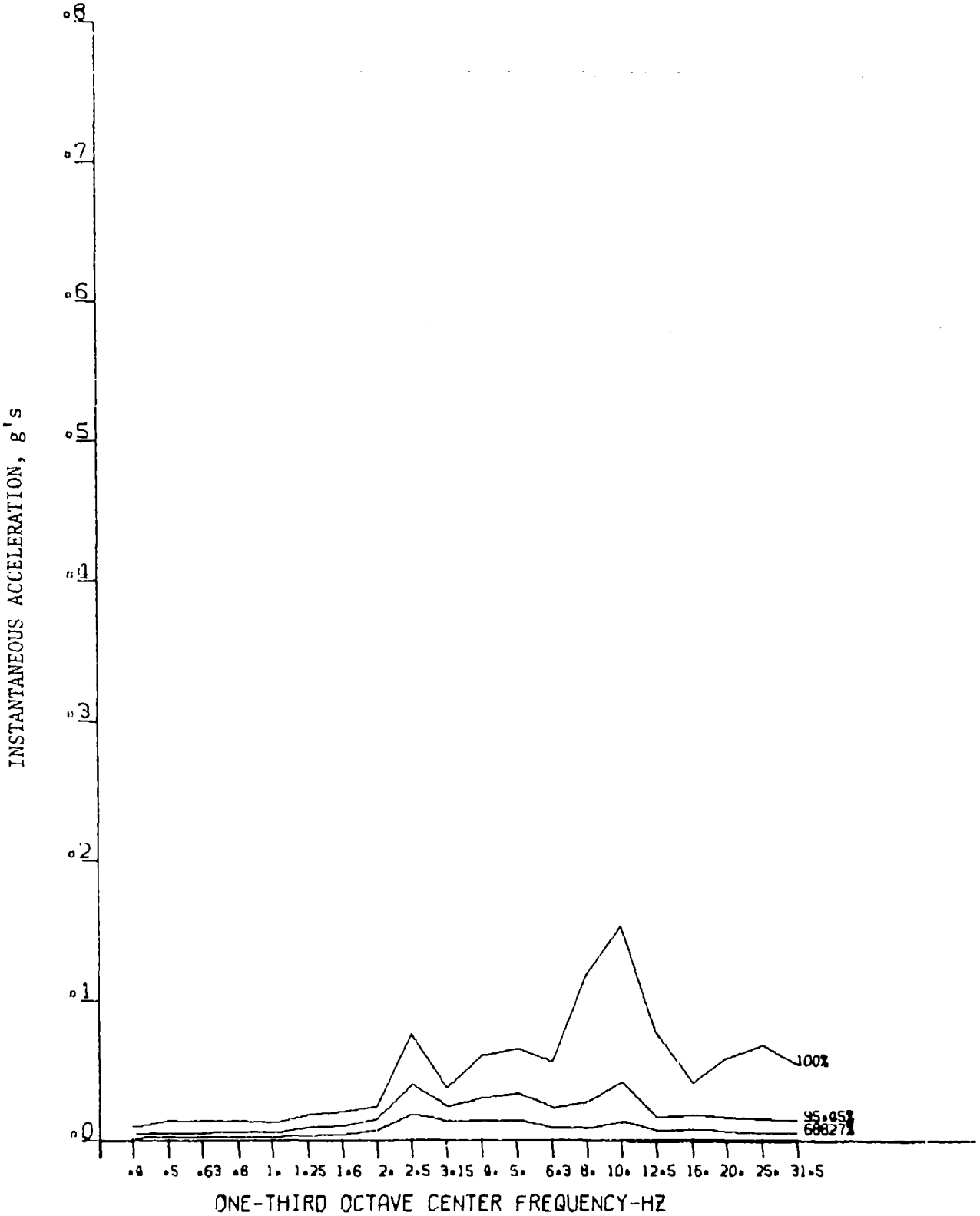

Figure 53. Lateral Landing Acceleration, Left Front Cargo Deck.

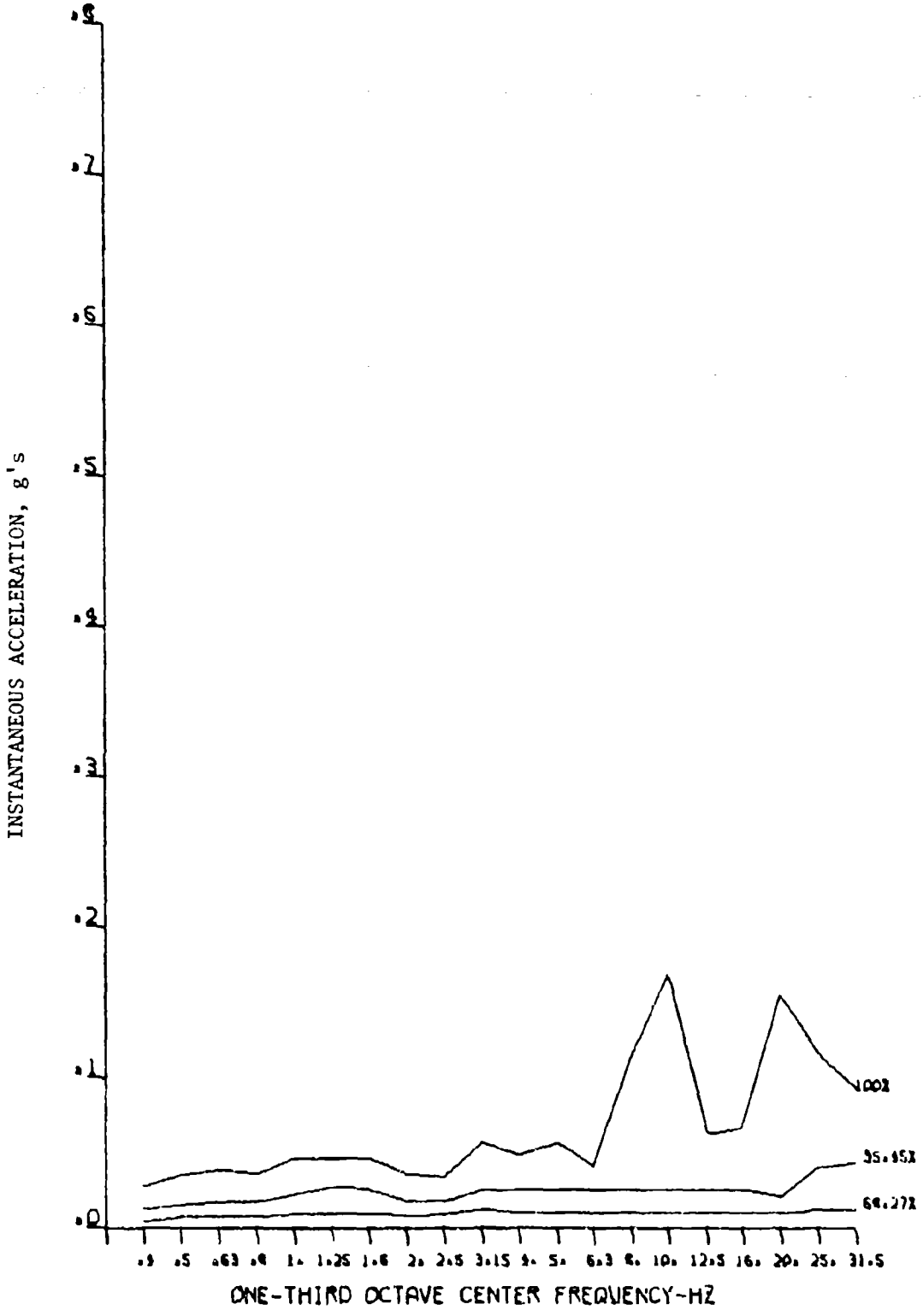

Figure 54. Vertical Landing Acceleration, Right Center Cargo Deck.

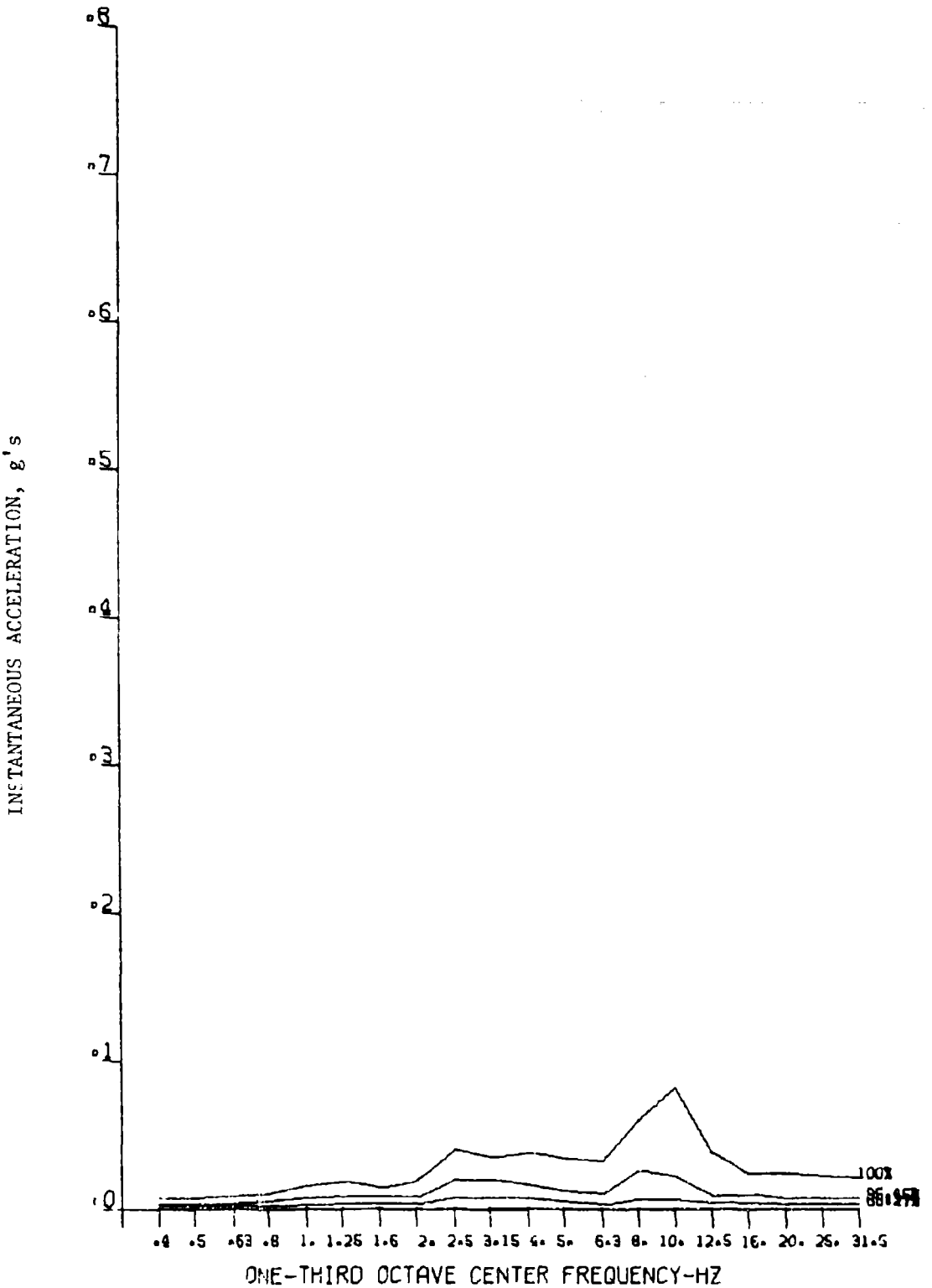

Figure 55. Longitudinal Landing Acceleration, Right Center Cargo Deck.

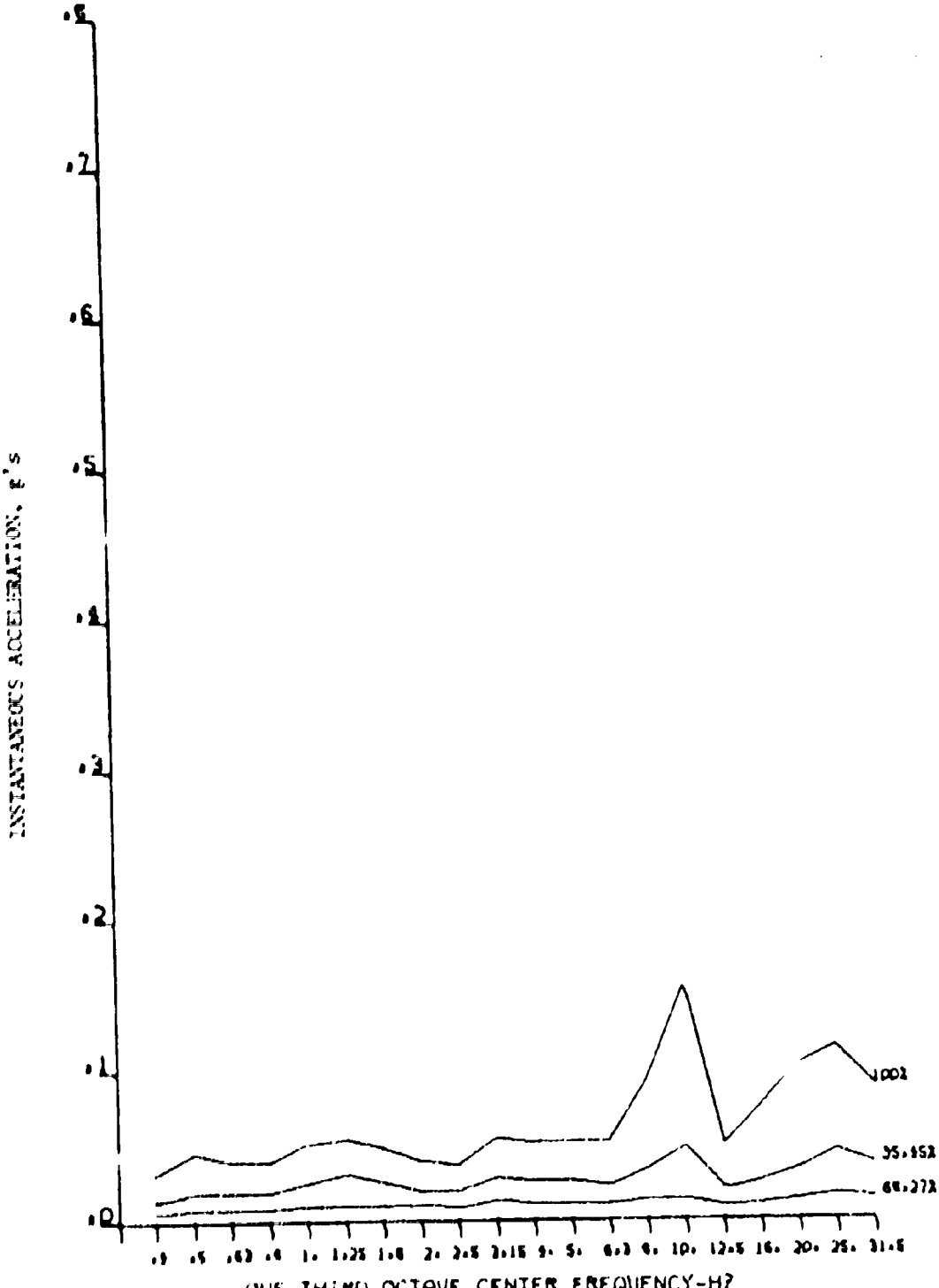

Figure 56. Vertical Landing Acceleration, Left Center Cargo Deck.

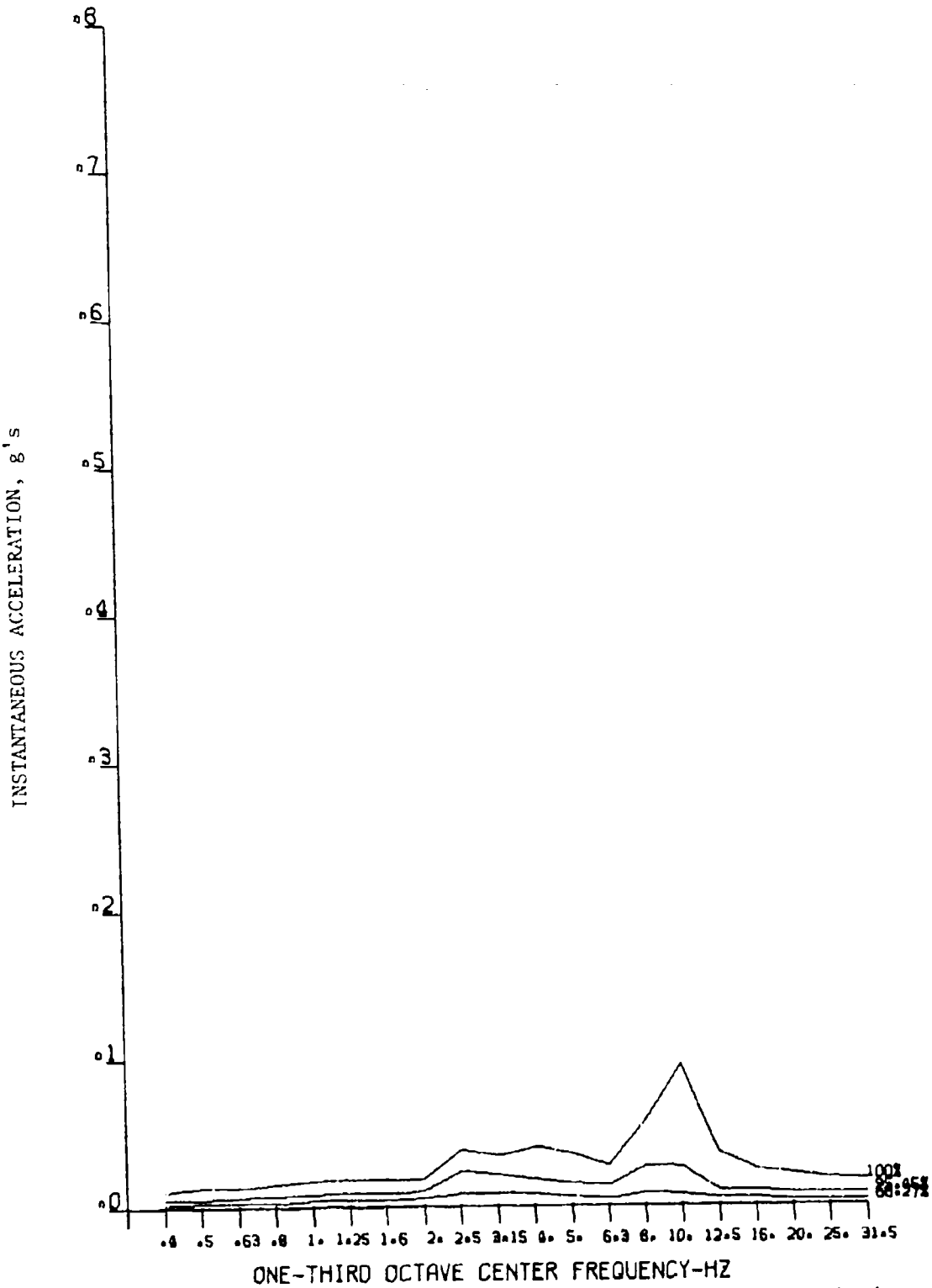

Figure 57. Longitudinal Landing Acceleration, Left Center Cargo Deck.

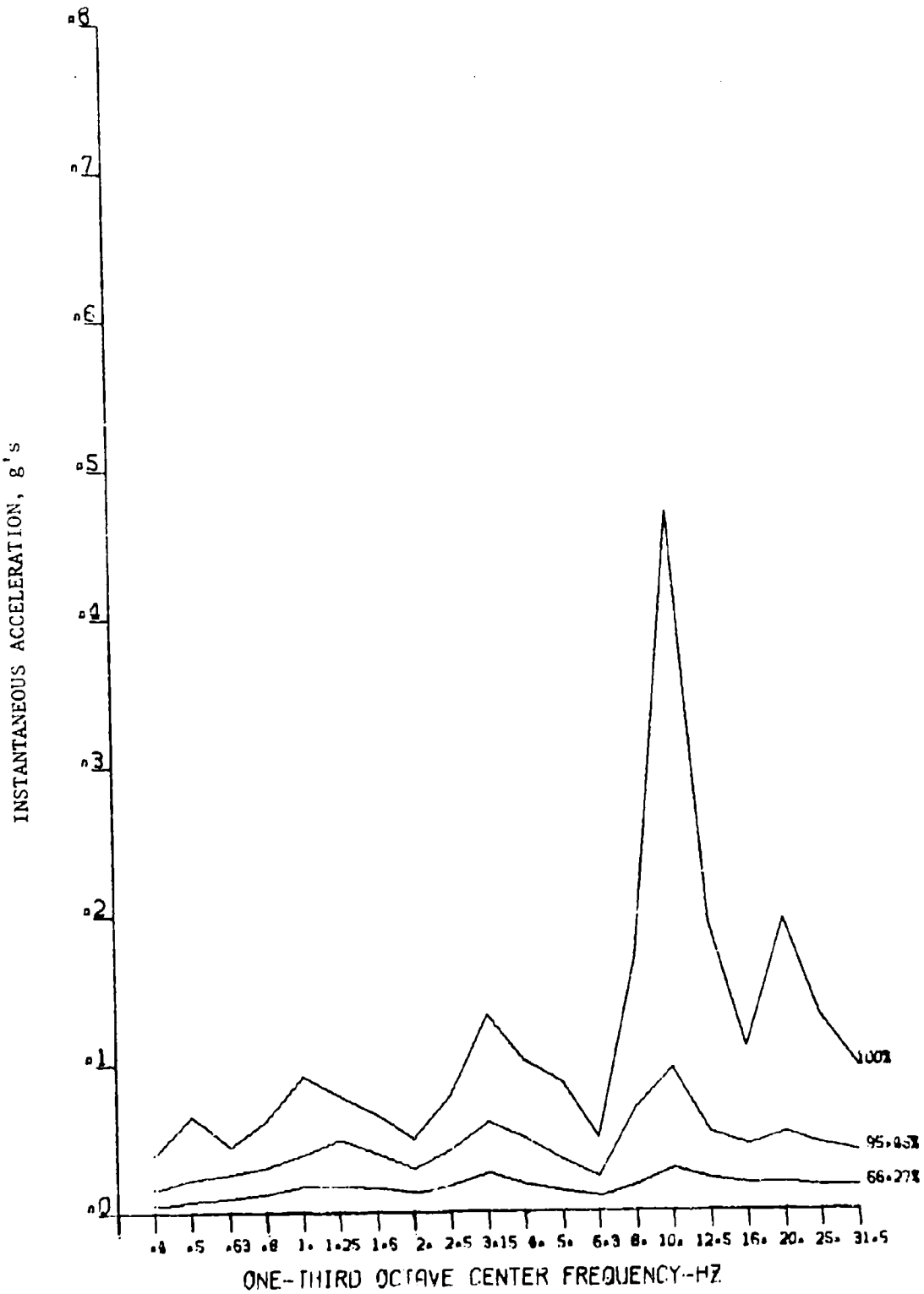

Figure 58. Vertical Landing Acceleration, Right Rear Cargo Deck.

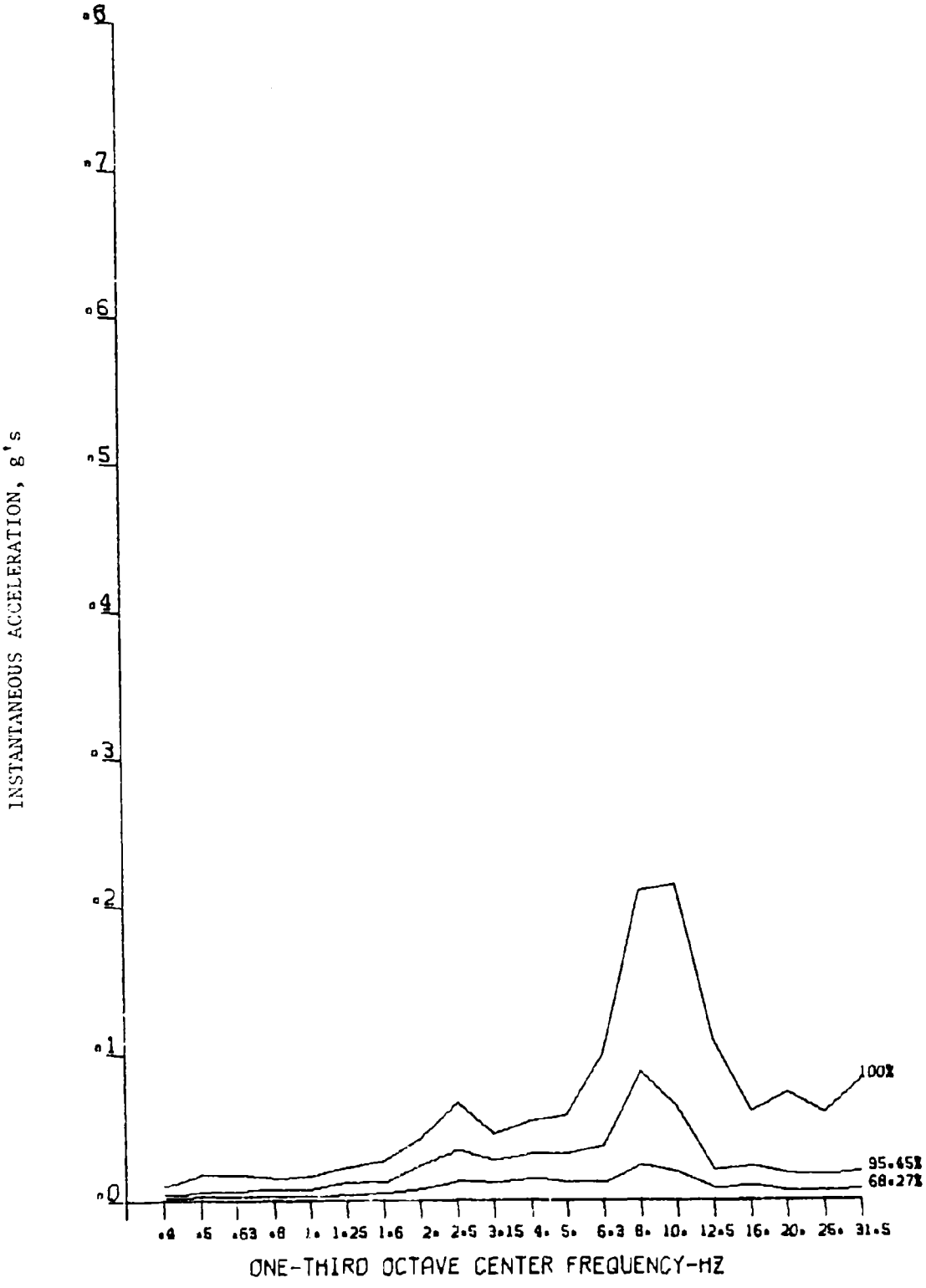

Figure 59. Lateral Landing Acceleration, Right Rear Cargo Deck.

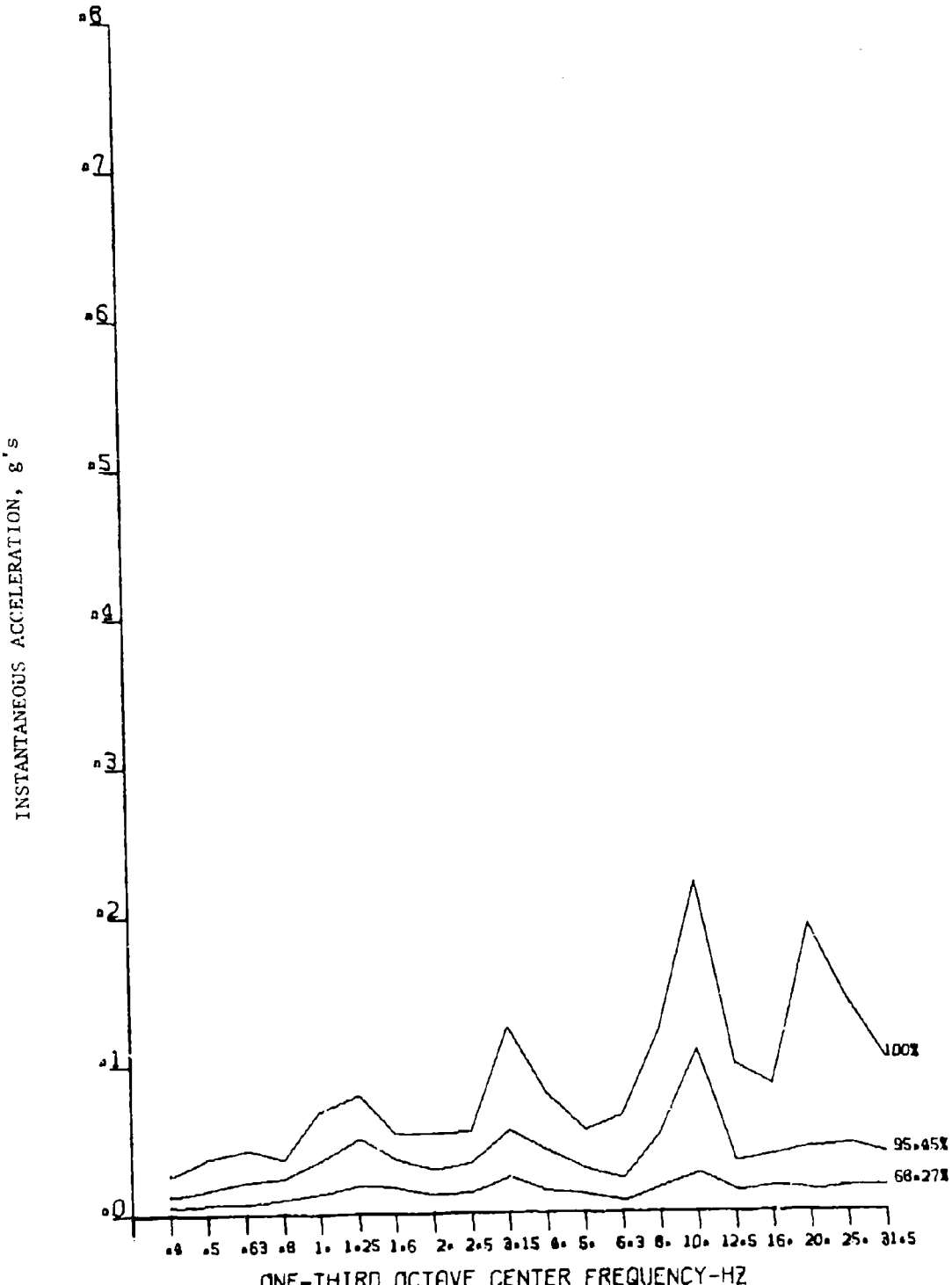

Figure 60. Vertical Landing Acceleration, Left Rear Cargo Deck.

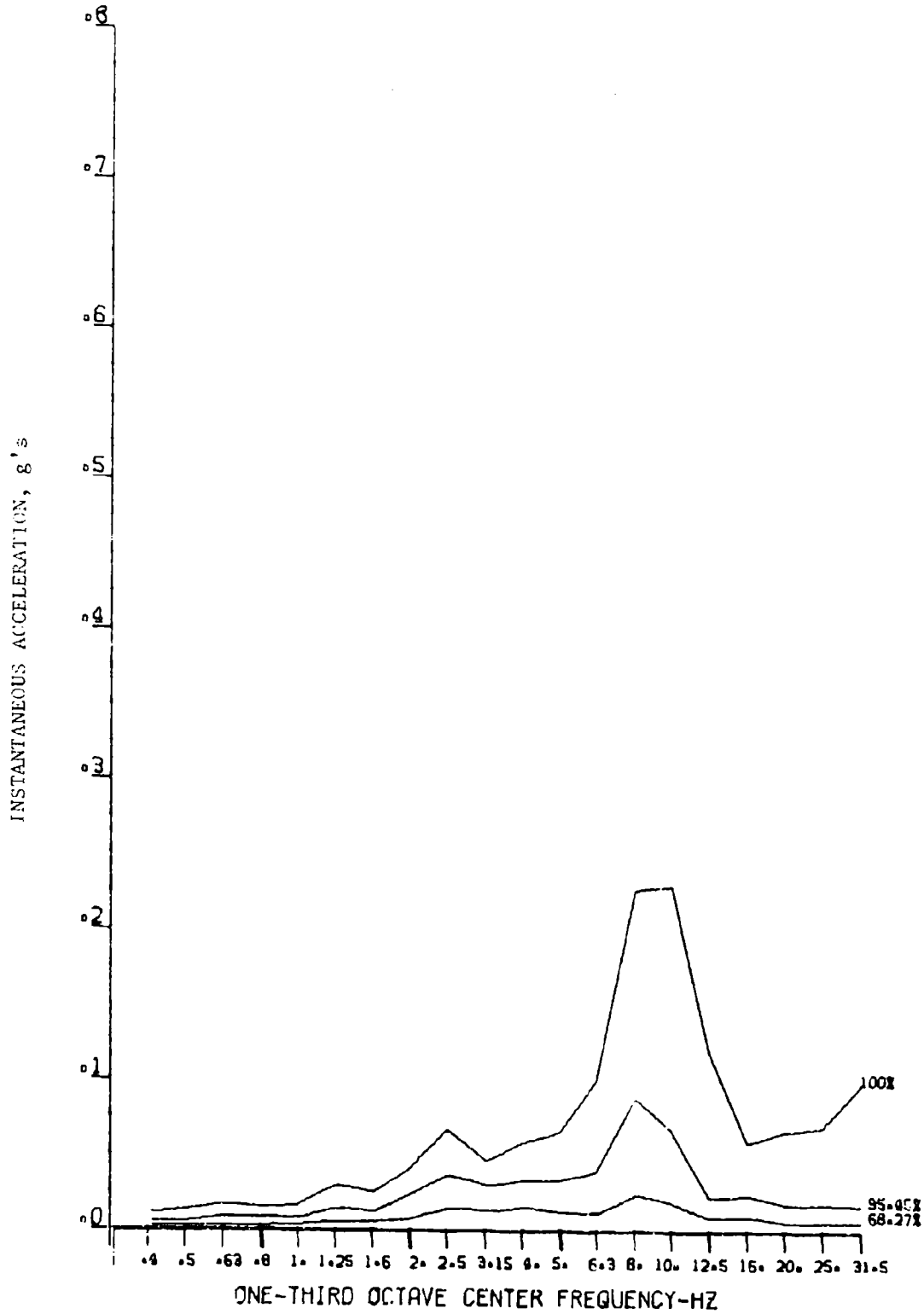

Figure 61. Lateral Landing Acceleration, Left Rear Cargo Deck.

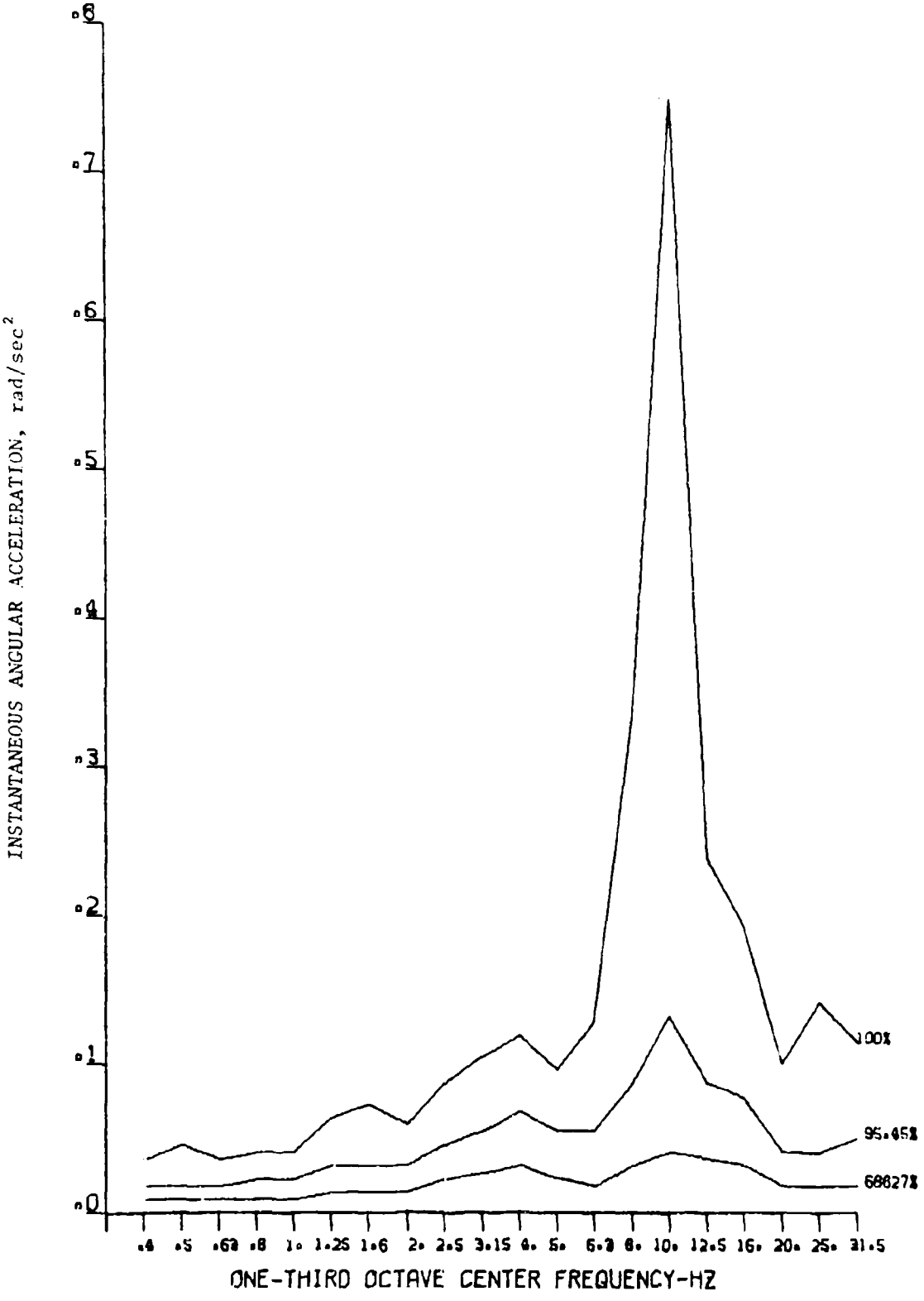

Figure 62. Roll Angular Acceleration During Landing.

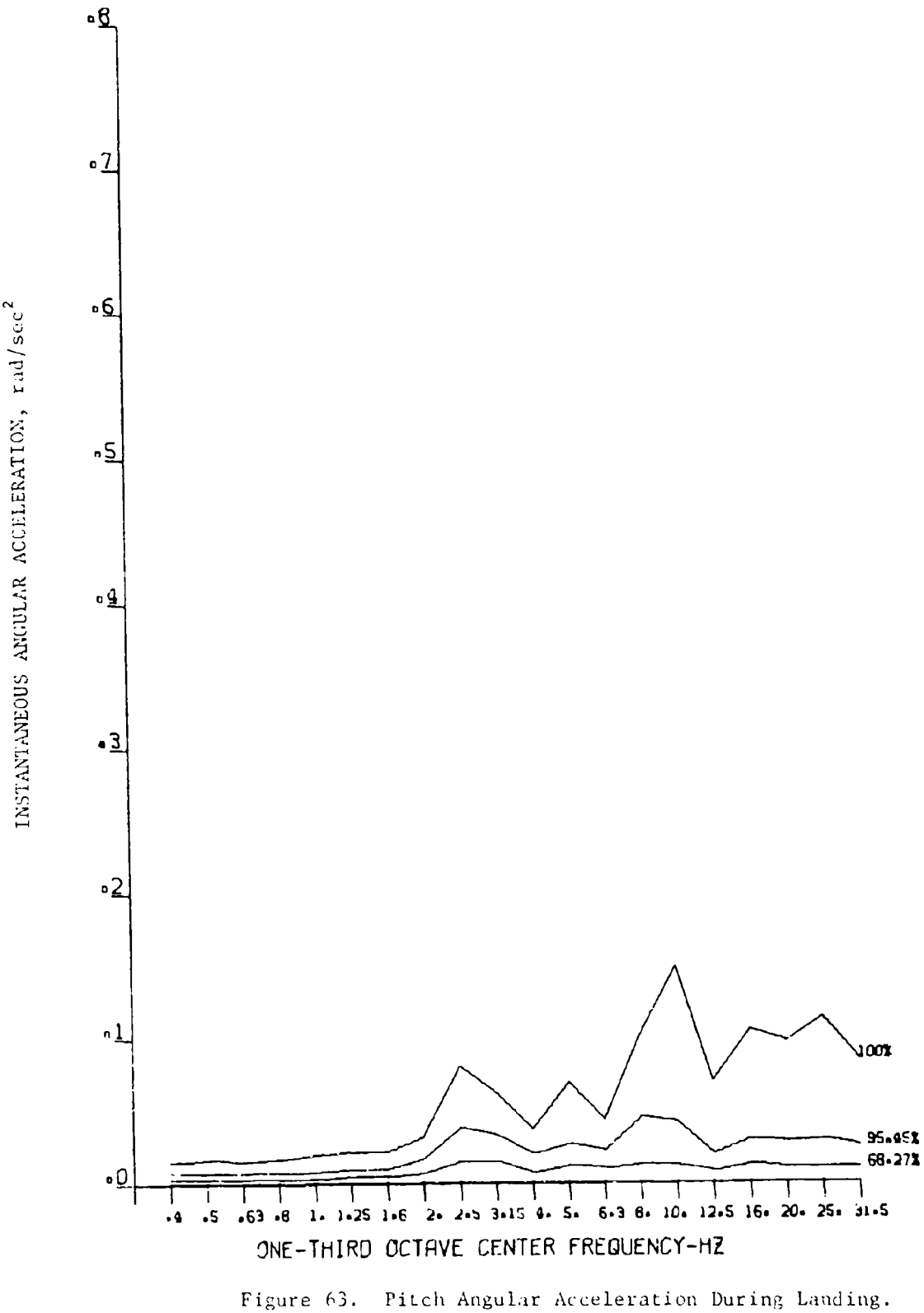

Figure 63. Pitch Angular Acceleration During Landing.

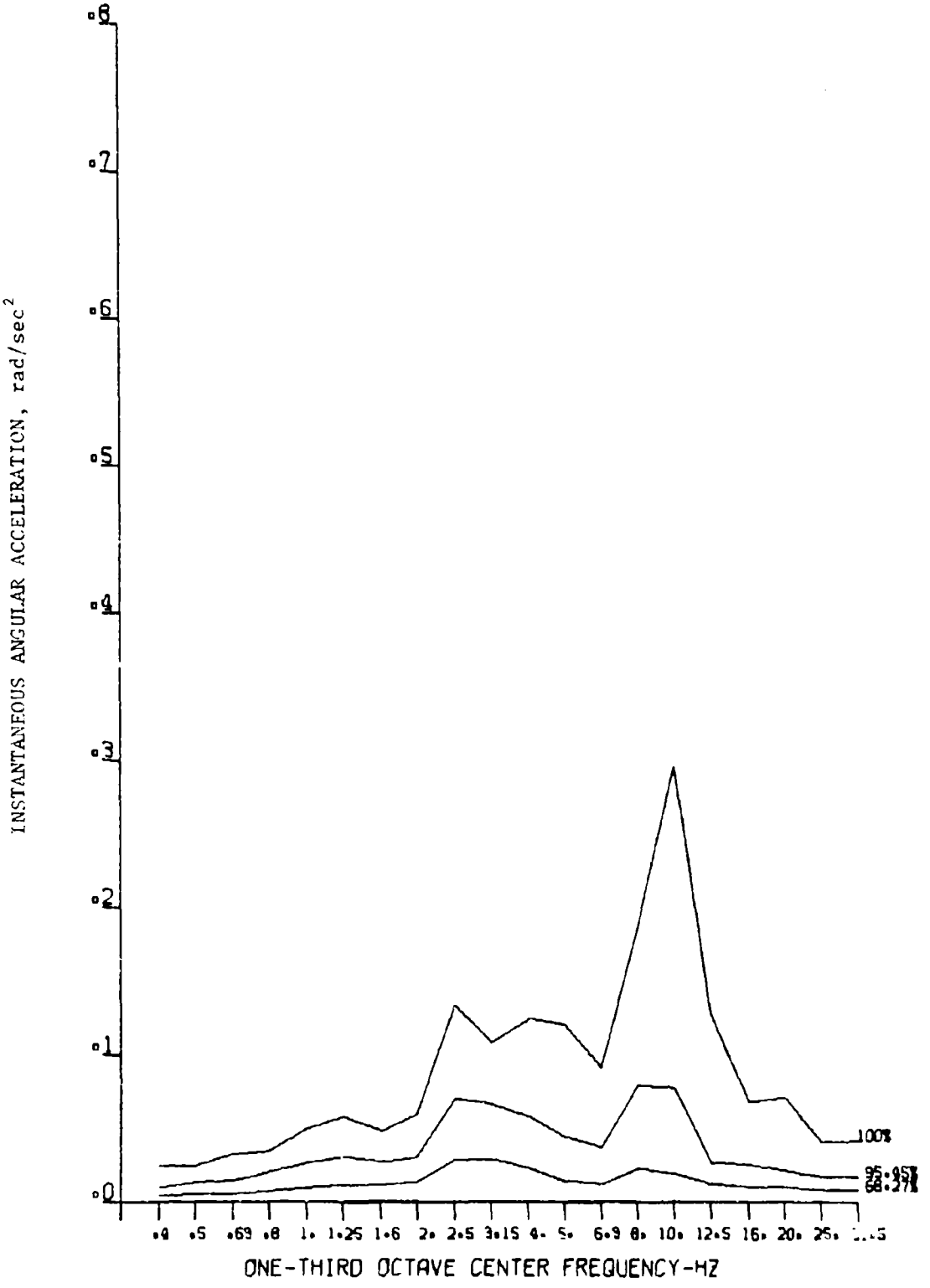

Figure 64. Yaw Angular Acceleration During Landing.

Table 1. PEAK VERTICAL LANDING ACCELERATIONS, RIGHT FRONT CARGO DECK

Landing Number	Maximum Instantaneous Acceleration, (g)		
	8 Hz Band	10 Hz Band	12.5 Hz Band
1	0.043	0.038	0.051
2	.032	.038	.048
3	.051	.078	.067
4	.030	.032	.054
5	.089	.097	.089
6	.070	.118	.124
7	.013	.226	.092
8	.094	.094	.057
9	.097	.121	.094
10	.078	.070	.097
11	.083	.070	.089
12	.043	.073	.089
13	.054	.070	.075
14	.059	.043	.067
15	.065	.062	.083
16	.051	.059	.065
17	.073	.083	.118
18	.083	.081	.065
19	.038	.046	.089
20	.065	.075	.075
21	.132	.116	.073
22	.073	.129	.067
23	.062	.057	.078
24	.043	.046	.038
25	.113	.132	.067
26	.057	.059	.059
27	.057	.067	.059

Table 3. PEAK VERTICAL LANDING ACCELERATIONS, LEFT FRONT CARGO DECK

Landing Number	Maximum Instantaneous Acceleration, (g)		
	8 Hz Band	10 Hz Band	12.5 Hz Band
1	0.045	0.048	0.053
2	.053	.045	.048
3	.034	.074	.064
4	.029	.029	.045
5	.069	.082	.103
6	.077	.156	.135
7	.119	.233	.074
8	.101	.095	.125
9	.066	.111	.066
10	.061	.053	.074
11	.109	.127	.106
12	.098	.106	.090
13	.085	.045	.077
14	.042	.058	.050
15	.077	.064	.048
16	.117	.098	.069
17	.058	.053	.114
18	.093	.090	.098
19	.034	.045	.114
20	.056	.056	.066
21	.082	.109	.069
22	.032	.090	.045
23	.058	.040	.058
24	.040	.045	.050
25	.095	.101	.074
26	.045	.042	.095
27	.095	.066	.111

Table 4. PEAK LATERAL LANDING ACCELERATIONS, LEFT FRONT CARGO DECK

Landing Number	Maximum Instantaneous Acceleration, (g)		
	8 Hz Band	10 Hz Band	12.5 Hz Band
1	0.028	0.037	0.034
2	.027	.052	.041
3	.025	.034	.035
4	.018	.022	.025
5	.059	.064	.034
6	.066	.152	.077
7	.124	.121	.045
8	.084	.107	.036
9	.088	.108	.038
10	.044	.063	.047
11	.036	.054	.023
12	.060	.083	.030
13	.036	.045	.027
14	.033	.035	.033
15	.036	.050	.029
16	.055	.086	.025
17	.043	.063	.047
18	.056	.109	.039
19	.018	.043	.027
20	.038	.071	.038
21	.056	.103	.028
22	.049	.084	.035
23	.027	.042	.026
24	.023	.025	.018
25	.049	.069	.044
26	.046	.057	.023
27	.036	.053	.030

Table 5. PEAK VERTICAL LANDING ACCELERATIONS, RIGHT CENTER CARGO DECK

Landing Number	Maximum Instantaneous Acceleration, (g)		
	8 Hz Band	10 Hz Band	12.5 Hz Band
1	0.034	0.036	0.044
2	.065	.039	.028
3	.049	.080	.057
4	.028	.026	.034
5	.078	.067	.039
6	.101	.166	.062
7	.103	.119	.028
8	.070	.044	.031
9	.036	.028	.028
10	.070	.039	.031
11	.106	.114	.052
12	.101	.090	.039
13	.065	.052	.031
14	.036	.036	.031
15	.093	.049	.031
16	.111	.093	.034
17	.067	.054	.034
18	.083	.083	.044
19	.028	.047	.034
20	.062	.067	.031
21	.067	.111	.041
22	.034	.101	.083
23	.044	.039	.036
24	.039	.028	.034
25	.101	.140	.034
26	.028	.054	.036
27	.093	.065	.034

Table 6. PEAK LONGITUDINAL LANDING ACCELERATIONS, RIGHT CENTER CARGO DECK

Landing Number	Maximum Instantaneous Acceleration, (g)		
	8 Hz Band	10 Hz Band	12.5 Hz Band
1	0.021	0.012	0.012
2	.017	.017	.021
3	.012	.012	.015
4	.010	.008	.009
5	.042	.049	.024
6	.060	.062	.038
7	.052	.065	.021
8	.056	.038	.022
9	.026	.025	.021
10	.022	.038	.021
11	.063	.091	.045
12	.045	.051	.023
13	.027	.042	.021
14	.023	.029	.016
15	.046	.057	.029
16	.037	.100	.062
17	.044	.061	.016
18	.040	.054	.035
19	.022	.030	.020
20	.033	.024	.020
21	.056	.069	.036
22	.040	.124	.117
23	.031	.053	.019
24	.016	.023	.016
25	.070	.119	.049
26	.018	.029	.013
27	.041	.048	.017

Table 7. PEAK VERTICAL LANDING ACCELERATIONS, LEFT CENTER CARGO DECK

Landing Number	Maximum Instantaneous Acceleration, (g)		
	8 Hz Band	10 Hz Band	12.5 Hz Band
1	0.043	0.049	0.046
2	.055	.043	.052
3	.046	.072	.046
4	.043	.032	.034
5	.112	.095	.037
6	.072	.086	.055
7	.057	.057	.032
8	.060	.072	.040
9	.037	.052	.026
10	.049	.043	.034
11	.083	.106	.034
12	.037	.037	.032
13	.055	.069	.037
14	.060	.040	.037
15	.049	.052	.040
16	.063	.086	.040
17	.069	.063	.040
18	.063	.057	.037
19	.043	.046	.060
20	.063	.066	.055
21	.129	.129	.040
22	.072	.155	.135
23	.049	.055	.040
24	.029	.043	.029
25	.101	.172	.089
26	.046	.049	.029
27	.040	.063	.032

Table 8. PEAK LONGITUDINAL LANDING ACCELERATIONS, LEFT CENTER CARGO DECK

Landing Number	Maximum Instantaneous Acceleration, (g)		
	8 Hz Band	10 Hz Band	12.5 Hz Band
1	0.025	0.023	0.016
2	.019	.014	.023
3	.030	.063	.024
4	.017	.010	.015
5	.064	.063	.018
6	.057	.076	.033
7	.050	.054	.019
8	.062	.048	.023
9	.033	.027	.019
10	.034	.050	.030
11	.066	.090	.048
12	.041	.034	.018
13	.047	.054	.019
14	.024	.022	.019
15	.039	.050	.017
16	.039	.108	.059
17	.054	.068	.019
18	.042	.044	.025
19	.025	.037	.025
20	.029	.030	.022
21	.064	.084	.026
22	.078	.132	.122
23	.041	.058	.022
24	.019	.025	.016
25	.063	.133	.068
26	.026	.038	.022
27	.034	.034	.023

Table 9. PEAK VERTICAL LANDING ACCELERATIONS, RIGHT REAR CARGO DECK

Landing Number	Maximum Instantaneous Acceleration, (g)		
	8 Hz Band	10 Hz Band	12.5 Hz Band
1	0.075	0.122	0.125
2	.067	.119	.163
3	.138	.166	.151
4	.039	.070	.083
5	.106	.117	.101
6	.163	.470	.192
7	.135	.319	.101
8	.109	.176	.104
9	.083	.091	.083
10	.093	.117	.156
11	.200	.436	.169
12	.151	.213	.086
13	.112	.096	.125
14	.091	.143	.065
22	.101	.119	.151
23	.088	.138	.109
24	.044	.091	.075
25	.119	.234	.080
26	.065	.060	.101
27	.122	.184	.091

Table 10. PEAK LATERAL LANDING ACCELERATIONS, RIGHT REAR CARGO DECK

Landing Number	Maximum Instantaneous Acceleration, (g)		
	8 Hz Band	10 Hz Band	12.5 Hz Band
1	0.050	0.035	0.043
2	.057	.039	.052
3	.115	.091	.070
4	.030	.025	.020
5	.164	.114	.048
6	.136	.213	.108
7	.210	.131	.049
8	.144	.162	.046
9	.099	.063	.041
10	.112	.092	.054
11	.102	.103	.060
12	.208	.137	.058
13	.142	.102	.027
14	.097	.058	.026
15	.076	.089	.052
16	.181	.148	.055
17	.100	.068	.042
18	.143	.173	.041
19	.033	.050	.052
20	.095	.089	.047
21	.189	.194	.060
22	.154	.168	.137
23	.073	.067	.046
24	.050	.045	.037
25	.149	.105	.051
26	.064	.085	.035
27	.130	.088	.035

Table 11. PEAK VERTICAL LANDING ACCELERATIONS, LEFT REAR CARGO DECK

Landing Number	Maximum Instantaneous Acceleration, (g)		
	8 Hz Band	10 Hz Band	12.5 Hz Band
1	0.041	0.077	0.084
2	.053	.096	.132
3	.031	.067	.098
4	.041	.048	.053
5	.141	.220	.072
6	.124	.218	.093
7	.122	.206	.074
8	.168	.218	.079
9	.091	.115	.093
10	.077	.129	.084
11	.079	.175	.060
12	.062	.141	.079
13	.134	.153	.093
14	.060	.053	.079

Table 12. PEAK LATERAL LANDING ACCELERATIONS, LEFT FRONT CARGO DECK

Landing Number	Maximum Instantaneous Acceleration, (g)		
	8 Hz Band	10 Hz Band	12.5 Hz Band
1	0.050	0.038	0.045
2	.063	.036	.054
3	.030	.031	.061
4	.031	.027	.021
5	.175	.116	.053
6	.144	.226	.119
7	.227	.139	.061
8	.146	.176	.048
9	.107	.069	.044
10	.126	.094	.056
11	.114	.112	.068
12	.223	.151	.059
13	.137	.112	.033
14	.104	.063	.026
15	.078	.093	.060
16	.185	.158	.060
17	.112	.069	.044
18	.147	.183	.040
19	.038	.054	.055
20	.108	.092	.056
21	.206	.200	.064
22	.162	.162	.136
23	.073	.066	.044
24	.050	.048	.037
25	.161	.115	.051
26	.072	.089	.039
27	.142	.092	.030

Table 13. RISK CALCULATION FOR NORMAL DISTRIBUTION
(VERTICAL ACCELERATION, RIGHT REAR CARGO DECK)

Flight Condition	Accel. a,(g)	100% Level,(g)	68.27% or rms Level σ,(g)	Band Center Freq. f,(Hz)	Flight Time T, (s)	Probability of Exceeding a $P=2fT\ \exp(-a^2/2\sigma^2)$	$1-P_i$	Overall Probability $1 - \Pi(1-P_i)$
Taxi	0.1	0.072	0.024	1.25	500	0.212	.788	
Climb	.1		.01	1.25	1500	0	1	
Cruise	.1		.002	1.25	9800	0	1	
Turbulence	.1	.08	.02	1.25	1000	.0093	.9907	
Descent	.1		.0033	1.25	1200	0	1	
Landing	.1	.076	.018	1.25	2.50	.000001	.999999	
Taxi	.1	.072	.024	1.25	1500	.2547	.7453	
Overall							.5818	.4182

Table 14. RISK CALCULATION FOR BINOMIAL DISTRIBUTION (VERTICAL ACCELERATION, RIGHT REAR CARGO DECK)

Flight Condition	Accel. a,(g)	100% Level,(g)	68.27% or rms Level σ,(g)	Band Center Freq. f,(Hz)	Flight Time T, (s)	Probability of Exceeding a $P=2fT\exp(-a^2/2\sigma^2)$	$1-P_i$	Overall Probability $1-\Pi(1-P_i)$
Taxi	0.3	0.20	0.024	10	920	0	1	
Climb	.3		.014	10	5000	0	1	
Cruise	.3		.003	10	31000	0	1	
Turbulence	.3	.04	.008	10	1700	0	1	
Descent	.3		.006	10	3800	0	1	
Landing	.3	From Table 13, 0.3g was not exceeded on 17 out of 20 landings. Then $P = 1-(\frac{17}{20})^1 = .15$				.15	.85	
Taxi	.3	.20	.024	10	920	0	1	
Overall							.85	.15

*U.S. Government Printing Office: 1976 — 657-020/809